Impact of temperature on the development and function of *Drosophila melanogaster's* olfactory system

Dissertation

Zur Erlangung des Grades

Doktor der Naturwissenschaften

Am Fachbereich Biologie

Der Johannes Gutenberg-Universität Mainz

Institut für Entwicklungsbiologie und Neurobiologie

Letícia Leandro Batista

geb. am 20.10.1997 in Uberlândia, Brasilien

Mainz 2026

Dekan: Prof. Dr. Eckhard Thines

1. **Gutachter:**
2. **Gutachter:**

Tag der mündlichen Prüfung:

List of abbreviations

L3	Third Larval Instar
E	Ecdysone
20E	20-Hydroxyecdysone
EcR	Ecdysone Receptor
USP	Ultraspiracle
MB	Mushroom Body
WPP	White Pre-Pupa
APF	After Puparium Formation
C4da neurons	Class IV Dendrite Arborization Neurons
TOR	Target Of Rapamycin
Imp	IGF-II Mrna-Binding Protein
NO	Nitric Oxide
NOS	Nitric Oxide Synthase
EM	Electron Microscopy
NMJ	Neuromuscular Junction
CNS	Central Nervous System
ORNs	Olfactory Receptor Neurons
ORs	Odorant Receptors
AL	Antennal Lobe
PNs	Projection Neurons
uPNs	Uniglomerular Projection Neurons
mPNs	Multiglomerular Projection Neurons
LNs	Local Neurons
GABA	γ-Aminobutyric Acid
ALT	Antennal Lobe Tract
mALT	Medial Antennal Lobe Tract
mlALT	Medial Lateral Antennal Lobe Tract
adPN	Antero-Dorsal PN Lineage
lPN	Lateral PN Lineage
vPN	Ventral PN Lineage
LH	Lateral Horn
KCs	Kenyon Cells
LHNs	Lateral Horn Neurons
LHLN	Lateral Horn Local Neuron
LHON	Lateral Horn Output Neuron
LH	Lateral Horn
PBS	Phosphate-Buffered Saline

LC-MS/MS	Liquid Chromatography Tandem Mass-Spectrometry
AUC	Area Under The Curve
RT-qPCR	Real-Time Quantitative PCR
CT	Cycle Threshold
BRP	Bruchpilot
ROI	Region Of Interest
SEZ	Subesophageal Zone
LH-AM	Lateral Horn Anterior Medial Region
LH-PM	Lateral Horn Posterior Medial Region
LH-AL	Lateral Horn Anterior Lateral Region
UTD	Universal Temperature Dependance
MaA	Makisterone A
MuA	Muristerone A
IR	Ionotropic Receptor
TCA cycle	Tricarboxylic Acid Cycle
ETC	Electron Transport Chain
OXPHOS	Oxidative Phosphorylation
Acsl	Acyl-Coa Synthetase Long-Chain
Gpdh1	Glycerol-3-Phosphate Dehydrogenase 1
G3P	Glycerol-3-Phosphate
GPO1	Glyerophosphate Oxidase 1
Hsp	Heatshock Proteins

List of figures

Figure 1. Detail from an illustration by Maria Sibylla Merian depicting metamorphosis. 3
Figure 2. Life cycle of the fruit fly *Drosophila melanogaster* at 25°C..... 5
Figure 3. 20-hydroxyecdysone dynamics during development and its regulation of gene expression. 7
Figure 4. Mushroom body γ neurons undergo stereotypic remodeling at metamorphosis. 9
Figure 5. Schematics of the olfactory system in the *Drosophila melanogaster* brain.. 19
Figure 6. Development at 18°C increases the number of postsynaptic partners of DM1-ORNs detected by trans-Tango. 37
Figure 7. Postsynaptic partners of DM1-ORNs developed at 18°C are functionally connected. 39
Figure 8. *Or42b*-ORNs display more and bigger synapses when developed at 18°C 40
Figure 9. DM1-ORNs contain more mitochondria when developed at 18 °C in comparison to 25°C..... 42
Figure 10. Temperature-dependent scaling of postsynaptic partners across olfactory glomeruli 44
Figure 11. Developmental temperature modulates the number of postsynaptic partners in DM1-ORNs exponentially across temperatures. 46
Figure 12. Impact of developmental temperature in odor-driven behavior. 49
Figure 13. Odor-evoked calcium responses of ORNs are enhanced at lower developmental temperatures, while PN responses remain consistent..... 51
Figure 14. Multiglomerular projection neuron activity in the lateral horn is similar across developmental temperatures. 52
Figure 15. Lower developmental temperature increases PN–LHN connectivity..... 54
Figure 16. BacTrace reveals temperature-dependent variability in PN–LHN connectivity 56
Figure 17. Calcium response of PD2a1/b1 neurons in flies developed at 18 and 25°C..... 57
Figure 18. Temperature dependence of DM1-ORN postsynaptic connectivity and developmental timing. 60
Figure 19. Example of uniform and non-uniform scaling..... 62
Figure 20. Temporal scaling of projection neurons development across developmental temperatures. 63
Figure 21. Conceptual model of temperature scaling and validation of ecdysone-responsive gene expression profiles. 65

Figure 22. Comparison of temporal gene expression at 18 °C and 25 °C during pupal development 66
Figure 23. Effect of developmental temperature on pupal development duration and experimental designs. 69
Figure 24. Temporal profiles of ecdysteroids across developmental temperatures. 70
Figure 25. Comparison of RNA-seq and RT-qPCR temporal profiles for ecdysone downstream genes across developmental temperatures. 72
Figure 26. Temporal expression profiles of olfactory and ionotropic receptor genes across developmental temperatures. 75
Figure 27. Coordinated upregulation of glycolytic and TCA cycle enzymes across developmental temperatures. 76
Figure 28. Coordinated upregulation of electron transport chain genes across developmental temperatures. 78
Figure 29. Expression of mitochondrial-encoded electron transport chain (ETC) genes across developmental temperatures. 80
Figure 30. Temporal expression of genes involved in lipid metabolism across developmental temperatures. 81
Figure 31. Temporal expression of heat shock protein genes is mostly upregulated at lower temperatures. 83

List of tables

Table 1. Fly strains used in this work, separated by used name, full genotype and figure in which it appears. 23
Table 2. Summary of duration of development percentages across temperatures.. 30
Table 3. Molecules quantified by LC-MS/MS, with precursor and fragment ion. Bold indicates the quantified fragment ion. 32
Table 4. Primer sequence of the evaluated genes, containing Forward and Reverse strands for each gene. 34

Table of Contents

1 Abstract 1

2 Zusammenfassung 2

3 Introduction 3

3.1 Metamorphosis 4

3.2 Developmental transitions are tightly regulated 6

3.3 Brain development throughout metamorphosis 8

3.3.1 Pruning regulation 10

3.3.2 Regrowth regulation 11

3.4 Neurodevelopment in the connectome era 12

3.5 Developmental plasticity in brain wiring 13

3.6 The role of the environment: the case of temperature 14

3.6.1 Effect of temperature on brain development 15

3.7 Drosophila's olfactory system 18

3.8 Aims of this dissertation 21

4 Materials and Methods 23

4.1 Experimental model and fly husbandry 23

4.2 Immunohistochemistry and confocal imaging 24

4.2.1 Image segmentation and quantification 25

4.3 Behavioral experiments 26

4.3.1 Spherical treadmill. 26

4.3.2 Free-walking assay. 27

4.4 In vivo calcium imaging 28

4.4.1 Optogenetics. 28

4.4.2 Odor delivery 29

4.5 Connectome analysis 29

4.6 Ecdysteroids quantification 29

4.7 RT-qPCR assays 32

4.7.1 Total RNA extraction 32

4.7.2 cDNA synthesis 33
4.7.3 RT-qPCR 33
4.8 Bulk RNA-seq 34
5 Results 36
5.1 Developmental temperature shapes ORNs connectivity and synaptic architecture 36
5.1.1 ORN connectivity scales across developmental temperatures 36
5.1.2 DM1-ORNs partners reported by trans-Tango at 18°C are functionally connected 38
5.1.3 DM1-ORNs present more active synaptic zones when developed at 18°C 40
5.1.4 DM1-ORNs present more mitochondria when developed at 18°C 41
5.1.5 Connectivity of other ORNs also scale with developmental temperature 43
5.1.6 DM1-ORNs connectivity scales exponentially across developmental temperatures 45
5.2 Functional consequences of changes in wiring 48
5.2.1 Odor-driven behavior is impacted by developmental temperature 48
5.2.2 Odor coding in the antennal lobe is impacted by developmental temperature 50
5.2.3 Lateral horn neurons connectivity to PNs is affected by developmental temperatures 53
5.3 A metabolic theory explains brain wiring at different developmental temperatures 58
5.3.1 Developmental temperature induces a non-uniform scaling of neuronal growth 61
5.4 Molecular correlates of temperature-dependent circuit remodeling 63
5.4.1 Ecdysone signaling regulates gene programs controlling circuit wiring 64
5.4.2 Temporal scaling of ecdysteroids levels is conserved across developmental temperatures 67
5.4.3 Temporal scaling of gene expression across developmental temperatures 71
5.4.4 Expression of genes involved in lipid metabolism (β-oxidation and lipogenesis) 80
5.4.5 Expression of genes involved in heat and cold stress responses 82
6 Discussion 85
6.1 Temperature-dependent modulation of neural connectivity during pupal development 85
6.2 Functional robustness of the antennal lobe to changes in developmental temperature 88
6.3 Developmental temperature shapes pn–lhn connectivity and behavioral responses 89
6.4 Developmental tempo and circuit assembly: linking body growth to brain wiring 91
6.5 Temporal dynamics of ecdysteroid are temperature-independent 93
6.6 Regulation of metabolic pathways by developmental temperature 93
6.7 Concluding remarks 96

7 Bibliography 98

8 Acknowledgments 127

9 Curriculum vitae 129

10 Eigenständigkeitserklärung 132

1 Abstract

The assembly of neural circuits during development is shaped by both intrinsic genetic programs and extrinsic environmental conditions. In insects, brain development undergoes extensive remodeling during metamorphosis, and temperature is a key environmental determinant of ectothermic development. However, how temperature-dependent changes in neuronal growth translate into circuit wiring and function remains poorly understood. Therefore, in this dissertation, I address four central questions: (1) how developmental temperature influences wiring in the *Drosophila melanogaster* olfactory system; (2) whether temperature-induced changes in wiring alter olfactory processing; (3) how changes in wiring due to temperature can be mechanistically linked to biophysical effects on growth; and (4) which developmental and molecular pathways mediate temperature-dependent effects on neural circuits. I show that developmental temperature systematically scales olfactory receptor neurons connectivity within the olfactory pathway, altering synaptic organization and neural growth. Odor representations remain robust, even as network connectivity is rescaled. In contrast, odor-driven behavior is stronger in flies developed at lower temperatures, which could be explained by a modified connectivity to the next downstream area. To explain these findings, I introduce a biophysical model in which temperature-dependent differences in metabolic reaction rates across cell types generate temporal mismatches during development, leading to predictable changes in neural wiring. At the molecular level, I find that temperature-induced rewiring does not arise from major changes in systemic developmental timing signals. Instead, temperature modulates the timing of downstream transcriptional programs: ecdysone-responsive transcription factors and genes involved in central energy metabolism are expressed earlier at lower temperatures. These results suggest that temperature shapes developmental outcomes by altering the temporal coordination of transcriptional and metabolic programs. Together, this work provides a multi-level view of how temperature influences neural development, linking environmental conditions to metabolism, developmental tempo, and circuit organization. It highlights how layers of the nervous systems can remain functionally robust while retaining flexibility in wiring to environmental variation, offering new insights into the effects of temperature into brain development.

2 Zusammenfassung

Die Bildung neuronaler Schaltkreise während der Entwicklung wird sowohl durch intrinsische, genetische Programme, als auch durch extrinsische Umgebungsbedingungen beeinflusst. Bei Insekten unterliegt die Gehirnentwicklung während der Metamorphose einer umfassenden Umgestaltung, wobei die Temperatur ein entscheidender Umweltfaktor für die Entwicklung von Ektothermen ist. Wie sich temperaturabhängige Veränderungen im neuronalen Wachstum jedoch auf die Vernetzung und Funktion der Schaltkreise auswirken, ist ungeklärt. Daher befasse ich mich in dieser Dissertation mit vier zentralen Fragen: (1) Wie beeinflusst die Entwicklungstemperatur die Vernetzung im Geruchssystem der Fliege? (2) Beeinflussen temperaturbedingte Veränderungen in der Vernetzung die Geruchsverarbeitung? (3) Wie können temperaturbedingte Veränderungen in der Vernetzung mechanistisch mit biophysikalischen Auswirkungen auf das Wachstum in Relation gesetzt werden? (4) Welche Entwicklungs- und Molekularwege vermitteln temperaturabhängige Auswirkungen auf neuronale Schaltkreise? Ich zeige, dass die Entwicklungstemperatur die ORN-Konnektivität über die Geruchsbahnen hinweg systematisch skaliert und dabei die synaptische Organisation und das neuronale Wachstum verändert. Die Geruchsrepräsentationen bleiben robust, auch wenn die Konnektivität neu skaliert wird. Jedoch ist das geruchsgesteuerte Verhalten bei Fliegen, die bei niedrigeren Temperaturen entwickelt wurden, stärker ausgeprägt, was durch eine veränderte Konnektivität zum nächsten nachgeschalteten Bereich erklärt werden könnte. Um diese Ergebnisse zu erklären, stelle ich ein biophysikalisches Modell vor, in dem temperaturabhängige Unterschiede in den Stoffwechselreaktionsraten verschiedener Zelltypen zu zeitlichen Diskrepanzen während der Entwicklung führen, was vorhersehbare Veränderungen in der neuronalen Vernetzung zur Folge hat. Auf molekularer Ebene stelle ich fest, dass die temperaturbedingte Neuvernetzung nicht auf größere Veränderungen der systemischen Entwicklungssignale zurückzuführen ist. Stattdessen moduliert die Temperatur den Zeitpunkt der nachgeschalteten Transkriptionsprogramme: Ecdyson-responsive Transkriptionsfaktoren und Gene, die am zentralen Energiestoffwechsel beteiligt sind, werden bei niedrigeren Temperaturen früher exprimiert. Dies suggestiert, dass die Temperatur die Entwicklungsergebnisse beeinflusst, indem sie die zeitliche Koordination von Transkriptions- und Stoffwechselprogrammen verändert. Insgesamt liefert diese Arbeit eine mehrschichtige Sichtweise darauf, wie die Temperatur die neuronale Entwicklung beeinflusst, und verbindet Umweltbedingungen mit Stoffwechsel, Entwicklungstempo und Schaltkreisorganisation. Sie zeigt, wie die Schichten des Nervensystems funktionell robust bleiben und gleichzeitig ihre Flexibilität in der Vernetzung gegenüber Umweltveränderungen bewahren können, und bietet neue Einblicke in die Auswirkungen der Temperatur auf die Gehirnentwicklung.

3 Introduction

The dramatic transformations that convert a caterpillar into a butterfly or a tadpole into a frog have fascinated naturalists for centuries, raising fundamental questions about how complex biological systems are built and remodeled. In the early eighteenth century, the German naturalist Maria Sibylla Merian produced some of the earliest integrated life-history studies, recorded in *Metamorphosis insectorum surinamensium*, a book that established a new standard in natural history (Etheridge, 2011; Merian, 1705). Her depictions of insects across developmental stages, presented alongside their host plants, combined meticulous observation with detailed illustration, laying the groundwork for future studies in ecology and entomology (Figure 1) (Etheridge, 2011; Merian, 1705).

Figure 1. Detail from an illustration by Maria Sibylla Merian depicting metamorphosis. Adult *Arsenura armida* (family *Saturniidae*) alongside the flowering tree *Erythrina fusca*,

illustrating Merian's metamorphosis studies. The larvae shown belong to different species, not described in Merian's work.

Building on this long-standing interest in developmental transformation, this dissertation examines how environmental conditions shape the assembly and function of neural circuits during development. Specifically, I investigate how developmental temperature influences the assembly and function of a sensory circuit in the fruit fly's brain.

To provide the necessary context for this work, this introduction first defines metamorphosis, with a focus on holometabolous insects, and outlines the hormonal mechanisms that regulate major developmental transitions. I then describe how the insect brain is extensively remodeled across metamorphosis, transitioning from larval to adult circuits. Next, I discuss plasticity in neural wiring during development, highlighting the roles of intrinsic and extrinsic factors, before narrowing the focus to temperature as a key environmental determinant of brain development. Finally, I introduce *Drosophila melanogaster* as a model organism, outlining its experimental advantages, current knowledge of temperature-dependent development in this species, and the organization and assembly of its olfactory system.

3.1 Metamorphosis

Metamorphosis, defined as a change (meta) in form (morphē), is widespread across animal taxa. This developmental strategy has evolved independently on multiple occasions, including in fish, amphibians, and insects, where it satisfies common criteria yet varies substantially in the degree of morphological transformation (Truman, 2019; Werner, 1988).

The most dramatic metamorphoses occur in insects, a group accounting for more than 60% of described animal species. Insects dominate ecosystems in abundance, diversity and biomass (Berenbaum, 2017; Grimaldi & Engel, 2005). Insects can be categorized as hemimetabolous or holometabolous based on the extent of metamorphic change during development. Hemimetabolous insects undergo gradual metamorphosis, with nymphs resembling miniature adults. Holometabolous insects – including beetles, butterflies, bees, and flies – undergo total metamorphosis, with four distinct developmental stages: egg, larva, pupa, and adult. More than 80% of all insect species are holometabolous, highlighting the evolutionary success of complete metamorphosis (Grimaldi & Engel, 2005).

The fruit fly is a holometabolous insect, with three distinct stages in their post-embryonic life cycle: larva, pupa, and adult. After hatching from the egg, the animal enters first larval instar.

The larva growth is characterized by two molts, each producing a new cuticular covering for the body. At the end of each molt, the old cuticle is shed in a process called ecdysis. These molts divide the larval stage into three instars, the 1st, 2nd and 3rd larval instars that each last approximately 48h at 25°C (Fig. 2).

The larva is a fully functional organism with differentiated organs – including a complex nervous system and endocrine organs – that support its feeding, behavior, and growth. The larva contains rudimentary epithelial structures, called imaginal discs, which will proliferate and differentiate during the pupal stage to form most adult body organs. Therefore, in metamorphosis, the previous larval structures are destroyed while the adult ones are generated.

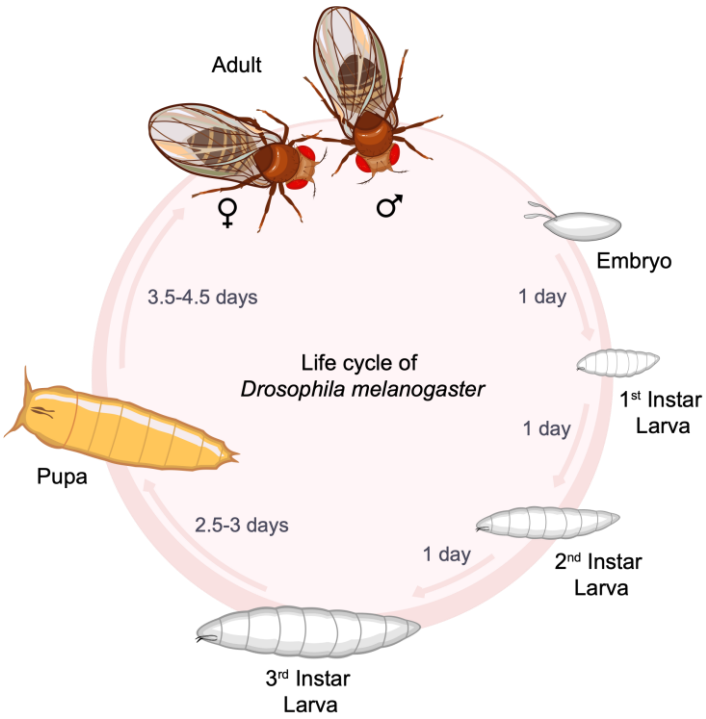

Figure 2. Life cycle of the fruit fly *Drosophila melanogaster* at 25°C. Following mating, fertilized eggs develop as embryos for one day before hatching into first-instar larvae. Larval development consists in three instars, each lasting one day. After 2.5-3 days, late third instar larva pupariates and enter the pupal stage. In the pupa most larval tissues are degraded and adult structures formed. Pupal development takes 3.5-4.5 days, after which the adult fly ecloses. (Drawings: Adobe Stock # 387850389).

At the end of third instar (L3), the larva switches from feeding into leaving the food and searches a site for pupariation. In the first minutes of puparium formation, the pupa is still white

(white prepupa – WPP). This stage is used as a time reference to pupa development, marking hour zero of the pupa – 0h after puparium formation (0h APF). As pupa development proceeds, the cuticle begins to tan, and becomes a protective shell around the metamorphosing insect. At 25°C, the whole developmental process takes 10 days. The duration of development is temperature-dependent, proceeding faster at higher temperatures and more slowly at lower temperatures (Davidson, 1944).

3.2 Developmental transitions are tightly regulated

Insect metamorphosis is tightly regulated through developmental programs: transitions between life stages are controlled by endocrine signaling pathways that coordinate growth, tissue remodeling, and maturation across the organism. These hormonal systems ensure that developmental progression occurs at the appropriate time and in response to both internal and external cues (Jindra et al., 2013; Koyama et al., 2025; Yamanaka et al., 2013).

In insects, postembryonic growth, metamorphosis, and many other developmental processes are controlled by Ecdysone (E), a hormone derived from cholesterol (Nakagawa & Henrich, 2009; Riddiford et al., 2003). Ecdysone function has been thoroughly dissected using the fruit fly, *Drosophila melanogaster*. It regulates developmental timing and its transitions through six steps: biosynthesis, secretion, circulation, transport, modification and gene expression regulation. Ecdysone is produced in the larval prothoracic gland, through Cytochrome P40 monooxygenases, encoded by Halloween genes, which convert cholesterol into Ecdysone (*Phantom*, *Disembodied*, and *Shadow*) (Chávez et al., 2000; Niwa et al., 2004; Warren et al., 2002, 2004).

In the intestine and fat body, Ecdysone is modified into its active form, 20-hydroxyecdysone (20E), by Shade, an enzyme also encoded by a Halloween gene (Petryk et al., 2003). The developmental effects of ecdysone are ultimately mediated through its active form, 20-hydroxyecdysone (20E), with transitions between developmental stages marked by pulses of elevated ecdysone titers that regulate stage-specific gene expression (Fig. 3A) (Bond et al., 2010; Schwedes & Carney, 2012).

20E regulates gene expression via its receptor heterodimer, which consists of the ecdysone receptor (EcR) and Ultraspiracle (USP) (Nakagawa & Henrich, 2009; Yao et al., 1993). The EcR/USP heterodimer binds to specific DNA sequences. Without 20E binding to EcR/USP, the receptor acts as a repressor of gene expression, in addition to recruiting other co-repressors as

histone deacetylases. However, once 20E binds to EcR/USP the co-repressors are released. This way, 20E binding to EcR/USP can can lead to relief of the repression – via releasing the co-repressors – or lead to a strong gene expression (Beatty et al., 2006; Devarakonda et al., 2003).

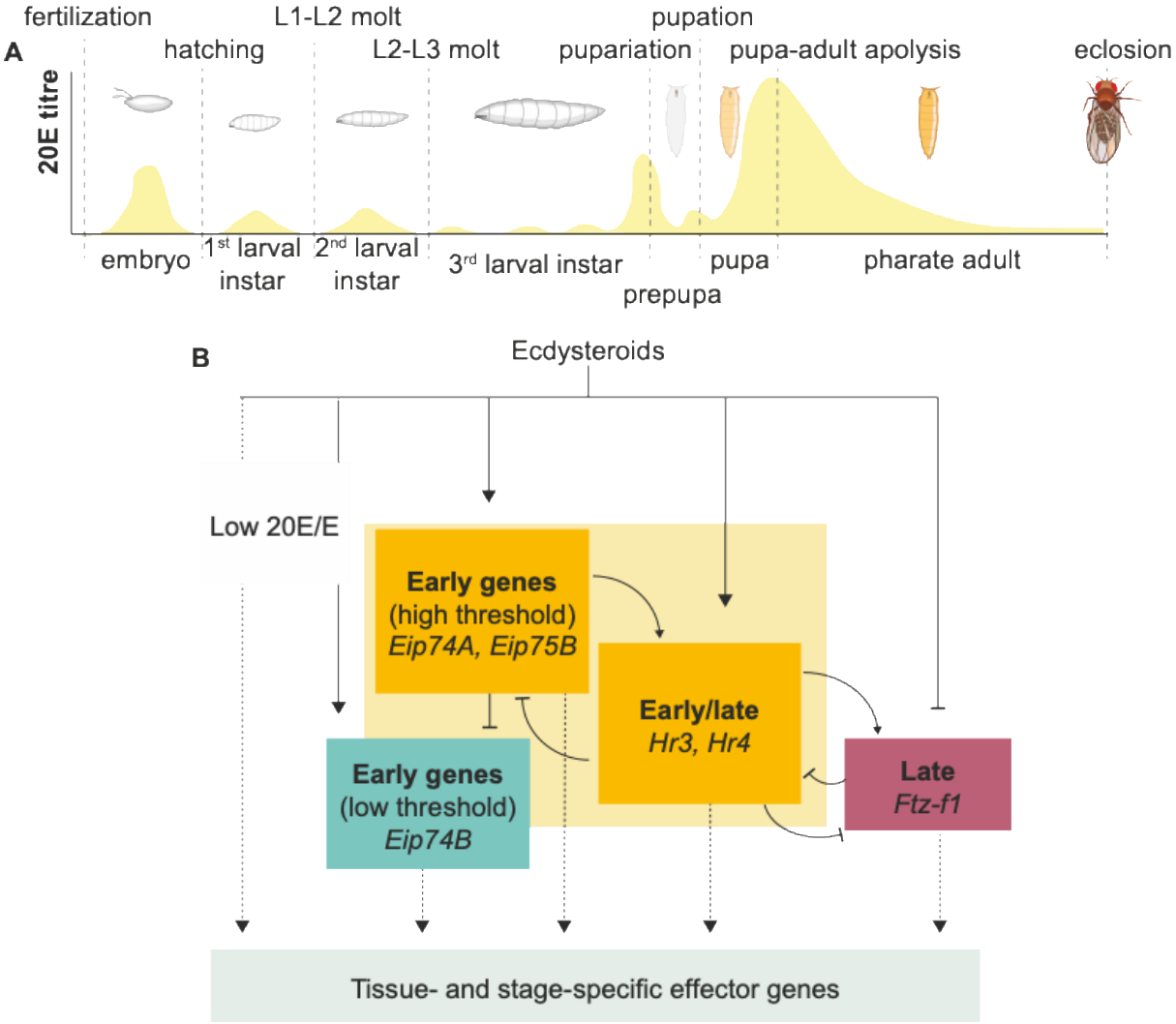

Figure 3. 20-hydroxyecdysone dynamics during development and its regulation of gene expression. (A) Temporal dynamics of 20-hydroxyecdysone (20E) during Drosophila development, with major developmental transitions and key events indicated. Adapted from Scanlan *et al.* (2023) (B) The Ashburner model, illustrating the hierarchical transcriptional cascade triggered by ecdysteroids. The binding of 20E to the ecdysone receptor (EcR) initiates a sequential activation of early transcription factors, which regulate one another and further control the expression of downstream effector genes. Adapted from Truman & Riddiford (2023).

Upon binding, a gene expression cascade is induced, described by the Ashburner model (Fig. 3B) (Ashburner, 1974). In this model, first we have the expression of a few early genes, that encode transcription factors. Early genes can be divided into high threshold (e.g., *Eip74A*,

Eip75B) or low threshold (e.g. *Eip74B*) depending on 20E reaching its concentration threshold that leads to gene transcription activation. Early genes then trigger feed-forward and feedback targets that turn off early response gene and increases the expression of multiple late downstream genes (e.g., *Hr3, Hr4, ftz-f1*). This way, target genes are regulated throughout development with different temporal patterns.

Despite uniform 20E pulses, there are spatial and tissue-specific developmental outcomes. Those could arise from either tissue-specific ecdysone receptor isoforms expression or activation of tissues-specific effector genes. The ecdysone receptor has three ecdysone isoforms (EcR-A, EcR-B1, and EcR-B2), expressed in different tissues and timepoints (Talbot et al., 1993; Truman et al., 1994). For example, in the nervous system, B-isoforms mediate pruning of larval neurons at metamorphosis (Lee et al., 2000), whereas EcR-A expression regulates cell death of ventral cord neurons upon adult emergence (Robinow et al., 1993).

Regarding tissue-specific effects, ecdysone signaling has been shown to terminate the proliferation of neural stem cells by reprogramming their energy metabolism (Homem et al., 2014). This process occurs through the Mediator complex, which assist embryonic stem cell to maintain pluripotency by binding to large regulatory regions (super-enhancers) and activating the transcriptional programs that sustain the stem cell state (Kagey et al., 2010; Whyte et al., 2013).

Ecdysone signaling can also carry out sex-specific consequences. In males, it contributes to the development of male-specific neurons in the brain, by interacting with FruBM-dependent transcriptional programs (Zhang et al., 2018). Meanwhile in females, the ecdysone-response factor E78 controls the niche formation and follicle survival in the ovary (Ables et al., 2015).

3.3 Brain development throughout metamorphosis

During metamorphosis, the larval brain is extensively remodeled: some larval neurons die, others prune and regrow new processes, and a large population of adult-specific neurons are generated, resulting in an adult brain with circuits and neuron types specialized for adult behaviors, as courtship and mating (Thum & Gerber, 2023; Truman & Riddiford, 2023; Winding et al., 2023).

Neuron types that persist through metamorphosis often undergo neuronal remodeling. In this process, most or all larval dendrites and/or axon branches are pruned, followed by developmental regrowth that forms the foundation of adult specific connections, completely

overriding the previous larval connectivity. Neuronal remodeling happens on different scales: small scale pruning (e.g. single synapses) occurs via retraction, while large scale pruning occurs via localized degeneration of axons and dendrites (Low & Cheng, 2006; Luo & O'Leary, 2005; Schuldiner & Yaron, 2015). However, even within the same neural structure, not all axons are remodeled during metamorphosis. For example, dendritic arborization neurons have their dendrites remodeled but their axons remain intact (Shimono et al., 2009).

The mushroom body (MB) is one of the major Drosophila neuropiles to undergo neuronal remodeling during metamorphosis. The MB is involved in learning and memory of olfactory cues in both larva and adults (Heisenberg, 2003), and consists of three types of neurons – γ, α/β and α'/β' – out of which only the γ neurons undergo remodeling (Lee, Lee, Arthur, et al., 1999; Truman et al., 2023) (Fig. 4). The MB γ neurons are one of the most studied neurons during metamorphosis, with a well described process and mechanism. As such, they will be presented as an illustrative example of neuron remodeling.

In the early phases of pupation, γ neurons dendrites undergo complete pruning, while its axons retract back to a characteristic branch point. Axonal fragmentation is typically finished by 18 hours after puparium formation (APF). By 24 h APF, axonal regrowth becomes detectable, and around 48 h APF, γ neurons have extended their axons again to establish a new, adult-specific medial lobe, accompanied by the emergence of a new dendritic arbor (Hakim et al., 2014; Rabinovich et al., 2015).

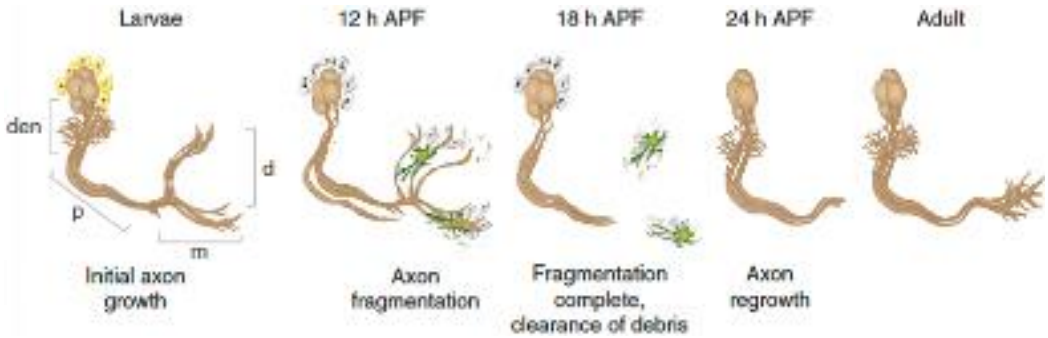

Figure 4. Mushroom body γ neurons undergo stereotypic remodeling at metamorphosis. At larval stage, Mushroom body (MB) γ neurons project a single axon that branches to form dendrites (den), a tightly bundled axon peduncle (p) that bifurcates to form the dorsal (d) and medial (m) lobes. Cortex glia (yellow) and astrocytes (green) instruct MB axon pruning. At 12 h APF, axon fragmentation is apparent, finished at 18 h APF. At 24 h APF, the MB γ neurons

begin to regrow toward the adult targets, forming the adult γ lobe. Modified from (Yaniv & Schuldiner, 2016).

3.3.1 Pruning regulation

Neural pruning is a tightly regulated processes, governed by both cell-autonomous mechanisms and interactions with neighboring cells. In the mushroom body (MB), the ecdysone receptor EcR-B1 together with its partner Ultraspiracle (USP) is required for pruning and subsequent axon extension (Lee, Liqun Luo, et al., 1999; Liou et al., 2018; Schubiger et al., 1998). Expression of EcR-B1 in the MB is tightly controlled, present only at the onset of pruning (Lee et al., 2000). This transcriptional control is regulated by multiple upstream pathways, including the cohesin complex, the nuclear receptor FTZ-F1, and TGF-β signaling (Boulanger et al., 2011; Schubiger et al., 1998; Schuldiner et al., 2008). The ecdysone pathway also relies on proper hormone delivery: ecdysone must be transported into the brain through the Ecl receptor, expressed on the surface of glial cells (Okamoto et al., 2018).

Building on this hormonal control, downstream cellular machinery drives the remodeling of MB γ neurons in response to ecdysone signaling. The ubiquitin–proteasome system is cell-autonomously required for γ-axon pruning, as loss of the E1 enzyme or proteasome subunits in MB neurons blocks pruning (Watts et al., 2003). In addition, endocytic and endolysosomal pathways, including UVRAG–class III PI3K complexes and localized endocytosis that regulates receptor and membrane turnover, have been shown in Drosophila sensory neurons to mediate dendrite pruning and are thought to act in analogous ways during axon and dendrite remodeling in other neurons (Issman-Zecharya & Schuldiner, 2014). In parallel, destabilization of cell-adhesion molecules such as Fasciclin II, for example via JNK-dependent down-regulation, facilitates axon branch withdrawal, highlighting a complementary mechanism that lowers axon–axon adhesion to permit pruning (Bornstein et al., 2015).

Different neuron types use overlapping but non-identical pruning machinery. For example, class IV dendrite arborization (C4da) sensory neurons in Drosophila have their remodeling driven by localized endocytosis, which promotes local loss of cell-adhesion molecules and membrane, leading to dendrite thinning and compartmentalization. This compartmentalization

allows localized calcium signaling and subsequent calpain activation, which execute dendrite degeneration (Kanamori et al., 2013, 2015).

Beyond cell autonomous mechanisms for dendrite pruning, neurons also interact with surrounding glia throughout the pruning process. Glia secrete the TGF-β ligand Myoglianin, which activates Baboon/Smad signaling in MB γ neurons and upregulates EcR-B1 expression (Awasaki et al., 2011; Hakim et al., 2014). Interestingly, astrocytes themselves require ecdysone signaling for their maturation into phagocytes and for effective infiltration of the MB γ neurons during metamorphosis (Tasdemir-Yilmaz & Freeman, 2014). Astrocytes then clear γ neurons debris following pruning by engulfing the fragments and degrading them through an endosomal-lysosomal pathway (Tasdemir-Yilmaz & Freeman, 2014).

3.3.2 Regrowth regulation

After pruning, regrowth takes place. Regrowth of neurons is regulated by a unique program, different from the neuronal growth during initial neurogenesis. In MB neurons, the nuclear receptor UNF, the target of rapamycin (TOR), and the ecdysone inducible protein Eip75B are involved in regrowth after pruning, but not in the initial neurogenesis (Marmor-Kollet & Schuldiner, 2016; Rabinovich et al., 2016; Yaniv et al., 2012). Both UNF and Eip75B function as nuclear receptor dimers in order to promote axon regrowth in MB γ axons , and exert its function via the TOR pathway (Rabinovich et al., 2016). Recent studies have identified the IGF-II mRNA-binding protein (Imp) as a key regulator of profilin mRNA trafficking and localization during the regrowth phase. As profilin plays a central role in actin polymerization (Prokop et al., 2013), these findings suggest that modulation of actin dynamics may facilitate axonal regeneration.

The transition between pruning and regrowth occurs quite rapidly, with nitric oxide (NO) as a possible switching mechanism in the MB neurons. Both UNF and Eip75B are activated by NO, demonstrated by the fact that both receptors bind a heme moiety – a sensor for monovalent gases, such as NO (de Rosny et al., 2008; Raghuram et al., 2007; Reinking et al., 2005). Moreover, Eip75B exhibits context-dependent activity in different NO environments by modulating its affinity for interacting partners (Cáceres et al., 2011; Johnston et al., 2011). A rapid decrease in NO levels, produced by neuronal nitric oxide synthase (NOS), is in fact necessary to permit axon regrowth. Experimental evidence indicates that reduced NO facilitates

the formation of a stable UNF–Eip75B complex, which is thought to activate a cohort of genes that drive the regrowth program (Rabinovich et al., 2016).

In contrast, elevated NO levels – produced by neuronal NOS in conjunction with calmodulin – are necessary for the normal progression of axon pruning. The transition from high NO during pruning to low NO during regrowth is developmentally controlled and occurs rapidly with precise temporal regulation (Rabinovich et al., 2016). Nevertheless, how NOS activity is finely tuned, and the mechanisms by which high NO promotes pruning, remain unresolved questions – and similar gaps in knowledge extend to other aspects of brain remodeling.

3.4 Neurodevelopment in the connectome era

The endpoint of the developmental process is the adult brain. In recent years, substantial effort has gone into generating brain-wide connectomes in both adult and larval flies – comprehensive reconstructions of all neurons and connections in the central brain of the fruit fly. A major milestone came in 2018, when the first complete Drosophila brain connectome was produced using electron microscopy (EM) imaging (Zheng et al., 2018). Ever since, increasingly comprehensive datasets have become available. A connectome encompassing half of the fly brain – comprising roughly 25,000 neurons and ~ 20 million synaptic connections – was published in 2020 (Scheffer et al., 2020), together with a full reconstruction of the olfactory system connectome (Bates et al., 2020). The FlyWire consortium subsequently released a complete female Drosophila brain connectome, containing ~140,000 neurons and 54.5 million connections (Dorkenwald et al., 2024). This was followed by a full nervous system connectome that includes all ~160,000 neurons in the fly, including the ventral nerve cord (Bates et al., 2025).

A reconstruction of the fly larval brain was also released, allowing the comparison of larval and adult brain features (Winding et al., 2023). The adult brain displays a more modular organization than the larval brain, characterized by an expansion of specialized compartments with distinct functions. This specialization is accompanied by a reduction in overall network density, indicating that the adult brain has structural domains that operate as functional hubs (Yadav et al., 2025). In addition, the adult network has scale-free properties, enhancing robustness to failures while simultaneously reducing wiring costs through decreased density (Yadav et al., 2025).

Despite recent developments, there are still limitations in connectomes. Notably, electrical synapses have not yet been characterized in Drosophila connectomes. Because the resolution of electron microscopy (EM) is insufficient to reliably identify electrical synapses, they are absent from current datasets (Scheffer et al., 2020; Zheng et al., 2018). Moreover, methodological differences across published connectomes may also introduce variability and affect particular features of the reconstructions.

Although it is now possible to reconstruct neural wiring at nanometer resolution, generating connectomes remains extremely costly, and their application to questions of individuality – or to understanding environmental influences on connectivity – is still in its infancy. Sample sizes remain very limited, complicating efforts to evaluate biological variability and individual differences. Finally, while most EM datasets are derived from animals reared at 25 °C – which facilitates comparison – this uniformity also constrains the scope of inference, excluding brains that developed under alternative environmental conditions.

3.5 Developmental plasticity in brain wiring

Brain development is highly plastic and emerges from a dynamic interplay between intrinsic developmental programs (e.g., genetic control of development), experience-dependent processes (e.g. spontaneous activity), and environmental influences such as nutrition and temperature (Boyce et al., 2020).

Experience-dependent processes (spontaneous or externally driven neuronal activity) play a central role in shaping neuronal structure and connectivity. Changes in activity levels in embryonic-born Drosophila olfactory projection neurons (Prieto-Godino et al., 2012) and in larval and adult motoneurons (Duch et al., 2008; Hartwig et al., 2008) modify dendritic size and complexity, thereby directly impacting synaptic connectivity. Likewise, manipulating neural activity in larval motoneurons alters presynaptic neuromuscular junction size and arbor complexity and changes presynaptic bouton morphology (Berke et al., 2013; Lnenicka et al., 2003; Mosca et al., 2005). At a finer scale, neurotransmission at newly formed synapses plays critical roles for subsequent circuit development (Bleckert et al., 2018; Bleckert & Wong, 2011). For example, GABAergic neurotransmission has been shown to affect cortical development through balancing excitation and inhibition in developing networks (Warm et al., 2022).

Beyond internal factors, environmental factors can also impact circuit connection and brain development. Nutrition has a big impact in circuit formation: for example, the variation in larval

diet that gives rise to queen versus worker female honey bees acts at least in part through DNA methylation changes in both the head and peripheral tissues (Kucharski et al., 2008; Shi et al., 2013; Wang et al., 2020). Additionally, a high conspecific density during development has been shown to increase the size of neuropiles in both flies and wasps (Groothuis & Smid, 2017; Heisenberg et al., 1995).

Together, these findings demonstrate that brain development is shaped by interacting intrinsic and environmental factors, with distinct features exhibiting varying levels of robustness and plasticity. Building on this, the following section focuses on temperature as a major environmental determinant of development.

3.6 The role of the environment: the case of temperature

Temperature is among the most influential environmental regulators of development, affecting biological processes from molecular kinetics to organismal function (Angilletta Jr., 2009; Hochachka & Somero, 2002). The development of ectotherms – organisms whose body temperature is largely determined by the surrounding environment – is particularly sensitive to thermal conditions.

The biological effects of temperature are usually explained by dependency of rates of biochemical reactions and biological processes on ambient temperature (Gillooly et al., 2001). Rates of biochemical reactions typically increase exponentially with temperature. This relationship is described by the Van't Hoff-Arrhenius law (Arrhenius, 1889). The relationship between metabolic rate and temperature has since been demonstrated in many ectothermic taxa, with metabolic rate typically increasing by a factor of 2–3 for every 10°C increase in temperature (known as the Q10 value) (Clarke, 2017; Havird et al., 2020; Seebacher et al., 2015).

Developmental temperature dictates the pace of growth in ectothermic animals (Angilletta et al., 2004; Gillooly et al., 2002). The duration of development depends on temperature, taking longer at lower temperatures (Gillooly et al., 2002). The Universal Temperature Dependance (UTD) model proposed that growth rate is linked to temperature through metabolism (Gillooly et al., 2001), being limited by its slowest reaction (rate limiting reaction), which determines the overall tempo of a process.

Developmental temperature is also a major driver of developmental plasticity. By modifying metabolic activity, temperature can shift the coordination and timing of developmental events

across tissues, effectively compressing or extending critical windows during which cells proliferate, differentiate, and form functional connections. For example, the developing zebrafish notochord is more sensitive to temperature increases than other tissues, most likely due to higher secretory activity and reliance on the unfolded protein response compared to other cell types (Dorrity et al., 2023).

These adjustments place increasing demands on the mechanisms that normally buffer development against perturbation—a phenomenon known as canalization, which promotes stable phenotypes despite environmental or genetic variation. Under substantial thermal stress, however, this buffering capacity can be weakened (decanalization), leading to greater variability in gene expression and, consequently, broader phenotypic diversity arising from the same genotype (Chen et al., 2015a). Consistent with this idea, developmental temperature has been shown to influence adult behavior across multiple modalities. In many ectotherms, individuals raised at higher-than-typical temperatures are smaller and display reduced locomotor performance (Sheridan & Bickford, 2011). Temperature during development also shapes exploration and thermal preference in frogs (Fan et al., 2021; Ohmer et al., 2023); locomotion and thermoregulation in lizards and skinks (De Jong et al., 2023); and learning and cognition in multiple reptile species (Amiel et al., 2014; Amiel & Shine, 2012). Comparable effects are observed in invertebrates: developmental temperature modulates mating and social behaviors in butterflies (Bear & Monteiro, 2013), as well as locomotion and foraging in flies (Manenti et al., 2021; Schou et al., 2017).

3.6.1 Effect of temperature on brain development

As behavior is driven by the brain, long-lasting behavioral changes imply that temperature has impacted also the brain (i.e. the specific neural circuits that control that behavior) – in its wiring or function. Brain development itself is strongly modulated by external factors, and temperature is among the most significant of these modulators (Cheung & Ma, 2015; Takesian & Hensch, 2013).

Cold-induced hibernation in ground squirrels triggers dendritic spine retraction in the hippocampus, illustrating that temperature shifts can rapidly reshape neural structures (Popov & Bocharova, 1992). Comparable patterns emerge during development across a range of ectotherms. In lizards, high temperatures (32.5 vs 26°C) upregulate genes involved in myelin

production and neurite outgrowth (Pallotta et al., 2017). In *Xenopus laevis,* motor neuron differentiation and activity is dependent on environmental temperature: exposure to warmer developmental temperatures reduce the differentiation and survival of motor neurons, while colder temperatures increase the number of spinal motor neurons, in part by increasing Ca^{2+} spike frequency in embryonic spinal cord neurons (Spencer et al., 2019).

Temperature can also affect brain structure, for example with elevated temperatures reducing the size of the brain in lizards (Amiel et al., 2014; Falibene et al., 2016). In honey bees (*Apis mellifera*), modest deviations in brood temperature during pupation impact MB microglomeruli numbers (Groh et al., 2004). In the beehive, brood temperature is normally tightly regulated through social thermoregulation. Controlled manipulations of brood temperature revealed that even small deviations from the colony-typical temperature during pupal development result in long-lasting alterations to the synaptic architecture of the mushroom body calyces. Bees reared at the natural brood temperature exhibit a higher density and more regular organization of synaptic complexes (microglomeruli), whereas individuals reared at slightly cooler temperatures show reduced synaptic density and disrupted MB organization (Groh et al., 2004). These structural changes have functional consequences, as altered brood temperature has been linked to impairments in odor learning performance (Jones et al., 2004; Tautz et al., 2003). These findings suggest that temperature can reshape neural structure during development, with potential consequences for sensory processing and behavior.

Despite the strong temperature dependence of cellular and synaptic processes, neural circuits can generate stable functional outputs across broad thermal ranges. In crustaceans, Marder and colleagues demonstrated that rhythmic motor patterns are preserved over large temperature shifts, even as the intrinsic membrane properties and synaptic interactions underlying these patterns change substantially (Marder, 2011; Tang et al., 2010).

A more detailed dissection of the effects of temperature in neural circuits and synapse formation has been done using the fruit fly, *Drosophila melanogaster. D. melanogaster* is a classic model organism in biology for more than a century, owing to its short generation time, easy husbandry, and the ability to screen large numbers of individuals in parallel (Hales et al., 2015). A major strength of the system is the availability of sophisticated molecular tools that allow proteins to be expressed in defined cell types with precise spatial and temporal control, for example, binary expression systems such as GAL4/UAS, LexA/LexAop and QF/QUAS (Caygill & Brand, 2016; Riabinina & Potter, 2016). These established toolkits enable targeted neuronal

manipulation, activity monitoring and neural circuit mapping, and they can be used across many genotypes and rearing conditions (Honda, 2022).

In Drosophila, flies developed at high temperatures present increased axonal arborization of neurons at the neuromuscular junction and mushroom body (Peng et al., 2007; Sigrist et al., 2003; Zhong & Wu, 2004). In Drosophila's larval neuromuscular junction (NMJ), the number of synaptic boutons increases when animals are reared at elevated temperatures (25–29°C or 32°C). This increase was interpreted not as a direct thermal effect on synaptogenesis, but rather as a consequence of increased neuronal activity at higher temperatures, leading to activity-dependent synaptic growth (Sigrist et al., 2003).

Temperature-dependent modulation of neuronal growth has also been observed in central brain circuits. In the mushroom body (MB), axonal arborization of Kenyon cells is enhanced when flies are reared at higher temperatures (30°C compared to 22°C) (Peng et al., 2007). Elevated temperature induces overgrowth of MB nerve terminals in the central nervous system (CNS), resembling the synaptic expansion seen at the peripheral NMJ (Zhong & Wu, 2004). Mechanistically, temperature was shown to act in a largely cell-autonomous manner by increasing neuronal excitability and spontaneous activity. This elevated activity is proposed to drive Ca^{2+} accumulation and activation of the cAMP signaling cascade, ultimately promoting activity-dependent changes in neuronal excitability and growth (Peng et al., 2007).

In Drosophila, photoreceptors of flies developed at lower temperatures presented increased axo-dendritic branching and higher synapse numbers (Kiral et al., 2021). Similar results were observed with dorsal cluster neurons. The difference in connectivity is proposed to arise from temperature-dependent filopodial dynamics at developing axon terminals. Filopodial dynamics are known to mediate synapse formation and partner choice (Kiral et al., 2020; Özel et al., 2019). Lower developmental temperatures slow filopodial dynamics but prolong the overall developmental period, likely extending filopodial lifetimes and the total time available for exploratory contacts, thereby increasing the probability of synapse formation. Conversely, higher temperatures accelerate dynamics but shorten the developmental window, reducing the total opportunity for filopodia to sample partners and stabilizing fewer synaptic contacts. (Kiral et al., 2021).

Collectively, these studies indicate that while individual neural components are sensitive to temperature, developmental temperature can nonetheless shape both robust and flexible features of brain architecture and function. In insects, temperature impacts brain development

during metamorphosis, a period marked by extensive neural growth and large-scale circuit reorganization. However, several key questions remain unresolved. Does developmental temperature influence the wiring of other neural circuits, such as the olfactory system? What are the functional consequences of temperature-dependent changes in circuit connectivity? Can alterations in circuit architecture account for observed differences in neural processing? And finally, why is there more connectivity?

In this dissertation, I use the fruit fly, *Drosophila melanogaster*, as a model to dissect how developmental temperature during pupa metamorphosis shapes the assembly and function of the olfactory system. To provide the necessary context for this work, the following section introduces the organization of Drosophila's olfactory system, focusing on the circuit architecture and its development.

3.7 Drosophila's olfactory system

D. melanogaster's olfactory system contains two sensory organs (antennae and maxillary palp) innervated by the olfactory receptor neurons (ORNs) (Bruyne et al., 1999). ORNs dendrites are housed in protrusions called sensilla, which are divided into three morphologically distinct categories: trichoid, coeloconic, and basiconic sensilla (Stocker, 1994). In those organs, odorants bind odorant receptors (ORs), expressed in the ORNs. Each ORN type expresses a single OR gene – which specifies the odor tuning of the neuron – in combination with the odorant co-receptor, Orco. The functional receptor consists of a heterodimeric complex of a specific odorant receptor protein and Orco (Benton et al., 2006; Neuhaus et al., 2005; Vosshall et al., 2000).

In the brain, ORNs innervate the antennal lobe (AL), the first odor processing center of the insect brain. The AL is organized into approximately 50 compartments, called glomeruli. ORNs expressing the same OR project to the same glomerulus in the antennal lobe (AL) (Vosshall et al., 2000). ORNs make excitatory synapses with secondary order neurons – projection neurons (PNs) (Fig. 5). Depending on how many glomeruli they innervate, PNs can be either uniglomerular (uPNs) or multiglomerular (mPNs) (Liang et al., 2013; Stocker et al., 1990; Strutz et al., 2014; Tanaka et al., 2004, 2012). Therefore, uPNs are postsynaptic to only one glomerulus (and therefore to only one ORN type) and mPNs are postsynaptic to many ORN types. Glomeruli are also interconnected by local neurons (LNs), which are mostly inhibitory, releasing the neurotransmitter γ-aminobutyric acid (GABA) (Chou et al., 2010).

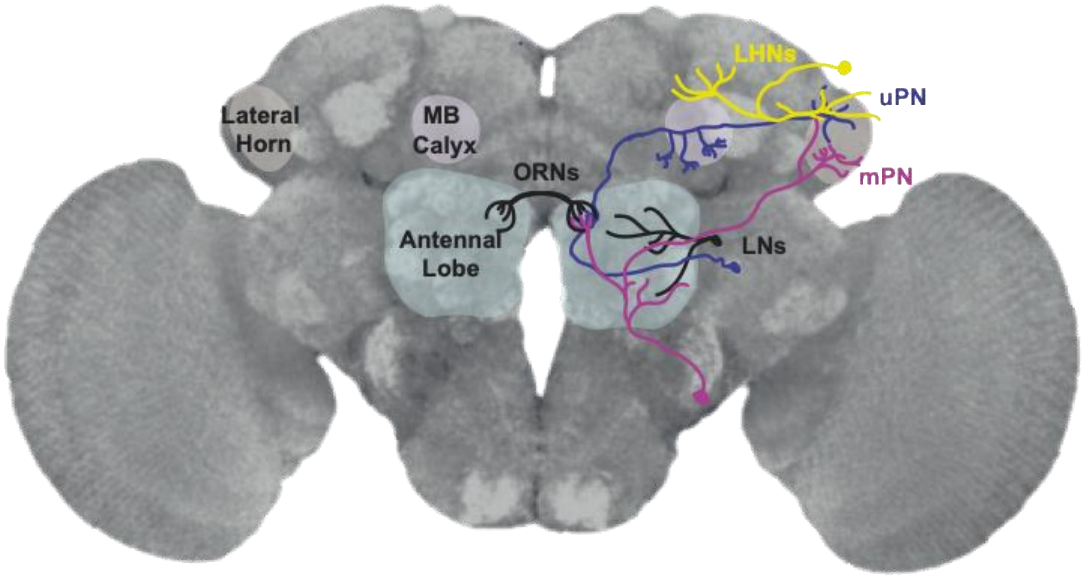

Figure 5. Schematics of the olfactory system in the *Drosophila melanogaster* brain. In grey: 3D projection of the nc82 stained female brain, from (Bogovic et al., 2020). Colored circles in the left half of the brain indicate main neuropiles related to the olfactory system: antennal lobe, mushroom body (MB) calyx and Lateral Horn. Neurons drawn represent the main neuron types in the olfactory system. Olfactory receptor neurons (ORNs) in black project to one glomerulus, innervating both ipsi- and contralateral antennal lobes. Local neurons (LNs) in black, innervate many glomeruli and are mostly inhibitory. Projection neurons are depicted separatly as uniglomerular projection neurons (uPN, in dark blue) and multiglomerular projection neurons (mPN, in dark pink). All those neurons have their cell bodies positioned surrounding the AL, which is a reflect of their neuroblast. uPNs project to the lateral horn via the medial antennal lobe tract (mALT) while mPNs use the medial lateral antennal lobe tract (mlALT). uPNs and mPNs connect to lateral horn neurons (LHNs), which are depicted in yellow. uPNs also connect to mushroom body intrinsic cells (Kenyon Cells) – not shown.

ORNs provide the major source of excitation to PNs. PNs are the main output from the AL, their combinatorial activity encodes odor identity and intensity, and this information is sent to higher brain areas. PNs can project to these higher brain areas through three antennal lobe tracts (ALT): the medial, medial lateral, and lateral ALT (Tanaka et al., 2012). PNs that project through the medial antennal lobe tract (mALT) are usually uniglomerular and excitatory, while the ones projecting via the medial lateral antennal lobe tract (mlALT) are mostly multiglomerular and inhibitory (Tanaka et al., 2012). Almost half of the glomeruli rely on only one uPN to transfer olfactory information to higher brain areas (Schlegel et al., 2021).

Projection neurons arise from different lineages, which determines by the cell body position in relation to the antennal lobe. PN numbers, identity, and birth sequence are consistent and predictable across and within individuals. PNs can originate from the antero-dorsal, lateral, or ventral lineages. The antero-dorsal PN lineage (adPN) generates PNs that are born in the embryo phase (17 neurons) and in the larval phase (22 neurons). The differentiation of the adPN line generates notch high and notch low siblings. The notch high is always apoptotic, and the notch low is always a PN (34 uPNs and 5 mPNs). The lateral PN lineage (lPN) are born during the larval phase only. The notch high sibling is a local interneuron (around 80 cells), with four different classes. The notch low is always a PN (~100, 48 types) englobing three olfactory PN classes but also auditory and subesophageal PN classes. The ventral PN lineage (vPNs) arise from the ventral neuroblast and, like the lPN lineage, produce a mixed lineage comprising both PNs and local interneurons (LNs) (Lai et al., 2008; Lin et al., 2012).

PNs are crucial for antennal lobe formation, determining glomeruli position (Jefferis et al., 2004; Sakuma et al., 2014). Coarse PN dendrite positioning is controlled by a Sema-2a/2b to Sema-1a gradient, whereas Capricious and Tartan act as glomerulus-specific recognition molecules (Hong et al., 2009; Sakuma et al., 2014; Sweeney et al., 2011). Furthermore, precise ORN-PN partner matching is mediated by Teneurins and Dscam (Hong et al., 2012; Sakuma et al., 2014; Zhu et al., 2006).

Projection neurons (PNs) relay glomerulus-specific odor information from the antennal lobe to two main neuropiles: the mushroom body – involved in learning and memory (Heisenberg et al., 1985) – and the lateral horn (LH) – which supports innate behavior (Jefferis et al., 2001; Marin et al., 2002; Wong et al., 2002).

In the mushroom body, PNs synapse onto its intrinsic neurons, the Kenyon cells (KCs) (Couto et al., 2005). Each KC samples input from a small, random subset of PNs, such that partner choice is combinatorial (Caron et al., 2013). This random connectivity allows an odor stimulus to be projected into an even higher-dimensional space (Luo et al., 2010) such that more precise associations can be established between an odor stimulus and a reinforcement or a context. This architecture positions the mushroom body as a core neuropil for associative odor learning and state-dependent modulation of odor-guided behavior (Aso et al., 2014; Devineni & Scaplen, 2021).

By contrast the lateral horn (LH) is associated with innate olfactory behavior (de Belle & Heisenberg, 1994; Heimbeck et al., 2001), as attraction to food-related cues, avoidance of

harmful volatiles, and pheromone-evoked courtship or aggression (Dolan et al., 2019; Frechter et al., 2019; Strutz et al., 2014).

Consistent with the idea that 'hardwired' neural pathways underly these innate behaviors, the axonal trajectory of each PN type is highly stereotyped across individuals, targeting specific subregions of the LH (Jefferis et al., 2007; Marin et al., 2002; Wong et al., 2002). On average, a single lateral horn neuron (LHN) receives excitatory input from ~ 6-7 PNs (Bates et al., 2020; Jeanne et al., 2018). In general, LHNs receive input from sparse and stereotyped combinations of glomeruli that are co-activated by particular odors and certain combinations of glomeruli seem to be over-represented (Fişek & Wilson, 2014; Jeanne et al., 2018; Luo et al., 2010; Schlegel et al., 2021). However, it is still not clear weather PN-LHNs across individuals is random – as in the PN-KCs in the MB –, stereotypic – in line with the anatomical projections –, or if it PN-LHNs connections lays halfway.

The LH circuit anatomical and physiological characterization are not as advanced as other neuropiles due to lack of neuron-specific and sparce transgenic lines. This has been overcome recently with the creation of over 2400 lines that target 89 different LHN cell types (Dolan et al., 2019). Those allowed substantial progress in the field, as the division of LHNs into LH local neurons (LHLNs) and LH output neurons (LHONs) (Dolan et al., 2019; Frechter et al., 2019), and cell-type specific circuit mapping.

Those tools allowed studies that shed light into PN-LHN connections, which exhibit higher variability and complexity than previously thought. Using the presynaptic labeling tool BAcTrace, Cachero and colleagues revealed substantial variability in synaptic connectivity across and within individuals. The lateral horn neuron AV1a1 receives input from different sets of glomeruli across animals and even between hemispheres, indicating that projection neurons do not form strictly stereotyped synaptic partnerships with LH neurons (Cachero et al., 2020). This observation raises the possibility that PN–LHN connectivity is not hard-wired, but instead variable. Whether such variability contributes to evolutionary fitness, functional flexibility, or reflects developmental noise remains an open and testable question.

3.8 Aims of this dissertation

Despite extensive work on how developmental temperature shapes neuronal growth and connectivity, it remains unclear how these effects influence the wiring and function of olfactory

circuits in Drosophila. In particular, how temperature-dependent alterations in neuronal growth translate into changes in circuit wiring and function remains poorly understood.

This work examines the effects of temperature on a defined developmental window in Drosophila melanogaster: the pupal stage. Because the pupa is a closed, non-feeding, and immobile system, temperature manipulations can be applied with precise temporal control. This approach allows us to probe fundamental principles of developmental organization in ectotherms, revealing how nervous systems are shaped by environmental temperatures.

In specific, I aim to address four central questions: (1) how developmental temperature influences ORN and PN wiring along the olfactory pathway; (2) whether these wiring changes impact olfactory processing; (3) how changes in wiring and biophysical properties due to temperature can be mechanistically linked; and (4) which developmental and molecular pathways, including transcriptional and hormonal regulation, mediate these temperature effects on neural circuits.

4 Materials and Methods

4.1 Experimental model and fly husbandry

To investigate how developmental temperature affects olfactory circuit assembly and function, I used *Drosophila melanogaster* as a model organism. Flies were raised on standard molasses-based food at 65% relative humidity under a 12:12 hour light-dark cycle. All flies were kept at 25°C, except during pupa development. Flies were placed at different temperatures (12°, 18°, 25°, and 31°C depending on the experiment) between the third-instar larva stage (L3) and the end of metamorphosis. Since the length of pupa stage varies with temperature, the end of metamorphosis (therefore adult eclosion) was defined as 100% of development. Fly genotypes are described below (Table 1).

Table 1. Fly strains used in this work, separated by used name, full genotype and figure in which it appears.

Name	Genotype	Figure
Or42b > trans-Tango	*w+,UAS-myrGFP.QUAS-mtdTomato-3xHA; trans-Tango / CyO ; Or42b-Gal4 / +*	Fig. 6, Fig. 10D, Fig. 11
Or42b > trans-Tango QUAS-GCaMP6s	*w+ 10x QUAS-GCaMP6s; trans-Tango / UAS-CsChrimson; Or42b-Gal4 / +*	Fig. 7
Or42b > Brp^{Short} GFP	*;+;UAS-BRP D3::GFP/Or42b-Gal4*	Fig. 8
Or42b > mito-GFP	*+; UAS-mito-HA-GFP; Or42b-Gal4*	Fig. 9
Or7a > trans-Tango	*w+, UAS-myrGFP.QUAS-mtdTomato-3xHA; trans-Tango / Or7a-Gal4*	Fig. 10E
Or10a > trans-Tango	*w+, UAS-myrGFP.QUAS-mtdTomato-3xHA; trans-Tango / Or10a-Gal4*	Fig. 10F
isoD1	*w+; ; (isoD1)*	Fig. 12, Fig. 21-22, Fig. 24-31
GH146 > GCaMP6f	*w+; UAS-GCaMP6f/ GH146-Gal4*	Fig. 13, Fig. 20
Orco > GCaMP6f	*w+; UAS-GCamp6f / +; orco-Gal4 / +*	Fig. 13
MZ699 > GCaMP8f	*w+; UAS-GCaMP8f/+; MZ699-Gal4/+*	Fig. 14

PD2a1 > *retro-Tango*	*y w+ QUAS-mtdTomato-3xHA; retro-Tango / + ; 10xUAS-retro-Tango/ R48F03-p65AD; R37G11-Gal4DBD / +*	Fig. 15
PD2a1/b1 > *BacTrace*	*w+, QUAS-mtdTomato,UAS-CD2/+; Syb::GFP, VT033006-LexAp65, LexAop-minQf-noV5-minSNAP25-HIVNES-Syntaxin/R48F03-p65AD; UASI-B3R.PEST,B3RT-B2B3RT-HBMBoNTa2xGFPnb, QUAS-mtdTomato::HA / R37G11-Gal4DBD*	Fig. 16B,C
AD1c1 > *BacTrace*	*w+, QUAS-mtdTomato,UAS-CD2/+; Syb::GFP, VT033006-LexAp65, LexAop-minQf-noV5-minSNAP25-HIVNES-Syntaxin/R55C09-GAL4; UASI-B3R.PEST,B3RT-B2B3RT-HBMBoNTa2xGFPnb, QUAS-mtdTomato::HA / +*	Fig. 16E
AV4a1 > *BacTrace*	*w+, QUAS-mtdTomato,UAS-CD2/+; Syb::GFP, VT033006-LexAp65, LexAop-minQf-noV5-minSNAP25-HIVNES-Syntaxin/ R34C08-p65.AD; UASI-B3R.PEST,B3RT-B2B3RT-HBMBoNTa2xGFPnb, QUAS-mtdTomato::HA / R22C12-GAL4DBD}*	Fig. 16D
PD2a1/b1> *GCaMP6f*	*w+; UAS-GCaMP6f/ R48F03-p65AD ; R37G11-Gal4DBD / +*	Fig. 17

4.2 Immunohistochemistry and confocal imaging

Female flies (9 to 11 days after eclosion, unless stated otherwise) were anesthetized with ice and briefly immersed in 70% ethanol. Flies were dissected on cold phosphate-buffered saline (PBS) for no longer than 20 minutes and fixated for 50 minutes in 2% paraformaldehyde (Polysciences, diluted in PBS) while rotating at room temperature. Pupa brains were fixated similarly in 4% paraformaldehyde. All subsequent incubations and washes were performed under rotation and protected from light. Brains were washed three times in PBT (PBS with 0.5% Triton X-100, Roth) for 15 minutes and then blocked for 1 hour in 5% normal goat serum (Thermo Fisher Scientific, in 0.3% PBT). Samples were incubated in a primary anti-body mixture (chicken anti-GFP 1:1000 and mouse anti-nc82 1:25 for all samples, rabbit anti-DsRed 1:500 when indicated) for 48 hours at 4°C, then washed in PBT (3 washes of 15 minutes) and incubated in secondary antibody mix (goat anti- chicken Alexa Fluor 488 and donkey anti-

mouse Alexa Fluor 647 for all samples, donkey anti-rabbit Alexa Fluor 568 when indicated, all at 1:200) for 48 hours at 4°C. Last, brains were washed three times in PBT and mounted in VectaShield (Biozol).

Brains were imaged using a Leica SP8 confocal microscope with 20×, 40×, or 63× objectives, depending on the experiment. Images for segmentation and quantification were acquired with 63x objectives. For cell body counting, acquired images were annotated manually by Pascal Züfle using Fiji's cell counter plugin. Cell body numbers were classified according to the position around the AL: dorsal, lateral, or ventrolateral (including both ventrolateral and ventral clusters). **Pascal Züfle** performed either the dissection, staining or image acquisition for almost all experiments.

4.2.1 Image segmentation and quantification

4.2.1.1 Brp, nc82 and mito-GFP analysis

For both Brp^{Short}, nc82 and mito-GFP quantification across temperatures, the same process was employed. Confocal images of individual DM1 glomeruli were processed using a custom code in python, with the package pyclesperanto (https://github.com/clEsperanto). Images contained a Brp^{Short} and nc82 channel. Both channels were pre-processed using Gaussian Blur ($\sigma = 1.0$) and a top-hat box filter (kernel = 20 x 20 x 1). DM1-ORNs mask were generated from the Brp^{Short} channel, by applying Voronoi Otsu Labeling and then merging the touching labels. For the whole DM1 glomerulus mask, the DM1-ORN volume was closed using the function closing labels. Single nc82 puncta were labeled by Voronoi Otsu Labeling and restricted to the DM1 glomerulus mask using binary filter. The volume and mean fluorescence intensity of labeled regions were quantified using the *statistics_of_labeled_pixels* function in pyclesperanto.

4.2.1.2 Retro-Tango quantification

Retro-Tango confocal stacks were processed using a custom python script. For each AL, a manual mask was done to delimit the region of interest and crop the original images. Presynaptic neurons were preprocessed by applying Gaussian Blur ($\sigma = 1.0$) followed by top hat box (kernel = 10 x 10 x 1). Presynaptic neurons were segmented using Gauss-Otsu thresholding. Volumes of labeled regions were quantified using the *statistics_of_labeled_pixels* function in pyclesperanto

4.3 Behavioral experiments

4.3.1 Spherical treadmill.

Experiments were conducted at 32°C in a closed custom arena by **Näncy Benjamin with assistance of Constantin Müller**. The spherical treadmill consisted of a 15mm diameter polyurethane foam sphere (FR-7120 foam, General Plastics) floating on an air-column. The sphere was coated with two layers of classic wood glue (Ponal, 25% in water) and then a random non-uniform pattern was drawn using two layers of acrylic black paint (Black 3.0, Culture Hustle). All coats of paint were allowed to dry overnight. The odor delivery system was similar to the one described above for in vivo calcium imaging experiments, but with a differing airflow rate controlled by Alicat Scientific MFCs. Continuous clean airflow was 90 mL/min and both the odor and balancer airflows were 10 mL/min. Videos were acquired with a XIMEA xiQ video camera, placed 10cm from the treadmill. The treadmill ball was illuminated by a panel of 940nm LEDs (Solarox) and an extra LED on the air-column was visible in the video and turned on simultaneously to the odor stimulus to trigger the data.

4.3.1.1 Experimental protocol

For experiments, 9-10 days old female flies were cold anesthetized and secured to a needle at their thorax on the dorsal side using a UV-hardening glue (Bondic) and positioned on the sphere with the help of a 3D micromanipulator. Before recording, flies were acclimatized to walking on the sphere for 10-15 minutes with no stimulus presented. Subsequently, video recording and the odor stimulation were started. Videos were acquired using the XIMEA CamTool software (exposure: 10,725ms, gain: 2,6Db, framerate: 80fps). The odor stimulation was controlled through MATLAB by an Arduino UNO Rev3 and consisted of at least 19 repetitions of 5s long odor stimuli and 20s-long interval without odor.

4.3.1.2 Video processing and analysis

Fly moving speed was calculated a posteriori from the video recordings using the open-source software library FicTrac (Moore et al., 2014) which provided direction and walking speed of the animal for each frame in the video. The video recordings were also analyzed in MATLAB to extract the stimulus trigger from the LED placed in the field of view. Finally, the output data from FicTrac and the timepoints obtained from the video were analyzed in MATLAB so that

the moving speed during and outside odor presentation could be quantified. Flies that had a basal walking speed lower than 2mm/s were discarded.

4.3.2 Free-walking assay.

A free walking area was contained in a thermally controlled black box (100x45cmx45cm) shielded from room light, fully closed with a frontal door, and equipped with a heating system and thermostat (H-TRONIC GmbH, Product ID: 1114430). The box was heated up by an air stream created by a fan and homogeneously distributed by a diffuser. A blue LED stripe (470nm, Paulmann Licht GmbH, Product ID: 78979) was positioned around the walking arena to ensure stable illumination during experiments. Videos were recorded with a Basler Camera (Basler acA2040-90um) placed on the ceiling of the box and equipped with f12mm lens (Basler C10-1214-2M-S), using Pylon viewer (64-Bit, 6.3.0.10295). The walking arena had 40.2 cm diameter and 2 cm height and was composed of four stacked layers and three overlapping plates (glass or plexiglass). The bottom layer contained six holes, arranged at the corners of a hexagon, where 1.5mL glass vials (Fisherbrand 11565874) containing the test odor could be screwed in. On top of this, a Teflon® coated porous sheet (FIBERFLON GmbH & Co. KG, Product ID: 408.07 P) provides a walking surface for the flies hiding the odor location. The mid arena layer consists in a sloped (at 11°, 5 cm length) ring that defines the accessible walking area. To seal the walking arena, we used a glass plate coated with Sigmacote® (Sigma-Aldrich Co.) to prevent fly walking upside-down. This behavioral setup was built by the workshop of the Biology Department at Johannes Gutenberg Universität Mainz.

4.3.2.1 Experimental protocol

Female flies developed at 18°C or 25°C, 5-7 days post eclosion were tested by **Giovanni D'Uva, Christian Daniel** with assistance of **Polina Krasnova**. One hour before the experiment, flies were transferred into a vial with only a small piece of filter paper soaked in water and kept at room temperature. For experiments carried at 32°C, the fly vials were incubated for 15 minutes in a 32°C water bath. To create an odor gradient inside the arena, five minutes before the start of each experiment, a 1.5mL glass vial containing 1mL of test odor was placed in one of the six possible odor positions in the behavioral setup. For each trial, a fresh odor vial was used, and the position was pseudo-randomized. Each trial consisted of 10-15 female flies exposed to either apple cider vinegar (10^{-2} in MilliQ water), 2-butanone (10^{-2} in mineral oil), or tested with empty vials. Flies were gently pushed inside the arena using a custom fly transfer tube and the

recording was immediately started. All experimental videos were recorded at 20 fps for 15 minutes and saved in mp4 format. At the end of each trial, the flies were removed and discarded. The initial condition was restored by removing the odor vial and the cover glass plate, replacing the Teflon® sheet with a clean one, and letting the whole system ventilate for 5 minutes.

4.3.2.2 Video processing and analysis

All required steps to pre-process the raw videos were done using the Python 3.9.12 distribution ANACONDA (Version 4.13.0), by **Giovanni D'Uva and Christian Daniel.** Scripts were written using Virtual Studio Code (Version 1.81.1). Recorded mp4 videos were processed and the video was tracked with the software TRex (Version 1.1.8.3) (Tristan Walter & Iain D Couzin, 2021). The output files were analyzed using custom Python and MATLAB scripts. A threshold of 5cm was chosen to determine if the fly had located the odor source, variations of this threshold do not alter the results. Odor occupancy was calculated as the integral under the curve in the first 7 minutes, being 1 if all flies spend 100% of the time at the odor.

4.4 *In vivo* calcium imaging

Flies were developed at either 18°C or 25°C during pupa stage. At 9-11 days post eclosion, flies were anesthetized on ice and mounted on a custom holder using UV-cured glue (Bondic). Saline solution (5mM Hepes, 130 mM NaCl, 5mM KCl, 2 mM MgCl2, 2mM CaCl2, 36 mM Saccharose – pH 7.3) was added. The cuticle covering the fly's head, as well as obstructing trachea, were removed. Functional imaging was performed using an Investigator two-photon microscope (Bruker) coupled to a tunable laser (Spectraphysics Insight DS+) with a 25X/1.1 water-immersion objective (Nikon). The laser was tuned to 920 nm, with power kept below 20 mW at the specimen plane. Emitted light passed through a SP680 short-pass filter, a 560 lpxr dichroic filter and a 525/70 filter. PMT gain was set to 850 V. The microscope was controlled with the PrairieView (5.4) software. **Ana Sofia de Castro Brandão** collected 2photon Imaging data for all *GH146*-Gal4 > UAS-GCamp6s experiments, and helped in the collection of data for *Orco*-Gal4 > UAS-GCamp6s experiments.

4.4.1 Optogenetics.

For optogenetic activation, light from a 625nm LED was directed using an optic fiber to the fly's antenna. The LED was synchronized with the imaging software via an Arduino interface,

enabling simultaneous image acquisition and light stimulation. The light stimulus protocol consisted of 5s series of light pulses, presented 5 times with intervals of 30s. Stimulus intensity was measured at the fly position with this protocol.

4.4.2 Odor delivery.

Flies were exposed to a continuous clean air airflow (1L/min), in which either an odor stream (100mL/min) or a clean balancer airflow (100 mL/min) was redirected through a solenoid valve (LEE), so that the final airflow reaching the fly was 1.1L/min. For creating the gas dilutions, four mass flow controllers were used (Analyt-MTC) and controlled using a custom MATLAB (MathWorks) script and an Arduino board. Odors were prepared as a 5mL 10^{-2} volumetric dilution in 20mL glass vials (2-butanone and benzaldehyde in mineral oil, apple cider vinegar in MiliQ Water). The final volumetric gas dilution used was 10^{-5}. Odor stimulation consisted of three repetitions of a 5 seconds, with 30 seconds intervals in between.

4.5 Connectome analysis

The Hemibrain dataset (hemibrain:v.1.2.1) was used for connectome analysis. For the DM1 glomerulus, we considered all synapses from the Or42b-ORNs of the left and right antenna within the glomerulus of the right hemisphere, which were selected by clustering the synapses based on their 3D coordinates. The analysis was restricted to synapses of the right hemisphere, as postsynaptic partners are fully reconstructed only on this side. We calculated the number of synapses between each individual ORN and each individual post-synaptic neuron. Connections with less than 3 synapses from a single ORN were discarded. Moreover, postsynaptic neurons that received less than 10 total synapses were discarded. The number of synapses was normalized to the total number for this ORN type. Postsynaptic neurons were sorted based on the number of synaptic inputs they receive. The same procedure was used for DL1 and DL5. The percentages of LNs and mPNs are lower bounds, as calculated from the available annotations.

4.6 Ecdysteroids quantification

For ecdysteroids quantification, all flies (isoD1) where kept at 25°C until white pre pupae (P0). Pupa at P0 were identified, added to a clean food vial and then then transferred to the

experimental temperature (12°C, 18°C, 25°C or 31°C) until its respective developmental time (Table 2). Six developmental percentages were selected – 20, 35, 50, 65, 80 and 95% of development, in each of the four tested temperatures. Developmental percentage was calculated as having the eclosion time as 100% and the P0 collection as 0%. Each sample was collected in six replicates (each with n = 10 animals). At the correct developmental time, pupa were flash frozen using liquid nitrogen and stored at -80°C until until extraction.

Table 2. Summary of duration of development percentages across temperatures. Separated by different temperatures, considering the correspondent pupa development (0% being white prepupa, and 100% eclosion). Time after P0 indicate how many ours each sample was kept at the correspondent temperature until being processed.

Developmental temperature	**Pupa development**	**Time after P0 (hours)**
12°C	20%	103
12°C	35%	181
12°C	50%	258
12°C	65%	335
12°C	80%	413
12°C	95%	490
18°C	20%	43
18°C	35%	76
18°C	50%	108
18°C	65%	140
18°C	80%	173
18°C	95%	205
25°C	20%	19
25°C	35%	34
25°C	50%	48
25°C	65%	62
25°C	80%	77
25°C	95%	91
31°C	20%	17
31°C	35%	29
31°C	50%	42
31°C	65%	55
31°C	80%	67
31°C	95%	80

Tissue extraction and LCMS-MS was performed using an adapted protocol from (Lavrynenko et al., 2015), as following. Frozen pupae were homogenized with a pestle in 200 µL of cold 100% methanol containing 0.5 pmol Muristerone A as an internal standard. The pestle was rinsed with additional 800 µL of the solution. Samples were vortexed and kept rotating overnight at 4°C. For a first methanol extraction, samples were centrifuged (20xg for 15 minutes at 4°C), and the supernatant was collected. The pellet was resuspended in 100% methanol, vortexed and kept rotating for 40 minutes. Samples were centrifuged and resuspended two more times, with all supernatants combined into a glass vial and dried using liquid nitrogen. For a hexane/methanol extraction, samples were resuspended in 3mL of methanol, vortexed, and 3mL of hexane was added. After 20 minutes the lower fraction was transferred into a glass vial. This process was repeated one more time and the lower fractions combined. The solvent was evaporated under liquid nitrogen. Finally, ecdysteroids were purified and concentrated from the extract using a solid-phase extraction using a 96-wells C18 endcapped Chromabond column (Macherey Nagel. #738011.100M). The columns were pre-washed using 100% methanol followed by 70% methanol. Samples were resuspended in 70% methanol and added to the columns. The flowthrough was collected and dried using liquid nitrogen. Samples were then resuspended in 30µL of methanol 70% and kept at -20°C until further processing.

Targeted metabolite analysis was done with assistance of **Dr. Martin Schäfer** (Xu Lab, iomE) by Liquid Chromatography Tandem Mass-Spectrometry (LC-MS/MS). Before injection, all samples were centrifuged at 4500 rpm at 4°C for 15 minutes. Mass spectrometry was performed in a triple quadrupole mass spectrometer LCMS-8060 (Shimadzu) for all samples. Peaks from all molecules were integrated with LabSolution Insight Version 4.0 SP6 (Shimadzu). The amount of 20-hydroxyecdysone and Makisterone A were calculated by normalizing the area under the curve (AUC) of the selected fragment ion (Table 3) by the AUC of the standard's selected fragment ion, Muristerone A.

Table 3. Molecules quantified by LC-MS/MS, with precursor and fragment ion. Bold indicates the quantified fragment ion.

Molecule	Precursor ion, *m/z*	Fragment ion, *m/z*
20-hydroxyecdysone	481.32	**371.29**
		445.20
		165.30
		427.15
Makisterone A	495.33	**371.10**
		357.05
		179.15
		441.30
Muristerone A	497.31	**425.25**
		443.10
		279.10
		309.20

4.7 RT-qPCR assays

4.7.1 Total RNA extraction

Total RNA was extracted using TRIzol (Invitrogen) following the manufacture's recommendations. Each sample consisted of 10 pupae developed at 18°C or 25°C at five developmental percentages: 25, 30, 40, 58 and 85% of pupa development. Pupa were collected, kept at the correct temperature until the correct time. The tissue was then macerated using a pestle and 500 µL of TRIzol. Samples were vortexed for 1 minute and kept at -80°C until all samples were ready for the next step.

Samples were vortexed and centrifuged (12,000 × g, 10 min, 4 °C), followed by addition of 100 µL chloroform:isoamyl alcohol (24:1). Samples were again vortexed and left for 5 minutes at room temperature to reach phase separation. The homogenate was again centrifuged for 10

minutes to separate organic and aqueous phases. The upper aquous phase was transferred into a new tube for DNAse treatment. DNAse treatment was done with DNAse and RNAse inhibitors and incubated at 37°C for 30. RNA clean up was performed using RNeasy MinElute Cleanup Kit (Qiagen) following manufactor instructions.

4.7.2 cDNA synthesis

For cDNA synthesis, 200ng of RNA of each sample were mixed to 50 µM Oligo(dT) 20 primer and 10 mM dNTP mix and incubated for 5 minutes at 65°C. In addition cDNA synthesis mix was added (RT buffer, 25 mM MgCl2, 0.1 M DTT, 40U RNAse Out and 200U SuperScript III RT). The mix was incubated for 50°C for 50 minutes, and the reaction was terminated at 85°C for 5 minutes, cooled in ice. Afterwards, 1µL of RNase H was added and incubated for 20 minutes at 37°C.

4.7.3 RT-qPCR

Gene expression was quantified by real-time quantitative PCR (RT-qPCR). Primers were designed based on the genes sequence (FlyBase release B2023_05) and aligned against *D. melanogaster* genome to verify there was no overlap with other regions. Primers were designed by **Giovanni D'Uva** (except *Rpl15*, which was kindly provided by **Simone Renner**) (Table 4). As an endogenous control, the gene for ribosomal-like protein 15 (*Rpl15*) were used.

qPCR reactions were done simultaneously for target genes and housekeeping genes (*Rpl15*) in a 384-well plate, with n = 3 per group and technical triplicates. For each reaction consisted of 10µL ORA TM qPCR Mix, 200 nM of each primer pair, 20ng of cDNA template and MiliQ water to complete 20µL. The PCR reaction was carried out in a QuantStudio 5 Real-Time PCR System (Thermo) provided by the IMB Equipment Core Facility as follows: initial denaturation 95°C for 2 minutes, denaturation 40 cycles (95°C for 5 seconds) and annealing / extension 40 cycles (60°C for 30 seconds).

Cycle threshold (CT) values were determined automatically by QuantStudio 5 software as the first cycle showing a significant increase in fluorescence. CT values were used to calculate target mRNA expression in relation to the housekeeping gene (*Rpl15*). CT values were used for quantification according to the Livak and Schmittgen method (Livak & Schmittgen, 2001),

determined by $2^{-\Delta\Delta CT}$, where CT = cycle threshold, ΔCT = target gene CT – housekeeping gene (*Rpl15*) CT, ΔΔCT = ΔCT of sample – ΔCT of normalizing sample.

Table 4. Primer sequence of the evaluated genes, containing Forward and Reverse strands for each gene.

Gene	Sense	Primer	Fragment (bp)
Blimp-1	Forward	GCAGTCGCAGTCGAAGTCGC	315
	Reverse	AGCGCGCCTTATTCTTATCATTGGG	
Eip71CD	Forward	ACCACGCCCATCAAGAGGCA	301
	Reverse	TAAACTGCTCGATGCCGCCG	
Eip75B	Forward	TGCGATCCAGAACGGAGCCA	300
	Reverse	TTCTCGGTGTGCAGGGTGCT	
Hr3	Forward	CGGCGTGCATTACGGAGTGA	316
	Reverse	CGAGGGCGTCTGTGTGTCGTA	
Nrx-1	Forward	CGATGTGCCCTGCGATCACG	310
	Reverse	GGCTGGCGGGTGCGAAAATA	
RhoGAP100F	Forward	CCGCAGTCCGAGCAGTTGGA	290
	Reverse	GCGAGGCCAACGTTTCCAGT	
Liprin-alpha	Forward	TGGCCGAGCAGGAATGGGAA	301
	Reverse	CCGCGAGCCAGCAGGTTTAC	
Brp	Forward	CGGTCCCCAACAGGCACAG	314
	Reverse	CGCCCCTGACCTTCTCCAACT	
cac	Forward	CCGAGGTGAAAGGCGGTTCG	306
	Reverse	CGTTCCAATCTTCGCCAGTGAGG	
Eip93F	Forward	CTTGAACTCTACAAGCTGCTGACCC	305
	Reverse	ACGGACTTCACATCGCCGCTAA	
Ftz-f1	Forward	GCACGGGCGGTGTTATAGCC	311
	Reverse	GCCAGAATCGAAGCACAATTTCGAG	
Eip63F	Forward	GGGCATAAACGTGAGTGACGAACT	296
	Reverse	GCTCGTTCAAGGGCTCCCCA	
Rpl15	Forward	AGGATGCACTTATGGCAAGC	137
	Reverse	GCGCAATCCAATACGAGTTC	

4.8 Bulk RNA-seq

For bulk transcriptome during pupa development, flies were collected as described for ecdysteroids quantification. Allflies (isoD1) where kept at 25°C until white pre pupae (P0). Pupa at P0 were identified, added to a clean food vial and then then transferred to the experimental temperature (12°C, 18°C, 25°C or 31°C) until its respective developmental time (Table 2). Six developmental percentages were selected – 20, 35, 50, 65, 80 and 95% of development, in each of the four tested temperatures. Developmental percentage was calculated

as having the eclosion time as 100% and the P0 collection as 0%. Flies at L3 and P0 stage – at 25°C, before changing temperature – were also added. Each sample was collected in triplicates (each with n = 3 animals). At the correct developmental time, pupa were flash frozen using liquid nitrogen and stored at -80°C until processing.

RNA extraction and sequencing were performed by Novogene following their *in house* protocol. Preprocessing was done by **Dr. Federico Marini** (IMBEI), including read abundance quantification – performed using Salmon (Patro et al., 2017).

5 Results

In the following sections, I first present results describing how developmental temperature affects ORN connectivity patterns within the AL (Section 5.1). I then examine the functional consequences of these connectivity changes on olfactory processing within and downstream of the AL (Section 5.2). Next, I introduce a model that integrates these findings with biophysical principles to elucidate how temperature-dependent alterations in connectivity could arise during development (Section 5.3). Finally, I explore the developmental and molecular mechanisms underlying these effects, focusing on transcriptional changes revealed by RNA-seq and hormonal regulation assessed through analytical chemistry (Section 5.4).

5.1 Developmental temperature shapes ORNs connectivity and synaptic architecture

Developmental temperature impacts synaptic connectivity in *Drosophila melanogaster*, as demonstrated by Kiral et al., 2021. In this study, lower developmental temperatures increased the number of postsynaptic partners of photoreceptors and dorsal cluster neurons, and also affected dendritic development of descending neurons and motor neurons (Kiral et al., 2021). The inverse was found at flies developed at higher temperatures.

These findings raise a central question addressed in this present work: whether inverse scaling of connectivity with temperature represents a general principle across sensory modalities and circuit layers, or whether it manifests in circuit-specific manner. In this section, I examine if a similar scaling occurs in the first layer of the olfactory system and assess its impact on the circuits synaptic architecture.

5.1.1 ORN connectivity scales across developmental temperatures

To determine the effect of developmental temperature in synaptic connectivity in the olfactory system, I used trans-Tango – a transsynaptic tracing tool (Talay et al., 2017). This tool enables visualization of downstream neurons by expressing a reporter in postsynaptic cells and requires only a Gal4 driver to targets the presynaptic population.

I first evaluated postsynaptic partners of olfactory receptor neurons (ORNs) expressing the *Or42b* odorant receptor, which innervate the glomerulus DM1. In these experiments (*Or42b*-Gal4 > UAS-trans-Tango), presynaptic neurons expressed the trans-Tango components together with GFP, while postsynaptic partner neurons were labeled with dsRed (Fig. 6A' – See Methods, Section 4.1 for all genotypes used).

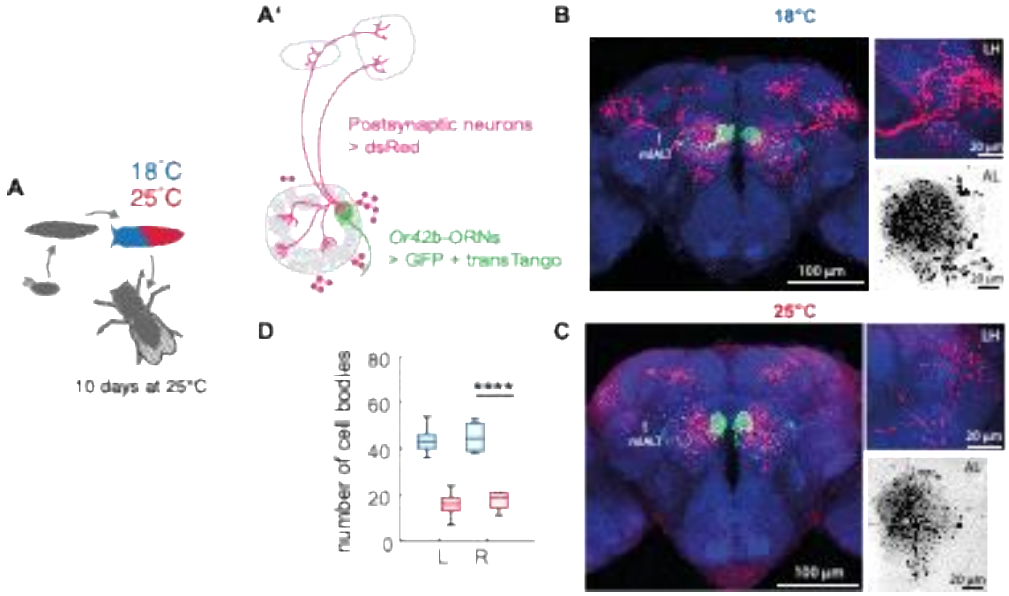

Figure 6. Development at 18°C increases the number of postsynaptic partners of DM1-ORNs detected by trans-Tango. (A) Schematic of temperature manipulation. Flies were kept during pupa stage at either 18 or 25°C. After eclosion, flies were kept at 25°C for 10 days before experiments. (A') Schematic of the trans-Tango system showing presynaptic *Or42b*-ORNs and post-synaptic partners. dsRed is expressed the membrane of postsynaptic neurons, allowing quantification of labeled cell bodies surrounding the antennal lobe (AL). (B-C) Representative brains from flies *Or42b*-Gal4 > UAS-trans-Tango developed at 18°C (B) and 25°C (C), stained for GFP (green, *Or42b*-Gal4), dsRed (red, postsynaptic neurons), and nc82 (blue, stains the presynaptic protein Bruchpilot). Arrows indicate the medial lateral antennal lobe tract (mlALT). Side panels show higher magnification of the LH and AL, where postsynaptic partners innervate. (D) Quantification of dsRed-positive cell bodies for the left (L) and right (R) ALs of flies developed at 18°C (blue) and 25°C (red). Flies reared at 18°C displayed more postsynaptic partners ($p < 10^{-7}$, Kruskal-Wallis test, n = 10 per group).

To isolate the developmental effects of temperature, manipulations were restricted to the pupal stage (18°C or 25°C, Fig. 6A), during which the fly does not feed or exhibit behavioral activity. In all other stages, including the 10 days between eclosion and dissection, flies were maintained

at the standard rearing temperature of 25°C. Data collection and analysis was performed by Pascal Züfle. This approach allowed us to visualize temperature-dependent differences in the number and distribution of postsynaptic partners in the DM1 glomerulus.

Fly brains were dissected and stained using antibodies against GFP (labeling DM1-ORNs), dsRed (labeling their postsynaptic partners) and nc82, which marks the neuropil structure by staining the presynaptic protein bruchpilot (BRP) (See Methods, Section 4.2). Postsynaptic partners were quantified by counting dsRed-positive cell bodies surrounding the antennal lobe (AL), where all ORN target neurons are present.

Flies developed at 18°C displayed visibly denser postsynaptic labeling in both the AL and LH compared to those developed at 25°C (Fig. 6B,C). Quantification of ds-Red positive cell bodies confirmed this observation. Flies reared at 18°C presented approximately twice as many postsynaptic partners as those reared at 25°C (Fig. 6D). This result indicates that lower developmental temperature leads to an increase in the number of postsynaptic partners formed by DM1-ORNs.

5.1.2 DM1-ORNs partners reported by trans-Tango at 18°C are functionally connected

To determine whether the postsynaptic partners identified by trans-Tango are functionally connected to DM1-ORNs, I adapted the system to combine optogenetic activation of presynaptic neurons with calcium imaging in their postsynaptic partners. Specifically, DM1-ORNs expressed CsChrimson – a red-shifted, light-gated cation channel – while postsynaptic neurons expressed GCaMP6s, a genetically encoded calcium indicator (Fig. 7A) (See Methods, Section 4.4.1).

Three regions of interest (ROIs) were defined for imaging and analysis: the DM1 glomerulus, adjacent glomeruli (referred as ‘rest of the AL’), and the medial lateral antennal lobe tract (mlALT). To determine the appropriate stimulation intensity, increasing light (0.02, 0.05 and 0.1 mW/mm^2) were tested while monitoring calcium transients in postsynaptic neurons in the DM1 ROI. Activity in this ROI mostly reflects the response from the uniglomerular DM1 projection neuron, which receives most of the ORNs input. In all intensities tested, calcium response within the DM1 glomerulus were consistent across developmental temperatures (Fig. 7B,C), suggesting that either the uPN connectivity remains constant or that the uPN activity is compensated by more inhibitory inputs.

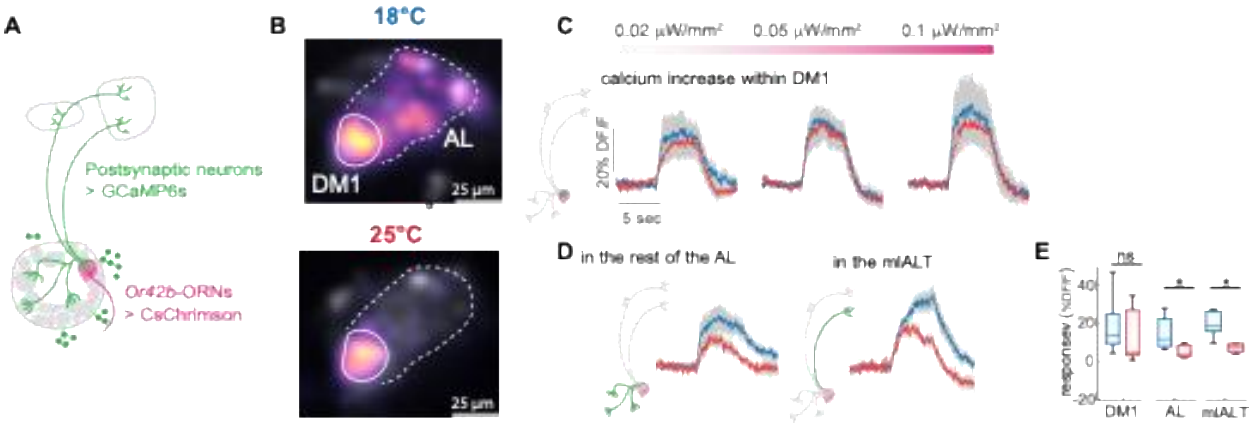

Figure 7. Postsynaptic partners of DM1-ORNs developed at 18°C are functionally connected. (A) Schematics of the modified trans-Tango system, expressing CsChrimson in the presynaptic DM1-ORNs and GCamp6s in their postsynaptic neurons. (B) Representative calcium imaging responses from flies developed at 18°C and 25°C. Color gradient indicates ΔF/F for each pixel. White outlines indicates the region of interest (ROIs) used for quantification in the AL: the DM1 glomerulus and adjacent AL glomeruli. (C) Optogenetically evoked calcium response to 0.05-0.1 mW/mm^2 light stimulation in the DM1 glomerulus. (D) Calcium responses to 0.05 mW/mm^2 light stimulation quantified in adjacent AL glomeruli and the medial lateral antennal lobe tract (mlALT). (E) Boxplot showing mean ΔF/F during the 9 s following stimulus onset (0.05mW/mm2). Significant differences were observed in the AL ($p = 0.02$, Kruskal-Wallis test, $n = 4$ at 18°C; $n = 7$ at 25°C) and in the mlALT ($p = 0.01$, $n = 4$ at 18°C; $n = 7$ at 25°C)

For subsequent experiments, a 0.05 mW/mm^2 stimulus was used. Upon red light stimulation, flies developed at 18°C exhibited larger calcium transients than those developed at 25°C in both the surrounding AL and the mlALT (Fig. 7D,E). This pattern is consistent with more postsynaptic neurons receiving functional input from the DM1-ORNs at the 18°C. A higher response in the AL could indicate the recruitment of either more local neurons or multiglomerular projection neurons. A higher response in the mlALT suggests an increase of activity and connection from ORNs to multiglomerular inhibitory PNs, that project to the LH through this tract (Tanaka et al., 2012; Wang et al., 2014). This is in agreement with notably more postsynaptic neurons in this tract at 18°C (Fig. 6B,C). Therefore, these results suggest that the increase in postsynaptic partners observed anatomically corresponds to an increase in functional connectivity.

5.1.3 DM1-ORNs present more active synaptic zones when developed at 18°C

The increase in functional partners observed could result either from a greater number of presynaptic active zones, a redistribution of synapses across postsynaptic partners, or a combination of both. To determine whether the number of active zones increased, I analysed data collected by Pascal Züfle, in which he expressed BRP-short^{GFP} (Chen et al., 2014) in DM1-ORNs (*Or42b*-Gal4 > UAS-BRP-short^{GFP}), providing a readout of presynaptic sites specifically within these neurons (See Methods, Section 4.2). However, the BRP-short^{GFP} seemed blobby and did not look like resembling real synapse size, and therefore we decided to stain and quantify endogenous BRP. The endogenous BRP (nc82) was stained using anti-nc82. This allowed us to also quantify synapses in the whole DM1 glomeruli and separate ORN synapses from other neuron types present in the neuropil (LNs and PNs).

Using a custom Python script and the pyclesperanto package, confocal images of the DM1 glomerulus were pre-processed, segmented and analyzed for synaptic quantification. The expression of BRP-short^{GFP} in DM1-ORNs was used to generate a 3D mask delineating the neuronal volume (Fig. 8A). The total volume of DM1-ORNs innervation did not differ across developmental temperatures (Fig. 8B). Within this mask – corresponding to DM1-ORNs axons – I quantified individual nc82-labeled puncta. Both the number, average size and intensity of nc82 puncta was significantly higher in flies developed at 18°C compared with those developed at 25°C (Fig. 8C,D).

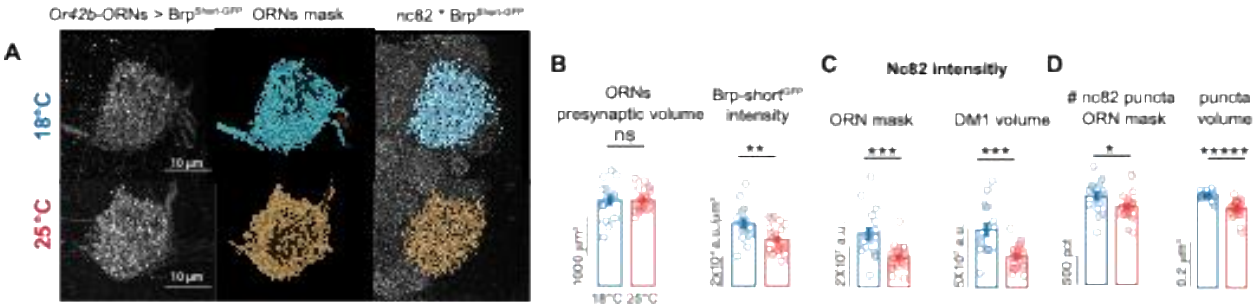

Figure 8. *Or42b*-ORNs display more and bigger synapses when developed at 18°C. (A) 3D representation (left to right) of DM1-ORNs expressing BRP-short^{GFP} (*Or42b*-Gal4 > UAS-BRP-short^{GFP}) in flies developed at 18°C (top) and 25°C (bottom); the corresponding binary mask delimiting DM1-ORNs volume; and segmented representations of endogenous nc82 (grey) and nc82 limited to the DM1 mask (blue and yellow). (B) Total volume of presynaptic DM1-ORNs is unchanged across developmental temperatures. Quantification of segmented

BRP-short^{GFP} mean fluorescence intensity. (C) Quantification of segmented endogenous nc82 puncta fluorescence intensity measured within the DM1-ORN mask (defined from the BRP-short^{GFP} expression on DM1 ORNs) and within the DM1 glomerular volume (defined as the expansion of the DM1-ORN mask). (D) Number of nc82 puncta within the DM1-ORN mask and their average volume. Error bars indicate SEM. Statistical significance was determined using the Kruskal-Wallis test (* indicates $p < 0.05$, ** $p < 10^{-2}$, *** $p < 10^{-3}$, ***** $p < 10^{-5}$; n = 16 hemibrains at 18°C; n = 25 at 25°C).

To assess whether this effect extended beyond DM1-ORNs, the initial mask was further expanded to approximate the entire DM1 glomerular volume. Using this volume, the endogenous BRP (nc82) signal in the whole DM1 glomerulus was used for puncta quantification. A similar increase in puncta intensity was in the presynaptic active zones of flies developed at 18°C both within DM1 glomeruli and within DM1-ORNs (Fig. 8D). Due to the spatial resolution of confocal microscopy, the larger puncta may reflect aggregates of multiple active zones that cannot be resolved. However, puncta quantification remain comparable across experimental conditions.

These findings demonstrate that a lower developmental temperature leads to an increase in both the number and size of presynaptic active zones in the first layer of the olfactory system. This is consistent with findings in DCN neurons, which present more BRP puncta when flies are developed at lower temperatures (Kiral et al., 2021).

5.1.4 DM1-ORNs present more mitochondria when developed at 18°C

The increased number and size of presynaptic active zones at lower developmental temperatures could cause a higher energetic demand for those neurons. Therefore, I next examined whether this structural change was accompanied by differences in mitochondrial abundance within DM1-ORNs (Fig. 9A). For that, I analyzed images acquired by Pascal Züfle. Mitochondria were visualized by expressing mito-GFP in DM1-ORNs (*Or42b*-Gal4 > UAS-mito-GFP), and the number of mitochondrial structures was quantified using a similar method for the BRP quantification (See Methods, Section 4.2.1).

Consistent with the increase in connectivity and synapse size and number, flies developed at 18 °C exhibited increased mitochondria numbers compared with those developed at 25 °C (Fig. 9B). This strong correlation between the number of active zones and mitochondrial content

could suggest an enhanced energetic support for synaptic function at lower developmental temperatures, potentially reflecting increased metabolic demands associated with greater synaptic connectivity. However, both active zones and mitochondria are quantified after the flies have been exposed to a common temperature (25°C) for 10 days after eclosion. Therefore the higher number of mitochondria of flies developed at 18°C could also be due to an adaptation response of those individuals to a new, higher temperature, in order to 'keep up' with differences in mitochondrial activity or efficiency.

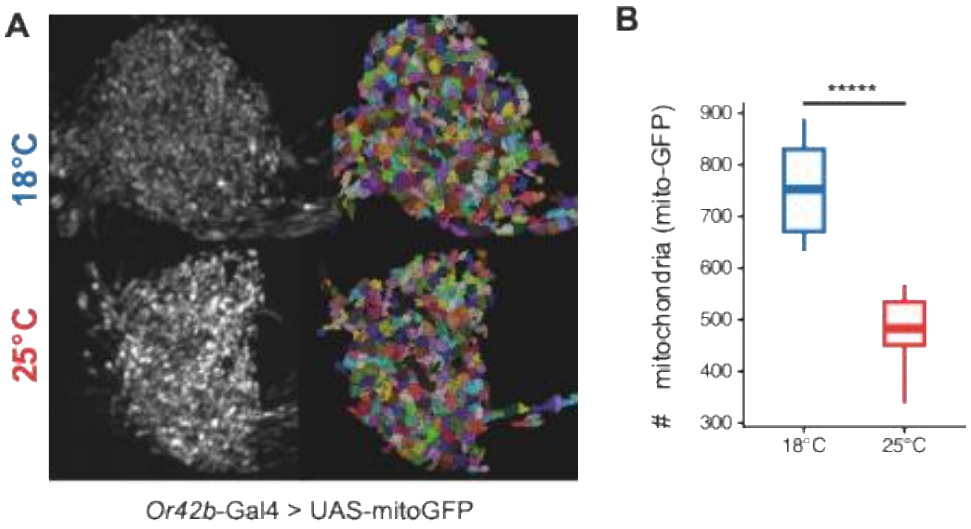

Figure 9. DM1-ORNs contain more mitochondria when developed at 18 °C in comparison to 25°C. (A) Representative images of DM1-ORNs expressing mito-GFP (*Or42b*-Gal4 > UAS-mito-GFP) in flies developed at 18 °C (top) and 25 °C (bottom). Left: three-dimensional projection of mito-GFP fluorescence signal. Right: segmentation of mitochondrial volume used for quantification. (B) Quantification of mitochondrial number across developmental temperatures. Flies developed at 18 °C exhibit a significantly higher number of mitochondria compared with those developed at 25 °C ($P < 0.0001$, t-test. n = 14 at 18°C; n = 16 at 25°C).

Additionally, an increase in mitochondria number does not necessarily result in more ATP production – for example when there is proton leak, and the protos migrate to the mitochondrial matrix independent of ATP synthase, not producing ATP. Therefore, future works quantifying not only the amount of mitochondria, but also its activity will be informative. Many techniques might be used as proxy for mitochondrial function, as oxygen consumption measurements and live imaging approaches using pyruvate or NAD+/NADH FRET sensors (Bulusu et al., 2017; Hemalatha et al., 2025).

5.1.5 Connectivity of other ORNs also scale with developmental temperature

To determine whether temperature-dependent connectivity changes are generalizable to other glomeruli, we examined the connectivity of two other glomeruli. Following the same approach described above, Pascal Züfle used trans-Tango to investigate the effect of temperature in the connectivity of Or7a and Or10a ORNs, which target DL5 and DL1 glomeruli (See Methods, Section 4.2).

These glomeruli have a similar synaptic distribution to DM1, as shown by an analysis of their partners using the hemibrain connectome (Fig. 10A, see Methods, Section 4.5). We hypothesize that the effect of developmental temperature in connectivity would follow the same magnitude across the antennal lobe. In this case, the increase of partners across temperatures should be comparable across glomeruli. Consistent with this, flies reared at 18 °C showed the same fold change in postsynaptic partners across all three glomeruli compared to flies developed at 25 °C (Fig. 10B).

We then examined the identity of the postsynaptic partners of these ORNs. Despite a similar scaling, the identity of postsynaptic partners could vary across glomeruli – depending on the available neurons within the glomerulus. As a starting point, we analyzed the connectome to account for which neuron types are postsynaptic partners to DM1, DL1 and DL5 ORNs at 25°C. More mPNs innervate the DM1 glomerulus compared to DL1 or DL5, which instead contain a higher proportion of mostly inhibitory LNs (Fig. 10C).

To understand if this impacts the identity of postsynaptic partners when flies are raised at lower temperatures, we used trans-Tango. To distinguish cell types in the trans-Tango data, we separate the postsynaptic neurons by the position of their cell bodies surrounding the AL (cell body clusters – dorsal, lateral and ventral) (Sakuma et al., 2014). In this case, cell body position can be used as a proxy for cell type, as it reflects the neuroblast from which the cell originated. Uniglomerular PNs originate from anterodorsal, lateral and ventral neuroblasts – which have correspondent cell body location in relation to the AL (Jefferis et al., 2001). LNs are also but not exclusively produced by the lateral and ventral lineages (Das et al., 2008; Lai et al., 2008; Lin et al., 2012).

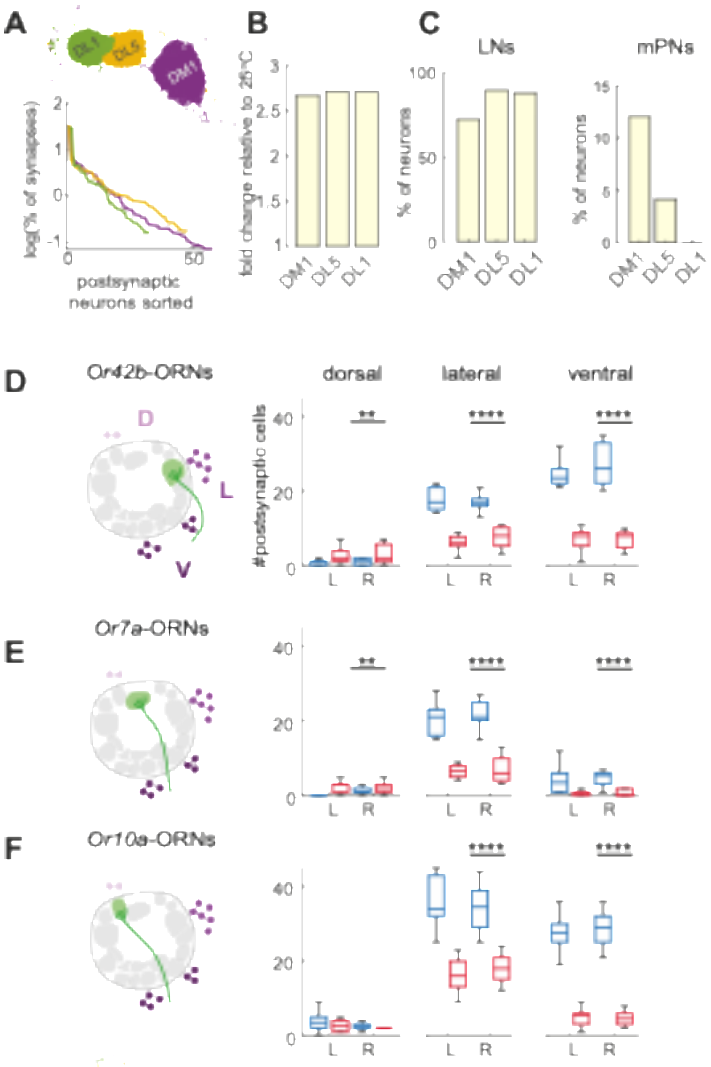

Figure 10. Temperature-dependent scaling of postsynaptic partners across olfactory glomeruli. (A) Connectomic (hemibrain) analysis of postsynaptic partners for the three tested glomeruli, showing the number of synapses for each postsynaptic neuron (x-axis), sorted in descending order of number of synapses. (B) Fold change in the number of postsynaptic partners reported by trans-Tango in flies developed at 18°C in relation to 25 °C for all three glomeruli. (C) Proportion of postsynaptic partners identified in the connectome that are local neurons (LNs, left) or multiglomerular projection neurons (mPNs, right) for each glomerulus. (D) Left: schematic showing the position of the DM1 glomerulus within the antennal lobe (AL) and cell body clusters position. Right: quantification of postsynaptic cell bodies in flies developed at 18 °C (blue) and 25 °C (red), separated by cluster position (dorsal - D, lateral - L, or ventral - L) across left and right ALs (* indicates $p < 0.05$, ** $p < 10^{-2}$, *** $p < 10^{-3}$, ***** $p < 10^{-5}$. Error bars indicate SEM. Kurskal-Wallis test, n = 20 at 18°C; n = 23 at 25°C). (E) Same as A for DL5-ORNs (*Or7a*-Gal4 > trans-Tango, n = 10 at 18°C and 25°C). (F) Same

analysis for DL1-ORNs (*Or10a*-Gal4 > trans-Tango, n = 10 at 18°C and 25°C). Boxplots indicate median and quartiles, whiskers indicate maximum and minimum values.

Trans-Tango labeling revealed that, when developed at 18°C, DM1-ORNs form more synapses with neurons located in the ventral and ventrolateral clusters (Fig. 10D), which contain the soma of approximately 66.6% of all multiglomerular projection neurons (mPNs) (Bates et al., 2020) including ventral PNs (Liang et al., 2013; Shimizu & Stopfer, 2017; Strutz et al., 2014). This is consistent with the pattern we observe in the connectome at 25°C (Fig. 10C). This pattern suggests that DM1-ORNs may drive stronger activity within this neuronal population when flies develop at 18 °C compared to 25 °C. Consistently, we observed increased calcium activity in the mlALT, the tract used by these neurons to project to the lateral horn (Fig. 7D,E, 10C).

In contrast, DL5 and DL1 ORNs displayed a prominent increase in connectivity with neurons in the lateral cluster (Fig. 10C,E,F), which contains a large population of LNs, and mPNs mostly of unknown function (Lin et al., 2012). This probable increase in LNs is consistent to the postsynaptic partners found in the connectome at 25°C for those glomeruli, indicating that developmental temperature could have distinct effects across circuits, depending on the spatially (and temporally) available partners.

For instance, R7 photoreceptors in flies reared at lower temperatures establish connections with postsynaptic partners that are not observed at 25 °C. Importantly, these partners are the same as those recruited when the principal synaptic target of R7 is unavailable, suggesting a shared compensatory wiring strategy (Kiral et al., 2021). Overall, lower temperatures are expected to increase local inhibition throughout the antennal lobe. In the case of DM1-ORNs, more input into mPNs might lead to a stronger modulation of the lateral horn, potentially affecting behavior.

5.1.6 DM1-ORNs connectivity scales exponentially across developmental temperatures

Having observed that the number of postsynaptic partners of DM1-ORNs approximately doubled between 25 °C and 18 °C, we next investigated whether this scaling continues across a broader range of developmental temperatures. To define the limits of this analysis, we first considered the known thermal boundaries for *Drosophila melanogaster* reproduction (Pétavy et al., 1997; Trotta et al., 2006), which range from approximately 11 °C to 31 °C. This experiment was done and analyzed by Pascal Züfle. Flies were reared under standard conditions

(25°C) until pupariation and then maintained at either 12, 18, 25 or 31°C for the total duration of pupal development (See Methods, Section 4.2).

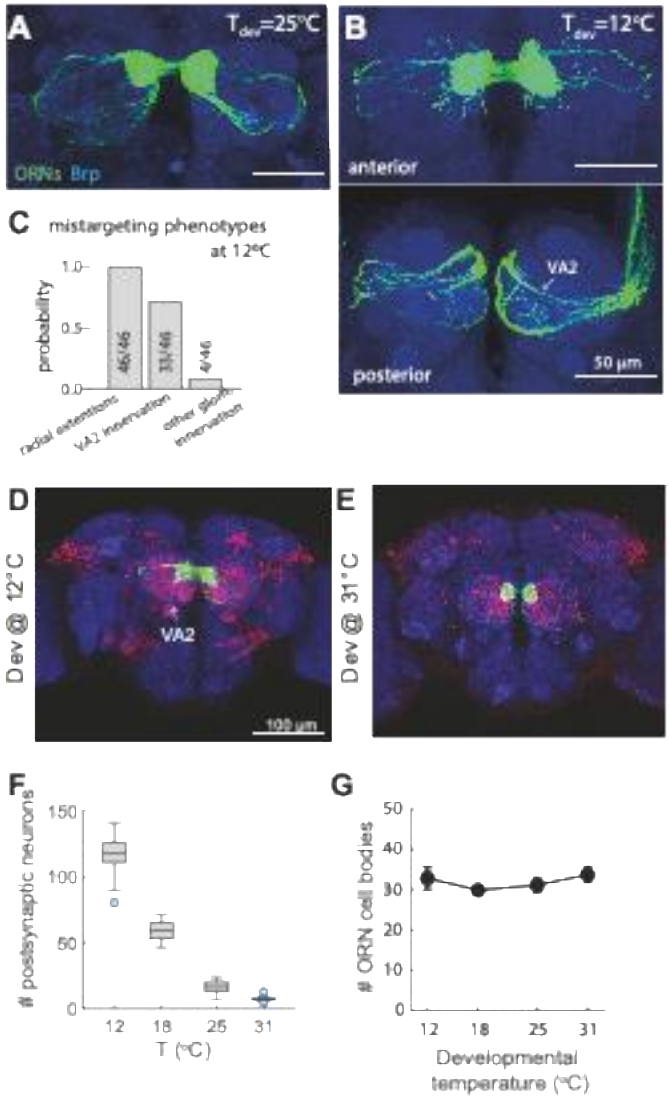

Figure 11. Developmental temperature modulates the number of postsynaptic partners in DM1-ORNs exponentially across temperatures. (A) Innervation pattern of DM1-ORNs in flies developed at 25°C. (B) DM1-ORNs project radially from DM1 (anterior, top) and innervate VA2 glomerulus (posterior, bottom). (C) Quantification of the mistargeting phenotypes at 12°C. (D-E) Representative trans-Tango labeling of DM1-ORNs (*Or42b*-Gal4 > trans-Tango) in flies developed at 12 °C (D) and 31 °C (E). Presynaptic neurons (*Or42b*-ORNs) are shown in green (GFP), postsynaptic partners in red (dsRed), and neuropiles in blue (nc82). (F) Quantification of postsynaptic cell bodies across developmental temperatures, showing a

strong increase in the number of partners at lower temperatures. (G) Number of DM1-ORNs cell bodies (counted in the antennae) across developmental temperatures.

At 12°C, DM1-ORNs grew axonal extensions radially from the DM1 glomerulus, and also innervated the VA2 glomerulus (Fig. 11A-C). Both of those phenotypes are not seen at 25°C. Correct ORN-glomeruli innervation is specified during development, ensured by precise ORN-PN partner matching (mediated by Teneurins and Dscam) (Hong et al., 2012; Sakuma et al., 2014; Zhu et al., 2006). Therefore, an increase in axonal innervation in a non-canonical glomerulus could be a result of mistargeted ORN-PN synapses during development – for example, between DM1-ORNs and VA2 PNs.

Using the trans-Tango system, we examined the postsynaptic partners of DM1-ORNs in flies developed at these extreme temperatures to assess whether the temperature-dependent increase in synaptic connectivity observed at 18 °C extends to the full range.

Flies developed at 12 °C exhibited a substantial increase in postsynaptic labeling, whereas those developed at 31 °C showed markedly fewer partners (Fig. 11D-F). At 12 °C, additional postsynaptic neurons were observed projecting toward the saddle region of the subesophageal zone (SEZ) – a region that is typically not innervated by neurons postsynaptic to ORNs at 25 °C. At 31°C, ORNs synapse into a 'minimal' circuit, consistent of the single uPN of DM1, few mPNs and LNs.

This shift in reported connectivity could be due to different cell numbers being labeled by the *Or42b*-Gal4 driver, which would bias our results. To ensure the number of DM1-ORNs remained consistent across all developmental temperatures, we verified it by counting *Or42b*-Gal4 cell bodies in the antennae (Fig. 10G), with data acquisition and quantification by Pascal Züfle. Therefore, at very low developmental temperatures, synaptic connectivity may extend beyond canonical olfactory circuits, potentially reflecting the recruitment of novel postsynaptic populations. Conversely, at very high temperatures, connectivity may be reduced to a minimal circuit backbone. Such core connections are likely evolutionarily conserved, ensuring reliable circuit assembly and function across a wide range of temperatures and supporting survival.

In summary, our data show that developmental temperature impacts the wiring of the Drosophila olfactory system, as ORN postsynaptic partners scale exponentially with developmental temperature. This is reflected in a greater number of synaptic partners, increased presynaptic active zone abundance, and elevated mitochondrial presence, consistent with higher

synaptic and energetic investment. Importantly, these changes are observed across multiple glomeruli, suggesting that temperature could have a global effect in scaling brain wiring.

5.2 Functional consequences of changes in wiring

The structural analyses presented in the previous section show that developmental temperature markedly reshapes the organization of olfactory circuits, resulting in increased ORN connectivity at lower temperatures. This observation naturally leads to the question of how such anatomical remodeling affects the circuit's functional properties and behavioral output. Therefore, in this section, I investigate the consequences of temperature-dependent wiring changes on behavior and neuronal activity.

5.2.1 Odor-driven behavior is impacted by developmental temperature

To determine whether the wiring consequences of developmental temperature affects odor-driven behavior, we tested flies developed at 18°C and 25°C in two behavioral paradigms.

In the first approach, flies were tethered to walk on a spherical treadmill in experiments conducted and analyzed by Ana Sofia Brandao, Näncy Benjamin and Constantin Müller (See Methods, Section 4.3.1). Individual flies, 10 days after eclosion, were tethered to walk on a spherical treadmill while their locomotor response to odor stimulation was recorded (Fig. 12A). On average, a puff of 2-butanone elicited a stronger increase in walking speed in flies developed at 18°C compared to those developed at 25°C (Fig. 12B). Results were also confirmed with vinegar as an odorant (see Züfle et al., 2025).

To test whether these findings were biased due to the assay, and to better understand the effect of developmental temperature on walking behavior, we employed a "free-walking" paradigm. These experiments were conducted and analyzed by Giovanni D'Uva, Christian Daniel and Polina Krasnova (See Methods, Section 4.3.2). In this setup, flies were allowed to explore a large circular arena (40 cm in diameter) containing a hidden odor source placed at a random position (Fig. 12C). At all times, more flies raised at 18°C visited the odor source and spent more time at the odor than flies raised at 25°C (Fig. 12D). The difference in behavior between flies developed at different conditions was more prominent in the first seven minutes of the

assay, when the odor landscape was novel. Similar results were obtained using vinegar as an odorant and when testing the flies at a higher assay temperature of 32°C (see Züfle et al., 2025).

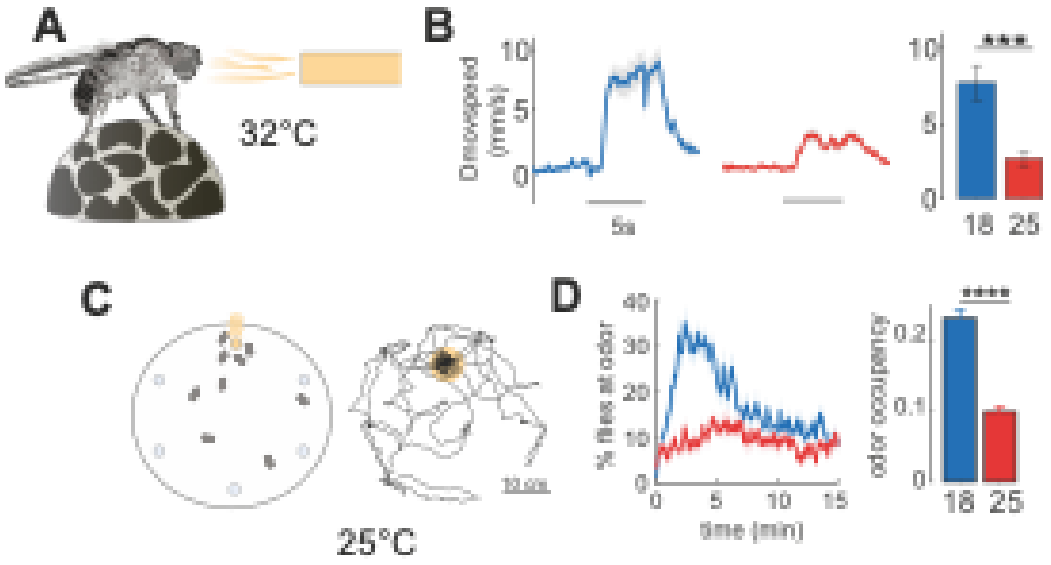

Figure 12. Impact of developmental temperature in odor-driven behavior. (A) Odor response was tested at 32°C on a spherical treadmill. (B) Odor response was calculated as change in moving speed as a function of time in response to 5s stimulation (Δ mov speed = speed - basal speed); bar plot, mean change in moving speed within the first 2 s of stimulation (n = 13 at 18°C and 25°C). (C) Odor-driven behavior was tested at 25°C in a free walking assay consisting in a circular arena of 40-cm radius with an odor source randomly placed in one of six possible locations. Flies were tracked for 15 min (D) Average percentage of flies at the odor source and odor occupancy (bar plot). Shaded area and error bars indicate SEM (*** indicates $p < 10^{-3}$, **** indicates $p < 10^{-5}$, n = 19 at 18°C and n = 20 at 25°C).

Together, these results argues that flies developed at lower temperatures display a higher approach behavior towards 2-butanone than flies developed at the reference 25°C. Such behavioral outcome suggests that there is a difference in odor perception and how they are acted upon.

Those behavioral changes provide evidence for functional consequences of the temperature-dependent circuit rewiring (Section 5.1). Notably, these effects are observed in flies after a 10 day re-adaptation to a reference temperature of 25 °C, indicating stable, developmentally encoded alterations rather than transient physiological states. However, behavioral changes do not directly reveal the underlying neural dynamics. To address this, I next examined how developmental temperature influences odor-evoked activity within the olfactory pathway.

5.2.2 Odor coding in the antennal lobe is impacted by developmental temperature

As we have a change in behavior, we hypothesized that there are changes in the odor signaling pathway across developmental temperatures. To assess this, I measured odor-evoked calcium responses in ORNs and in projection neurons (PNs), which are postsynaptic to ORNs and relay sensory information from the antennal lobe to higher brain centers.

Calcium imaging was performed in four glomeruli – DM1, DM4, DL1, and DL5 – while presenting three odors: benzaldehyde (aversive) and the appetitive odors vinegar and 2-butanone (See Methods, Section 4.2). This was done with the help of Ana Sofia de Castro Brandao. DM1 and DM4 ORNs from flies developed at 18 °C exhibited stronger calcium transients in response to appetitive odors than those developed at 25 °C, whereas responses to the aversive odor were comparable across temperatures (Fig. 13A). This enhanced ORN activity at 18 °C parallels the increase in synaptic partners and presynaptic structures observed anatomically. From the tested odors, DL1 and DL5 ORNs respond only to benzaldehyde. Across temperatures there was no increase in responses to benzaldehyde, which could suggest that the circuits for aversive odors might be more robust to shifts in developmental temperature.

The number of action potentials for DM1 and DM4 ORNs did not differ with temperature – see Züfle et al., 2025. Therefore, the increase in calcium transients would be caused by more and bigger synapses (Fig. 8), which would activate the corresponding uPNs more strongly at the onset of an odor stimulus. Surprisingly, uPNs displayed calcium responses that were consistent across developmental temperatures in all tested glomeruli (Fig. 13B, experiments performed by Ana Sofia de Castro Brandao).

This temperature independence suggests that odor-evoked activity is normalized within the antennal lobe, likely through inhibitory network mechanisms mediated by local interneurons. Consequently, the temperature-dependent differences in ORN response magnitude do not appear to propagate through the immediate downstream circuit.

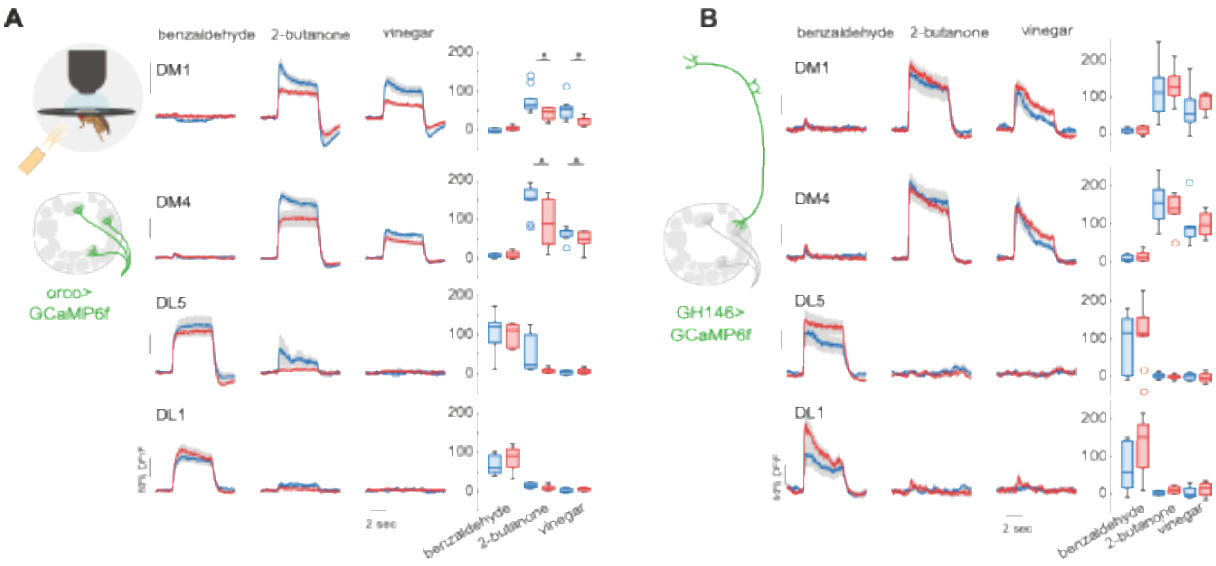

Figure 13. Odor-evoked calcium responses of ORNs are enhanced at lower developmental temperatures, while PN responses remain consistent. (A) Calcium responses recorded from olfactory receptor neurons (ORNs) (*Orco*-Gal4 > UAS-GCaMP6f) in flies developed at 18 °C (blue) and 25 °C (red). Traces show normalized fluorescence changes (ΔF/F) for four glomeruli—DM1, DM4, DL5, and DL1—during stimulation with three odors: benzaldehyde (aversive), 2-butanone, and vinegar (both appetitive). Boxplots to the right of each panel show the quantified peak ΔF/F values for each glomerulus and odor (* $p < 0.05$, P value calculated for the average activity during the first second of the stimulus, n = 6 at 18°C; n = 10 at 25°C). (B) Same analysis for projection neurons (PNs) (*GH146*-Gal4 > UAS-GCaMP6f), showing that PN calcium transients are consistent across developmental temperatures (n = 16 at 18°C; n = 18 at 25°C). Shaded areas indicate SEM.

Next, I examined the odor-evoked activity of multiglomerular projection neurons (mPNs), which convey integrated olfactory information from multiple glomeruli to the lateral horn (LH). mPNs have been shown to shape innate discrimination of closely related odors (Parnas et al., 2013) and encode both odor valence and intensity information to the LH (Strutz et al., 2014). Importantly, multiglomerular projection neurons (mPNs) form a parallel olfactory pathway to uniglomerular projection neurons (uPNs), which were examined previously using *GH146*-Gal4. Although no differences in odor coding were detected at the level of uPNs, this does not exclude potential temperature-dependent effects in mPNs. Given that mPNs integrate input from multiple glomeruli, in contrast to the single-glomerulus input characteristic of uPNs, they may be particularly sensitive to developmental perturbations. Therefore, I next examined how developmental temperature influences odor-evoked functional responses of mPNs.

To address this question, I used *Mz699*-Gal4 > UAS-GCaMP8f flies (see Methods, Section 4.4). The *Mz699*-Gal4 driver (Ito et al., 1997) labels a subset of PNs from the ventral lineage (vPNs) that project through the medial lateral antennal lobe tract (mlALT) and are not labeled by *GH146*-Gal4 (Lai et al., 2008). These vPNs labeled by *Mz699*-Gal4 are predominantly multiglomerular and GABAergic (Parnas et al., 2013; Shimizu & Stopfer, 2017).

Previous work has shown that *Mz699*-Gal4 labeled mPNs exhibit region-specific odor responses within the lateral horn (Strutz et al., 2014). Due to lack of landmarks in the neuropile, I performed calcium imaging in three distinct regions of interest (ROIs) within the LH, defined according to the spatial subdivisions described by (Strutz et al., 2014): LH-AM (anterior medial), LH-PM (posterior medial), and LH-AL (anterior lateral).

Similar to uPNs, calcium transients in mPNs were largely consistent across dev temp, indicating that the overall integrative output of the AL remains stable despite temperature-dependent changes observed in upstream connectivity (Fig. 14). The only exception was a decrease in responses to benzaldehyde within the posteromedial (PM) region of the LH in flies developed at lower temperatures.

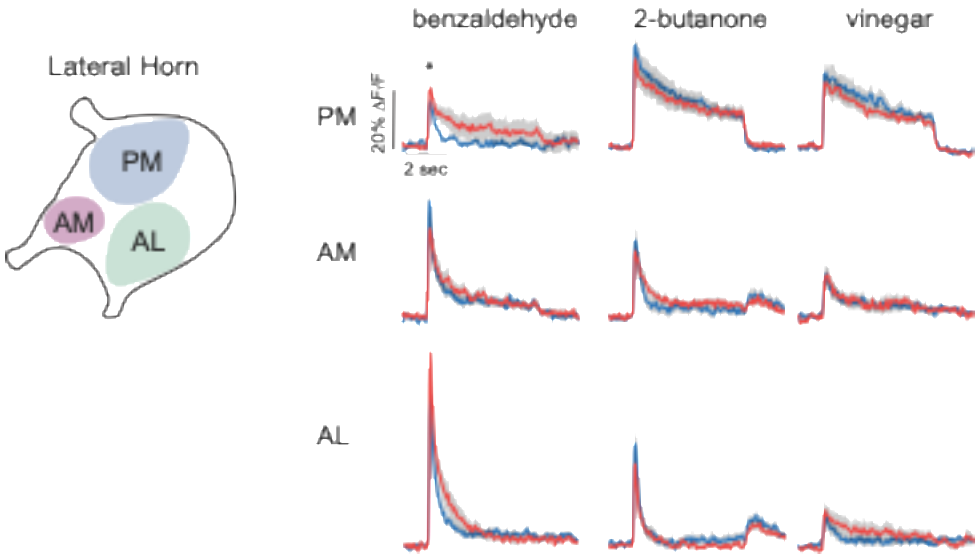

Figure 14. Multiglomerular projection neuron activity in the lateral horn is similar across developmental temperatures. (A) Schematic of the lateral horn (LH) showing the three regions of interest (ROIs) analyzed: AM (anterior medial), PM (posterior medial), and AL (anterior lateral), as defined in (Strutz et al., 2014b). (B) Odor-evoked calcium responses (ΔF/F) recorded in flies developed at 18 °C (blue) and 25 °C (red) for benzaldehyde, 2-butanone, and vinegar. Traces represent average fluorescence changes for each ROI. Across developmental

temperatures, calcium transients were comparable in all regions, except for a slight reduction in benzaldehyde responses in the PM region at 18 °C, indicating that overall mPN inputs to the LH activity remains robust to developmental temperature variation. * indicates $p < 0.05$. P value calculated for the average activity during the first second of the stimulus, n = 6 at 18°C; n = 10 at 25°C. Shaded areas indicate SEM.

Therefore, the odor representations from the AL to higher brain areas is robust to changes in developmental temperature, shown by the same response of uniglomerular and multiglomerular PNs across developmental temperatures. However, since *Mz699*-Gal4 labels only ventral lineage mPNs, it is unknown whether other mPN populations are equally robust to developmental temperature changes.

5.2.3 Lateral horn neurons connectivity to PNs is affected by developmental temperatures

Since the measured output activity of the AL is invariant to developmental temperature, the different behavioral phenotypes observed should result from differences downstream of the AL. I therefore examined the synaptic connections between PNs and lateral horn neurons (LHNs), the primary targets of PNs that integrate olfactory information in higher brain regions.

5.2.3.1 Pd2a1/b1 presents more presynaptic partners at lower developmental temperatures

To quantify the PNs-LHNs connectivity across developmental temperatures, I first focused on the PD2a1/b1 lateral horn neurons (LHNs), which were shown to be functionally connected to DM1 (Jeanne et al., 2018)

Using the retro-Tango system – a retrograde transsynaptic labeling tool that targets presynaptic partners of genetically defined postsynaptic neurons – we mapped all the presynaptic neurons connected to PD2a1/b1 across developmental temperatures (Fig. 15A). Here we focused on PNs, which cell bodies surround the AL in clusters defined by position (See Methods, Section 4.2). Cell bodies were manually counted and clustered by Pascal Züfle.

Consistent with findings from earlier stages of the olfactory pathway, flies developed at 18°C displayed approximately twice as many presynaptic partners as those developed at 25°C (Fig. 15B). The change in connectivity was larger in the ventral cluster, which contains mPNs (Fig. 15B).

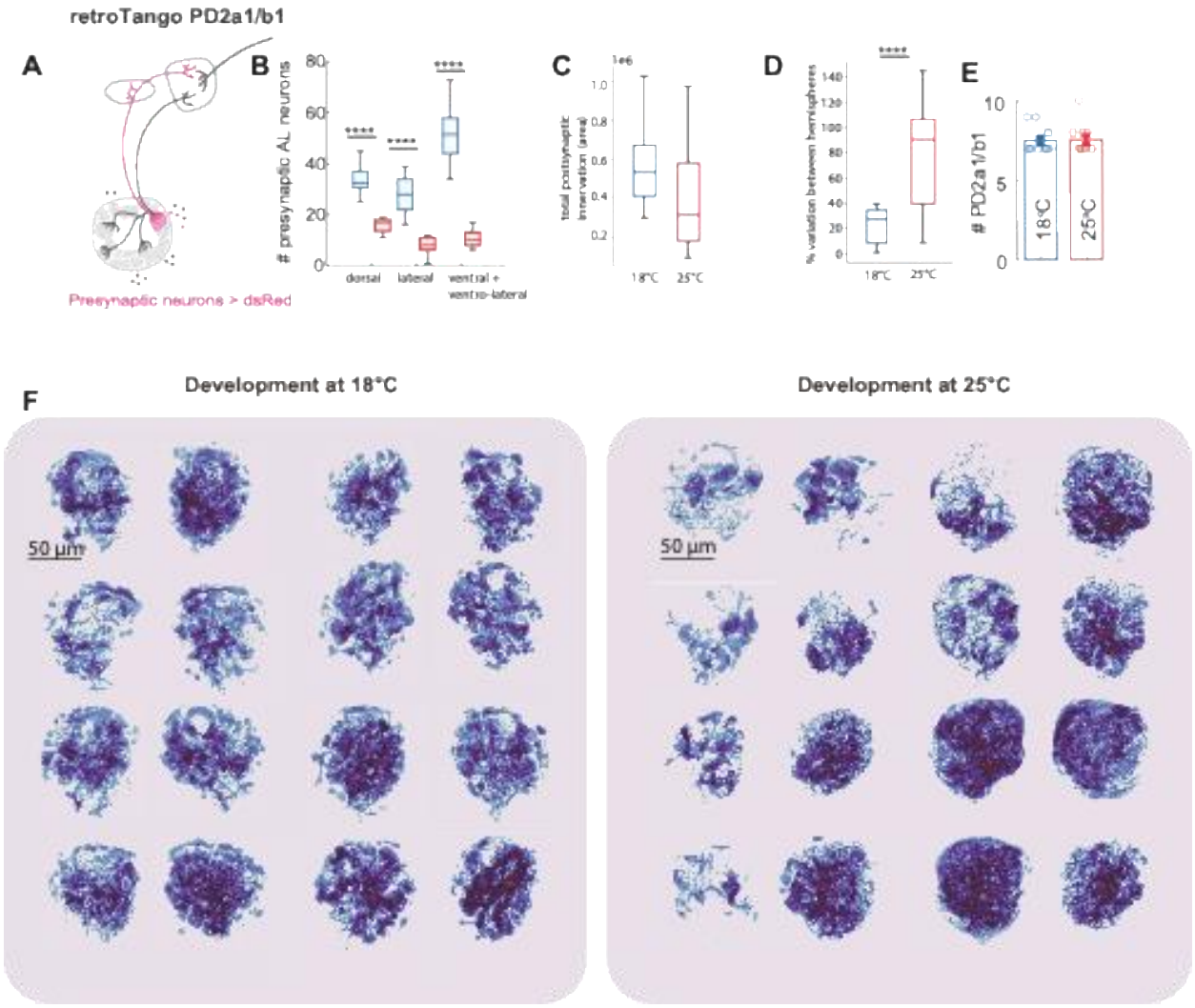

Figure 15. Lower developmental temperature increases PN–LHN connectivity. (A) Schematic representation of the retro-Tango experiment labeling presynaptic projection neurons (PNs) connected to PD2a1/b1 lateral horn neurons (LHNs). (B) Quantification of presynaptic neuron cell bodies surrounding the antennal lobe (AL) in flies developed at 18 °C (blue) and 25 °C (red), grouped by cluster position (dorsal, lateral, and ventral/ventrolateral) ($p < 10^{-4}$, n = 12 hemibrains at 18°C; n = 11 at 25°C). (C) Total area (in pixels squared) of the AL innervated by presynaptic partners at 18 °C and 25 °C. (D) Variation in total innervated area between left and right hemispheres, showing reduced bilateral variability at 18 °C. Variation was calculated as 100*(volume left–volume right)/(2*total volume) ($p < 0.0001$, t-test). (E) Number of PD2a1/b1 LHN cell bodies across developmental temperatures. (F) Representative z-projections of binarized presynaptic neurons in flies developed at 18 °C (left) and 25 °C (right)

To quantify AL innervations, I binarized the 3D image correspondent to the staining of presynaptic neurons in both hemispheres and accounted for its volume (See Methods, Section 4.2.1). Symmetry in AL innervation was calculated as the difference between the presynaptic neurons volume in the left AL vs. right AL, divided by double of the total volume. This was then calculated as a percentage. At 25°C, presynaptic neurons presented striking asymmetries across hemispheres and patchy innervations of the AL (Fig. 15B,C,F).

At 18°C, PD2a1/b1 neurons receive synapses from the AL in a denser and more symmetric way across hemispheres, in comparison to 25°C (Fig. 15 C,D). This would be consistent with a more reliable recruitment of mPNs at lower temperatures, which innervate bigger areas of the AL. to verify that these results are not due to a boas in expression, Pascal Züfle counted the number of PD2a1/b1 neurons labelled in flies developed at different temperatures. Flies developed at either temperatures presented the same amount of PD2a1/b1 cell bodies expressed by the chosen driver (Fig. 15E).

5.2.3.2 Connectivity of PNs-LHNs is affected by developmental temperatures

PD2a1/b1 neurons had more presynaptic partners across developmental temperatures, however, with retro-Tango it was not possible to distinguish which PNs (from which glomeruli) were connected at different temperatures. Therefore, we could not discern if there was only an increase in presynaptic PNs or if the combinatorial nature of these inputs was also modified across developmental temperatures. As we see a difference in behavioral output but a robust odor response from PNs across temperatures, the difference in behavior could arise from changes in the connectivity partners in a higher brain area.

To obtain a more detailed view of the identity of the glomeruli connect to the PD2a1/b1 lateral horn neurons (LHNs), I employed the BacTrace system, which enables the identification of presynaptic partners of genetically defined postsynaptic neurons (Fig. 16A) (See Methods, Section 4.2). Using the VT033006-LexA line, which labels uPNs from approximately 27 out of 51 antennal lobe glomeruli (Cachero et al., 2020), I mapped the PN–LHN connectivity profiles across developmental temperatures.

The lateral horn (LH) is thought to mediate innate olfactory behaviors; therefore, its connectivity with PNs would be expected to be highly conserved across individuals. Contrary to this expectation, I observed substantial variability in PN–LHN connectivity both across hemispheres and among individuals. At 25 °C, the most frequently connected PN (DM5) was detected in only ~60% of hemibrains (Fig. 16B,C). At 18°C, a similar variability was observed.

However, the probability of specific PN–LHN connections varies across temperatures (significantly for the VM2 glomerulus). This suggests a temperature-dependent bias in PN-LHN connectivity likelihood rather than circuit identity.

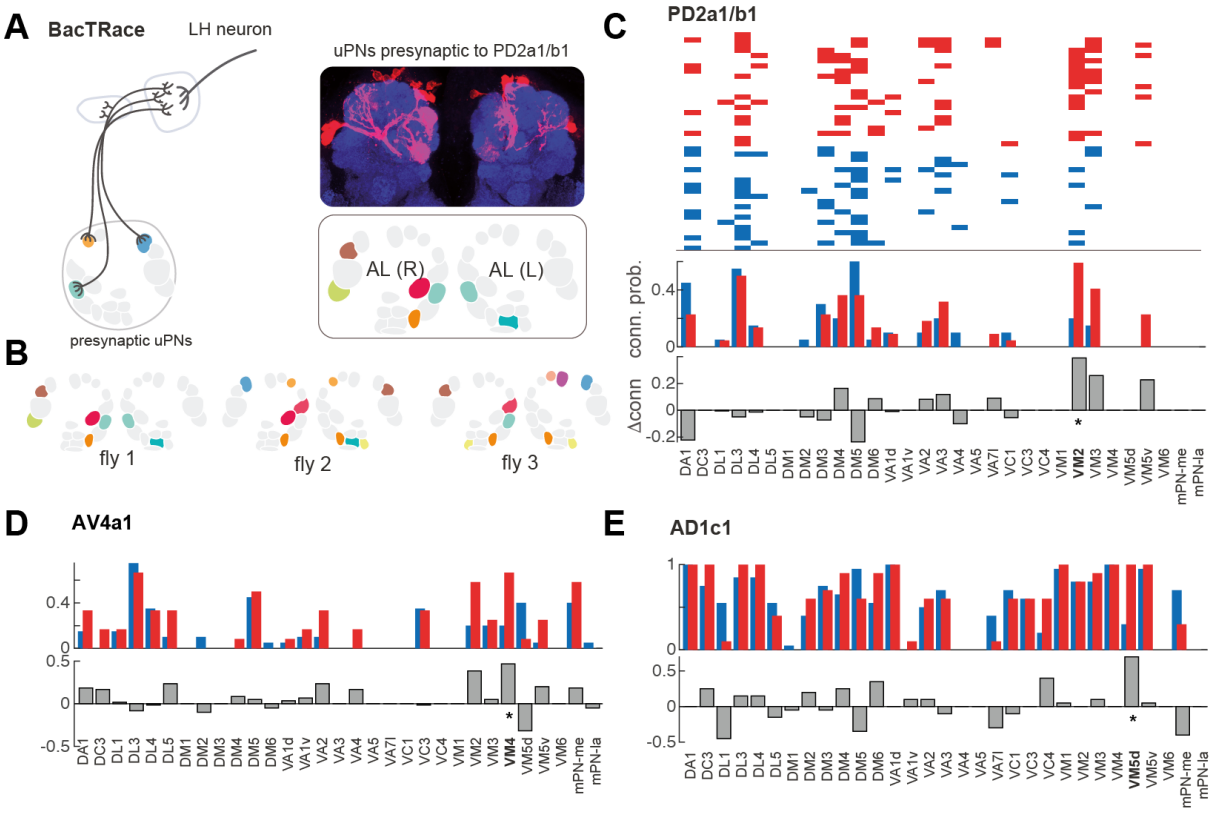

Figure 16. BacTrace reveals temperature-dependent variability in PN–LHN connectivity. (A) Schematic of the BacTrace approach showing presynaptic uniglomerular projection neurons (uPNs) connected to defined postsynaptic lateral horn neuron, PD2a1/b1. Right: Confocal image of uPNs presynaptic to PD2a1/b1 in the left and right hemispheres, with colored schematic glomeruli indicating identified presynaptic inputs. (B) Example illustrating interindividual variability in PD2a1/b1 connectivity patterns across flies. (C) Connectivity matrices for PD2a1/b1 in flies developed at 18 °C (blue) and 25 °C (red). Each row represents a single hemibrain and each column a glomerulus. The bar plot below shows the connection probability for each glomerulus, and the lower panel displays the difference in connectivity (25 °C – 18 °C) across glomeruli (* indicates $p < 0.05$, ** $p < 0.01$, chi-square test, n = 32 at 18°C; n = 26 at 25°C). (D–E) Equivalent analyses for AV4a1 (n = 12 at 18°C; n = 20 at 25°C) (D) and AD1c1 (E) lateral horn neurons (n = 10 at 18°C; n = 20 at 25°C).

To determine whether this variability is a general property of LHN connectivity, I extended the analysis to two additional LHNs, AV4a1 (Fig. 16D) and AD1c1 (Fig. 16E). Similar patterns

emerged: the identity of connected PNs remained largely consistent, but the relative connection probabilities differed across temperatures. Specifically, PD2a1/b1 received fewer inputs from the VM2 glomerulus at 18 °C compared with 25 °C, while AV4a1 showed reduced connectivity with VM4 and AD1c1 with VM5d under cooler developmental conditions.

5.2.3.3 Developmental temperature selectively alters the activity of PD2b1 subtype, but not PD2a1

To assess how temperature-dependent differences in PN–LHN connectivity influence neural activity, I performed calcium imaging in PD2a1/b1 lateral horn neurons (LHNs) (See Methods, Section 4.4). To separate a1 and b1 subtypes, two regions of interest (ROIs) were analyzed: one within the lateral horn (LH), where both PD2a1 and PD2b1 subtypes project, and another within the mushroom body (MB) calyx, which receives input exclusively from the PD2b1 subtype.

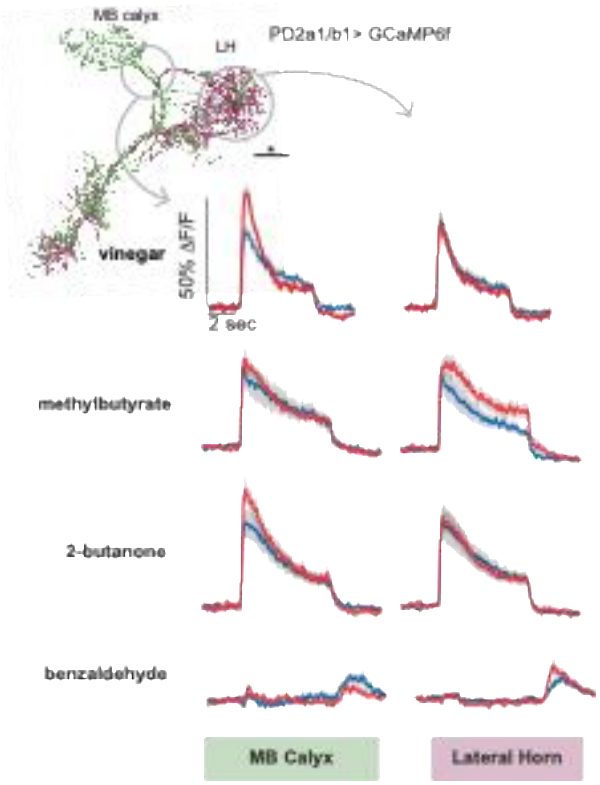

Figure 17. Calcium response of PD2a1/b1 neurons in flies developed at 18 and 25°C. Top: 3D reconstruction from electron microscopy data showing the skeletons of PD2a1/b1 lateral horn neurons (LHNs), with PD2b1 subtypes in green and PD2a1 in red. Bottom: odor-evoked calcium responses (ΔF/F) in flies developed at 18 °C (blue) and 25 °C (red) for four odors: vinegar, methyl butyrate, 2-butanone, and benzaldehyde. Traces represent average normalized fluorescence over time. Bottom left: calcium responses recorded in the mushroom body (MB)

calyx, innervated by the PD2b1 subtype. Bottom left: responses recorded in the lateral horn (LH), where both PD2a1 and PD2b1 subtypes project. PD2b1 neurons exhibit stronger responses at 25 °C, whereas activity within the LH remains comparable across developmental temperatures. * indicates $p < 0.05$. P value calculated for the average activity during the first second of the stimulus, n = 15 at 18°C; n = 15 at 25°C.

In flies developed at 25 °C, the PD2b1 subtype exhibited a higher odor-evoked calcium response in the MB calyx compared to flies developed at 18 °C, whereas calcium transients within the LH remained similar across temperatures (Fig. 17). These findings indicate that developmental temperature selectively alters the activity of the PD2b1 subtype, potentially reflecting the temperature-dependent changes in its presynaptic PN connectivity observed in the anatomical analyses. Therefore, while a general scaling of connectivity occurs across the brain, functional consequences are circuit specific and depend on the type of synaptic partners recruited.

In summary, in Section 5.1 we observed that developmental temperature induces shifts in ORN–PN connectivity, and in Section 5.2, we saw corresponding impacts on behavior. Here, we extend these findings to functional responses: while ORN calcium responses vary with developmental temperature, the responses of the next circuit layer – both uPNs and mPNs – remain largely unchanged across conditions. Examination of PN–LHN connectivity revealed that PN partner choice in the lateral horn is temperature-dependent, and at the level of the MB neuropile the LHN PD2b1 also show functional changes. Together, these observations suggest that the relative robustness of PN responses does not constrain temperature's effects on downstream circuits or their behavioral output. Beyond, behavioral alterations observed may arise from temperature-dependent changes in connectivity downstream of PNs, and the precise players will need to be dissected in future works.

5.3 A metabolic theory explains brain wiring at different developmental temperatures

In the previous sections we saw that developmental temperature affects behavior, physiology and connectivity. To understand the influence of developmental temperature in brain connectivity, we took a modeling approach.

We started from the observation that temperature determines **developmental time**, defined here as the time from pupa formation until the eclosion of the adult. Developmental temperature dictates the pace of growth in ectothermic animals (Angilletta et al., 2004; Gillooly et al., 2002). The duration of development depends on temperature, taking longer at lower temperatures (Gillooly et al., 2002) (Fig. 18A).

The Universal Temperature Dependance (UTD) model proposed that growth rate is linked to temperature through metabolism (Gillooly et al., 2001). The rate of any growing process is limited by its slowest reaction (rate limiting reaction), which determines the overall tempo of a process. Therefore, this model postulates that the rate of development scales with temperature proportionally to the Boltzmann factor ($e^{-\frac{E}{KT_k}}$) of a hypothetical rate-limiting metabolic reaction (Gillooly et al., 2002) with E being its activation energy.

Following this framework, we then assumed that flies eclose at a similar mass across temperatures (described in detail in Züfle et al., 2025), and reached a simple model that postulates that developmental time t should scale with the temperature T as $\frac{t}{t_0} = e^{-\frac{E}{KT_a^2}(T-T_0)}$. Here, t_0 indicates the developmental time at a reference temperature T_0 (in our conditions T_0 = 25°C); E is the highest activation energy of the rate limiting reaction; K is the Boltzmann constant; and T_a is the water freezing point (273K).

To verify this model with experimental data, Pascal Züfle measured the duration of developmental time (from puparium formation until eclosion) for flies developing at 12, 18, 25 and 31°C. The duration of pupa development increased exponentially with the temperature, and the model fits the data (Fig. 18B,C).

As both the developmental timing and number of postsynaptic partners scale exponentially with temperature, those phenomena could arise from the same first principles (Fig. 18D,E). This way, both the overall speed of growth and the formation of synaptic partners could be regulated by different metabolic rates, which accelerates with an increase in temperature (and decreases with a decrease in temperature).

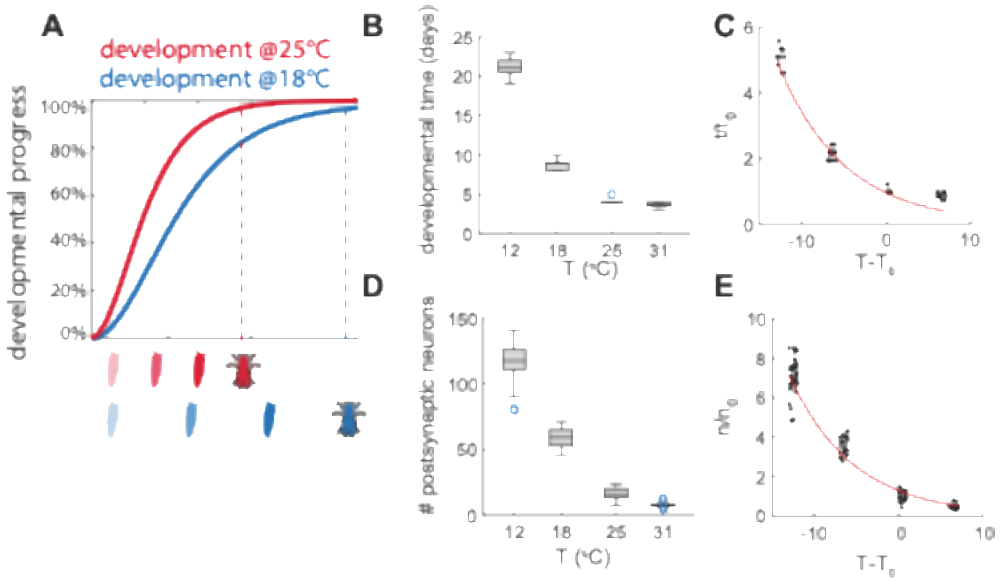

Figure 18. Temperature dependence of DM1-ORN postsynaptic connectivity and developmental timing. (A) Hypothetic growth curve showing effects of developmental temperatures in the duration of pupa development. Time of eclosion is indicated by dotted lines. (B) Developmental time for the four temperature regimes (days from puparium formation to adult eclosion). (C) Fold change in developmental time with respect to the temperature difference from 25°c and exponential fit (n = 8 to 20). Developmental time in days expressed relative to 25 °C and plotted against developmental temperature normalized to 25 °C. Red line indicates the corresponding exponential fit. (D) Boxplot of the number of postsynaptic partners labeled by trans-Tango from DM1 olfactory receptor neurons (ORNs) across developmental temperatures. (E) Single data points as in (D) normalized by the mean number of neurons connected at a reference temperature (25°C) and plotted as a function of the difference from the reference temperature (n = 20 to 38 hemibrains). Line indicates the exponential fit.

To account for the temperature-dependent wiring patterns observed in our data, we formulated the following hypothesis: if neural development were governed by the same underlying reaction rate as whole-organism ontogenesis (E), then the resulting connectivity should remain consistent across temperatures . Under this assumption, the developmental trajectories of both the nervous system and the organism would scale similarly in time across temperatures, leading to similar connectivity profiles. However, if the rate-limiting step in neural development was limited by a lower activation energy than that of general ontogenesis ($E' < E$), temperature changes would alter the pace of neural development in a different way, ultimately allowing distinct connectivity patterns. Previous results show that connectivity does, in fact, vary with developmental temperature (Fig. 18D,E). Therefore, we infer that nervous system development

is constrained by a reaction with lower activation energy than the other tissues. As a result, **the nervous system would progress at its own, faster developmental rate**, while the overall duration of development would still be determined by the pace of ontogenesis, resulting in more synapses.

To model the processes of nervous system development (i.e. axonal growth and synaptogenesis), we apply Kleiber's law, which postulates that in an organism, metabolic rate scales as the ¾ power of their mass. In this case, the mass would be a proxy for the stage of development, i.e. how advanced the developmental process is and the metabolic rate, its speed. The characteristic ¾ scaling emerges from the transport of nutrients through hierarchical branching networks – as the tracheal system in insects or the cardiovascular system in vertebrates (West et al., 1997). We assume that a similar scaling principle may apply to the nervous system development.

Based on this assumptions, we derived an analytical function for quantifying the scaling of synaptic connectivity with temperature: $\frac{n}{n_0} = e^{-4\frac{\Delta E}{KT_a^2}(T-T_0)}$ with $\Delta E = E - E'$ (see Züfle et al., 2025). We define $\beta = \frac{4\Delta E}{KT_a^2}$ as the scaling factor for synaptic connectivity. The model accurately captures the number of postsynaptic partners formed by DM1-ORNs at all developmental temperatures (with β = 0.133(± 0.011), Fig 18E), as well as for flies developed under temperature cycles (see Züfle et al., 2025).

Taken together, our results show that both synaptic connectivity and developmental duration scale exponentially with temperature. We established a first-principles framework that accounts for the scaling observed in these two traits, and predicts the nonuniform temporal scaling of neural development across temperatures. Moreover, predicts brain wiring under development at constant temperatures (shown in this section) and at temperature cycles (see Züfle et al., 2025).

5.3.1 Developmental temperature induces a non-uniform scaling of neuronal growth

Another prediction of the model concerns the relative speed of brain and body development. The duration of pupal developmental depends on temperature and can be normalized by defining pupariation (P0) as 0% and eclosion as 100% of development (as defined before). Using this normalization, we consider that the whole pupa (i.e, body) development scales uniformly across temperatures (Fig. 19A).

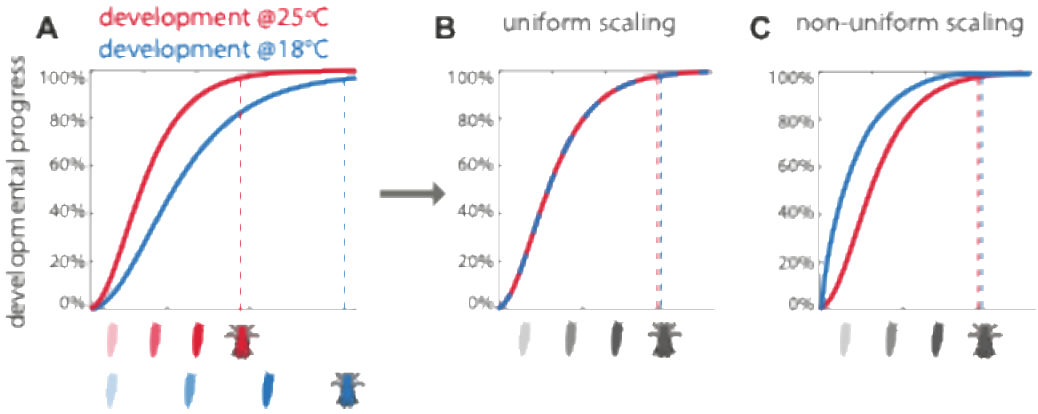

Figure 19. Example of uniform and non-uniform scaling. (A) Hypothetic growth curve showing effects of developmental temperatures in the duration of pupa development. Time of eclosion is indicated by dotted lines. (B) Representation of uniform scaling of a growth curve as in (A), normalized by the developmental time. (C) Representation of non-uniform scaling across developmental temperatures.

The developmental tempo of specific tissues (i.e. brain) may either follow the same uniform scaling, or exhibit non-uniform scaling patterns (Fig. 19B,C). As mentioned before, the model predicts that the increase of synaptic partners at lower temperatures is due to the nervous system progressing at its own, faster developmental rate. This would be in line with the nervous system following a non-uniform scaling in relation to the pupa developmental duration at different temperatures (Fig. 20A,B).

To test this model prediction in the fly, we examined the development of projection neurons (PNs) across pupal stages corresponding to 25%, 50%, and 75% of total pupal duration at 18 °C and 25 °C (Fig. 20C,D) (See Methods, Section 4.2). Previous studies (Jefferis et al., 2001) established that PNs begin to innervate the lateral horn (LH) around 30% of pupal development (30h APF). Consistent with these reports, PNs in flies developed at 25 °C did not reach the LH until after this stage (Fig. 20C'). In contrast, at 18 °C, PN axons were already observed innervating the LH as early as 25% of pupal development (Fig. 20D').

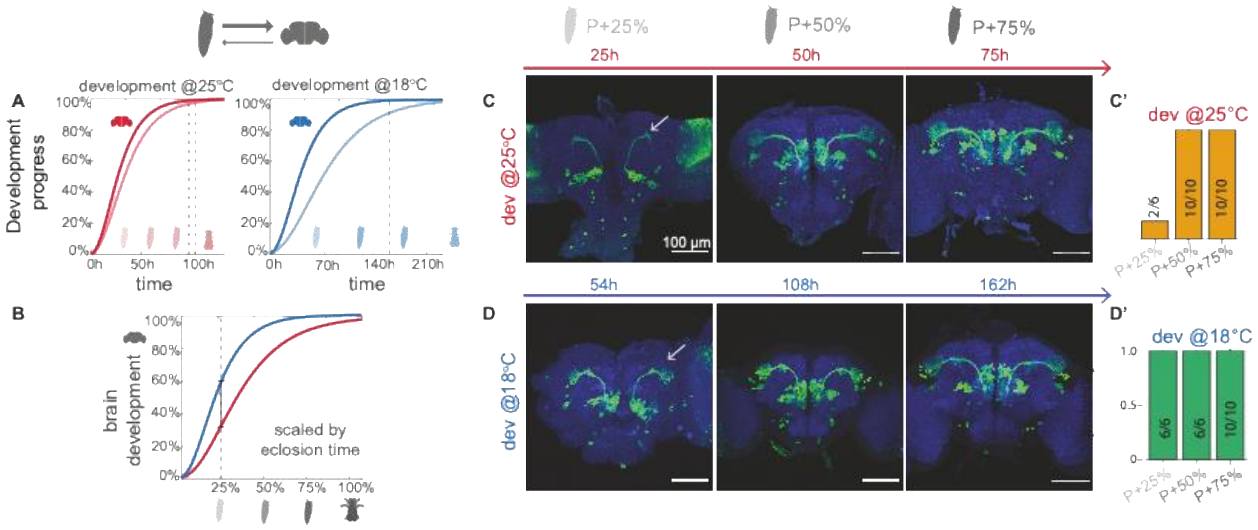

Figure 20. Temporal scaling of projection neurons development across developmental temperatures. (A) Schematics of the growth model showing percentage of development as a function of time for the brain and whole animal at two developmental temperatures. Parameters of the growth dynamics are hypothetical. (B) Brain growth curved scaled by body developmental time. (C) Staining of PNs labeled by *GH146*-Gal4 at three developmental times corresponding to 25, 50, and 75% of pupa development at 25°C. Arrow indicates the lateral horn (LH). (C') Probability that PN axon terminals innervate the LH (n = 6 to 10 hemibrains). (D and D') same as C and C' for 18°C.

These findings indicate that neural development at 18 °C progresses proportionally faster than at 25 °C, providing anatomical evidence that the brain develops slightly ahead of the body under lower temperatures. This supports the idea that neural tissues follow a distinct, non-uniform temporal scaling relative to the rest of the organism – consistent with the model predictions.

5.4 Molecular correlates of temperature-dependent circuit remodeling

The previous sections demonstrated that developmental temperature alters the wiring and function of olfactory circuits, and described evidence suggesting that brain development proceeds faster than overall body development, indicating a non-uniform scaling of brain developmental speed across temperatures. At the same body developmental percentage (25%), projection neurons displayed more advanced branching in the lateral horn at 18°C than at 25°C. However, the molecular basis of this observation remains unclear. This exciting finding

motivated me to test whether molecular regulators of development also scale uniformly – or non-uniformly – with temperature. To address this, I quantified levels of the developmental hormone ecdysone and analyzed gene expression patterns.

5.4.1 Ecdysone signaling regulates gene programs controlling circuit wiring

The duration of pupal development depends on temperature and can be normalized by defining pupariation (P0) as 0% and eclosion as 100% of development. Most biological process are expected to be slower at lower temperature, but we ask how they scale when we normalize the time to the total pupa development. Individual processes may follow the same uniform scaling or exhibit non-uniform scaling patterns (Fig. 21A).

Ecdysone, a steroid hormone derived from cholesterol, regulates developmental transitions in insects. It is converted into its active form, 20-hydroxyecdysone (20E), by the Halloween gene family (Chávez et al., 2000; Gilbert, 2004). 20E binds to the heterodimer of two nuclear receptors, – ecdysone receptor (EcR) and ultraspiracle – inducing downstream genes expression (Beckstead et al., 2005; Song et al., 2003). Among other functions, these target genes regulate wiring programs across the developing visual system, as shown by single-cell RNA-seq of the optic lobe (Jain et al., 2022). Since wiring varied across developmental temperatures, I hypothesized that the expression of these wiring-related genes might also be developmentally shifted, and therefore aimed at quantifying their expression across development at different temperatures.

I first examined whether the temporal dynamics observed in the optic lobe single-cell RNA-seq dataset could be reproducible using whole pupa samples. To this end, I performed RT-qPCR with the assistance of Giovanni D'Uva (See Methods, Section 4.7). We assayed flies developed at 25°C at five developmental time points (25, 30, 40, 50 and 80%). Out of the six genes observed to display the same temporal profile throughout all cells in the developing optic lobes (Jain et al., 2022), we choose four genes (transcription factors) with the most remarkable temporal profiles (*Blimp-1*, *Eip75B*, *Hr3*, and *ftz-f1*). Beyond that, we also selected two other classic ecdysone-inducible genes: *Eip63F-1* (early inducible gene) and *Eip93F* (regulates adult differentiation) (Cruz et al., 2024; Thummel, 2002).

Therefore, six genes downstream of 20E (*Eip63F-1, Hr3, ftz-f1, Blimp-1, Eip93F* and *Eip75B*) were selected for temporal expression quantification and comparison to the RNA-seq dataset.

Code for the analysis of the single cell RNA-seq dataset was kindly provided by Dr. Joachim Fuchs (see methods). Whole-pupa expression profiles recapitulated most of the temporal dynamics previously observed in the developing optic lobe (Fig. 21B). Even though there are a few differences in dynamics, seen in the expression of *Eip63F-1* and *Eip75B*, the overall similarity indicates that the characteristic 20E-driven transcriptional program is also detectable when pooling multiple tissues.

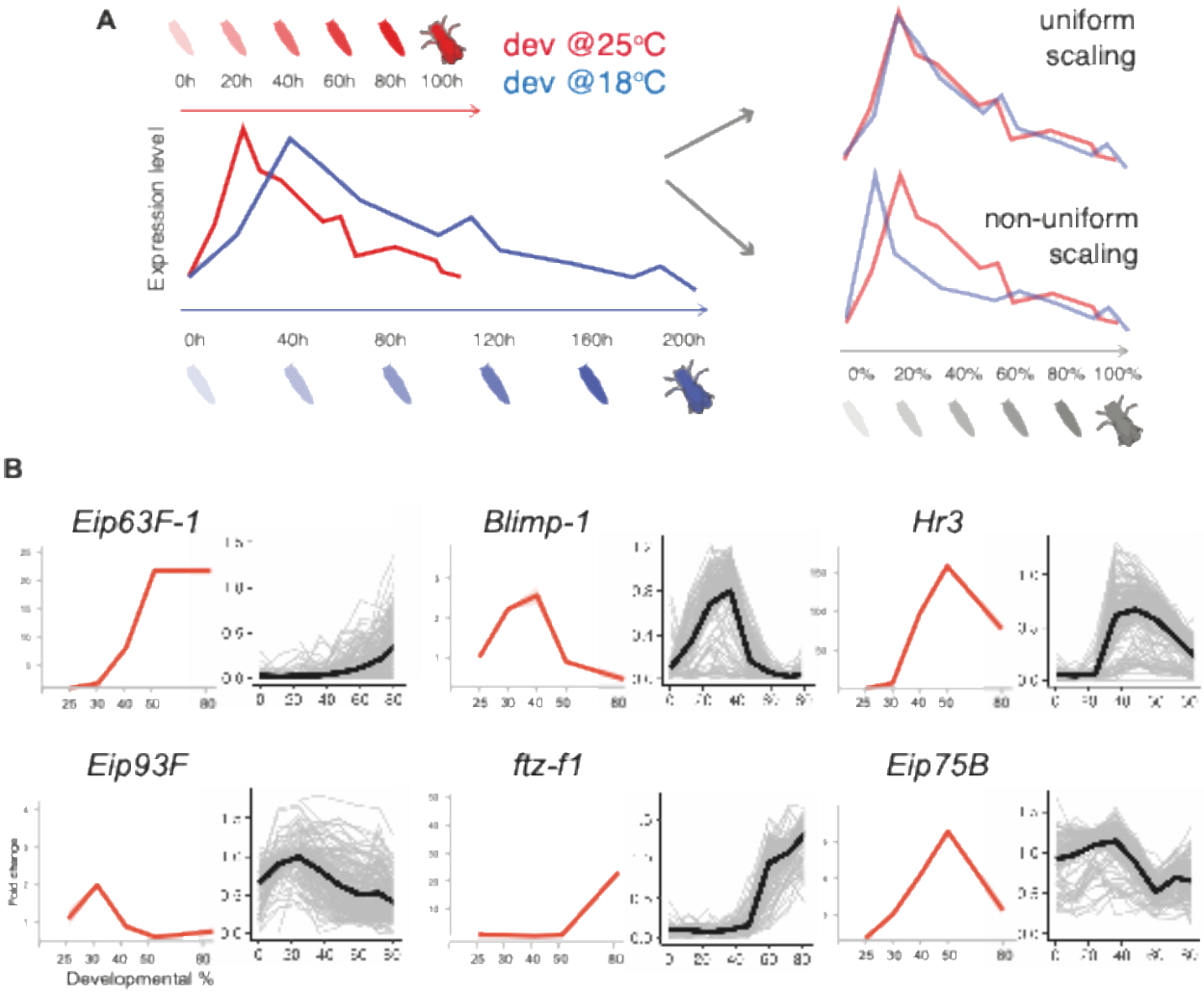

Figure 21. Conceptual model of temperature scaling and validation of ecdysone-responsive gene expression profiles. (A) Schematic representation of possible scaling of gene expression across developmental temperatures (18°C shown in blue, 25°C in red). Gene expression may scale uniformly with total pupal duration or non-uniformly, advancing or lagging relative to normalized developmental time (P0 = 0%, eclosion = 100%). (B) Expression of ecdysone pathway target genes at 25°C throughout pupa development. For each gene: (Left) RT-qPCR profiles from whole pupa, indicating fold change in relation to the first developmental time point; (Right) gene expression in the developing optic lobe, single-cell

RNASeq. Each trace displays the level of gene expression (log(reads)) for each cell cluster, with black line displaying the mean value across cells. Data plotted from (Jain et al., 2022).

Having established this reference profile at 25°C, I proceeded with comparing their temporal profile to pupa developed at 18°C. Samples were collected at corresponding developmental percentages, and two independent biological replicates were analyzed. Expression patterns for each replicate are shown in Figure 22 (top panel). While fold changes differed across replicates, the temporal profiles were consistent– therefore replicates are displayed separately to preserve within-replicate structure.

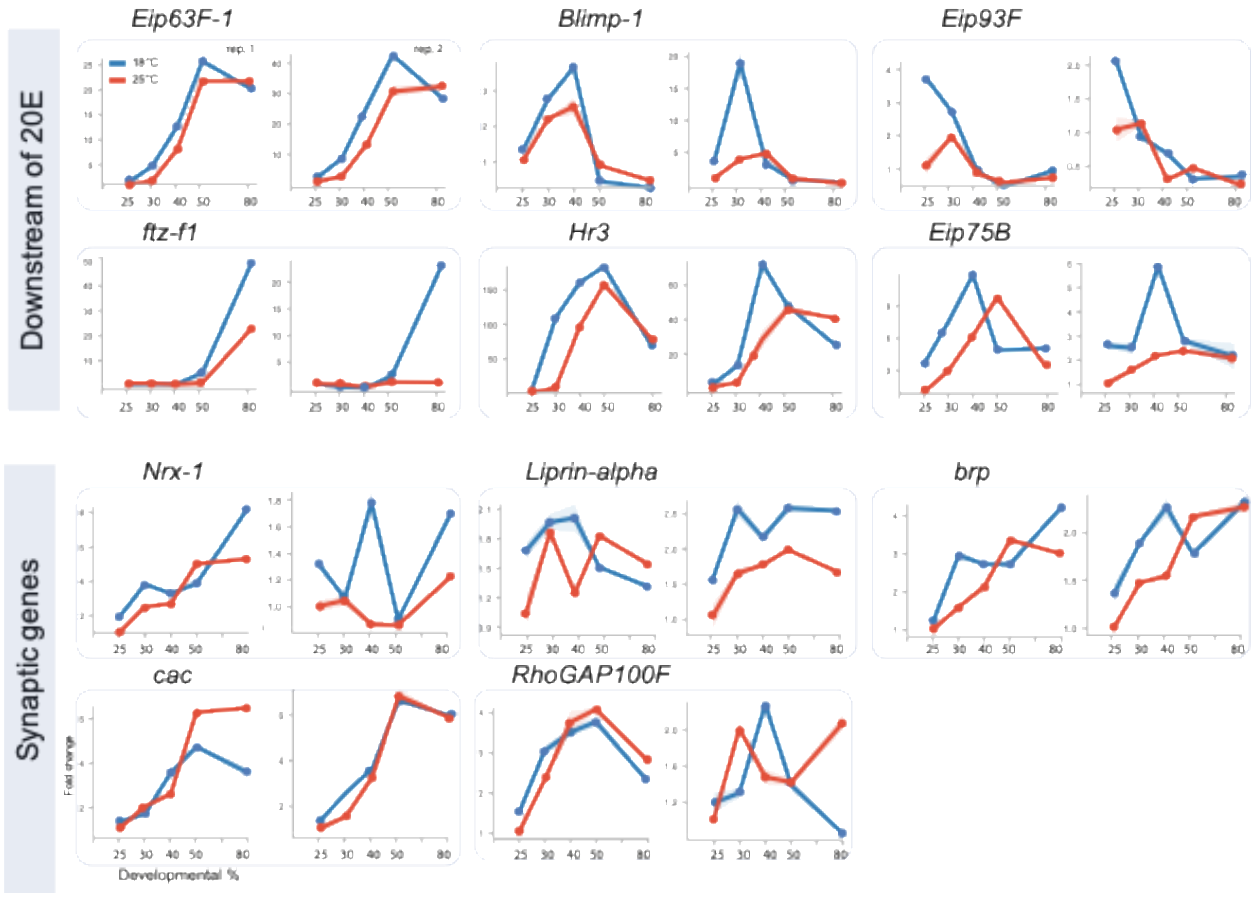

Figure 22. Comparison of temporal gene expression at 18 °C and 25 °C during pupal development. RT-qPCR of whole pupae across development at 18°C (blue) and 25°C (red). Each gene (enclosed by a rectangle) is represented by two independent biological replicates (left and right). Each time point presents three technical replicates for each temperature (represented as points). Fold change in gene expression was calculated using the $2^{-\Delta\Delta CT}$ method (Livak & Schmittgen, 2001), with *Rpl15* as the housekeeping gene. Fold change was calculated in relation to the first developmental time point at 25 °C.

When comparing across temperatures, overall expression levels tended to be higher at 18°C than at 25°C. Moreover, four out of six tested genes (*Eip63F-1, ftz-f1, Hr3,* and *Eip75B*) displayed an earlier increase in expression at 18°C. This result indicates that the activation of some 20E-responsive genes does not scale uniformly with overall pupal developmental timing. Instead, transcriptional activation of these genes appears to occur earlier (relative to body development) at lower temperatures, consistent with the hypothesis of non-uniform temporal scaling.

Since there are more synapses in the DM1 glomerulus at 18°C in relation to 25°C, as previously shown by quantification of BRP (nc82) puncta (Fig. 8C,D), I next examined whether genes involved in synaptogenesis or synaptic function exhibit temperature-dependent differences in expression. I quantified transcript levels of genes associated synaptic seeding (*Liprin-alpha* and *RhoGAP100F*) and synaptic active zones (*Nrx-1*, *brp*, and *cac*).

In contrast to ecdysone-responsive genes, these synaptic genes did not display a clear increase or temporal shift in expression between developmental temperatures (Fig. 22, bottom panel). This finding was unexpected, given the high number of synapses observed in adults developed at 18°C – where upregulation of gene expression might be anticipated. As we quantify synapses in 10 days old adults, this increase might be due to shifts in gene expression after 80% of pupa development – or alternatively this might not be related to gene regulation at the level of transcription but at translation (Formicola et al., 2021; Schuman et al., 2006; Thomas et al., 2014) . More broadly, this indicates that the non-uniform scaling observed for the selected ecdysone pathway genes is not a global feature of all developmental gene programs, but rather a specific property of some pathways, one being the hormonal.

Based on these results, I pursued two complementary approaches. First, I investigated whether the temporal shift observed in genes downstream of ecdysone originated at the level of the hormonal regulator itself. Second, I used bulk RNA sequencing to identify genes across the whole genome that scale uniformly or non-uniformly across developmental temperatures.

5.4.2 Temporal scaling of ecdysteroids levels is conserved across developmental temperatures

To obtain the temporal profile of ecdysone across developmental temperatures, I used liquid chromatography coupled to mass spectrometry (LC-MS/MS) to quantify three ecdysteroids in

a targeted manner. These experiments were done in collaboration with Dr. Martin Schäfer (Xu lab, iomE, JGU). We selected four ecdysteroids for the analysis: ecdysone, 20-hydroxyecdysone (20E), Makisterone A (MaA) and Muristerone A (MuA). 20E is the active form of ecdysone, synthesized from cholesterol and responsible for triggering developmental transitions. Makisterone A, derived from campesterol, is a structural analog of 20E that can also act as a signaling molecule in Drosophila. Muristerone A, another plant-derived analog and not present in flies, was used as an internal standard.

This approach allowed me to test whether the timing or amount of ecdysone differs across developmental temperatures, potentially explaining the non-uniform scaling observed in ecdysone-responsive gene expression.

Shortly, ecdysteroids were quantified in pupae collected at six developmental stages and four rearing temperatures (12, 18, 25 and 31°C) (See Methods, Section 4.6). All animals were kept at 25°C from embryo to pupariation (P0) and subsequently transferred to one of the four test temperatures until the desired developmental stage (20, 35, 50, 65, 80 and 95% of pupa development). Developmental percentages were calculated based on the total pupal duration at each temperature (Fig. 23). Tissues were stored at -80°C until extraction, which was performed by liquid-liquid fractioning with methanol and hexane, followed by solid-phase extraction of apolar compounds on a C18 column (see Methods, Section 4.6). Muristerone A was added as an internal standard during the first extraction step. Quantification of ecdysone, 20E, MaA and MuA was carried out using targeted liquid chromatography coupled to mass spectrometry (LC-MS/MS), with ion selection based on (Lavrynenko et al., 2015). Following mass spectrometry, peaks were manually integrated and normalized to the internal standard for each sample.

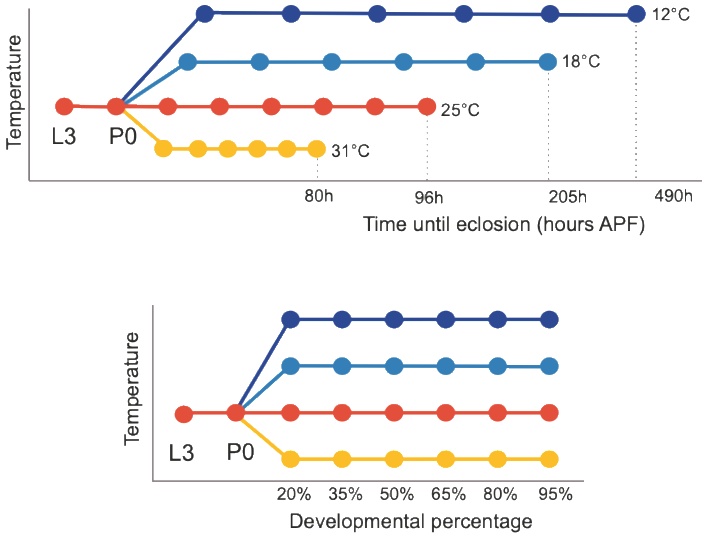

Figure 23. Effect of developmental temperature on pupal development duration and experimental design. Top: Developmental progression of flies reared at four temperatures (12 °C, dark blue; 18 °C, blue; 25 °C, red; 31 °C, yellow), with hours after puparium formation (h APF) shown on the x-axis until eclosion. Bottom: Normalized developmental time expressed as developmental percentage, allowing direct comparison of developmental progression across temperatures. Larval stages (L3) were maintained at 25 °C in all conditions. Pupae (P0) were transferred from 25 °C to the indicated developmental temperatures.

Ecdysone could not be properly quantified in our samples, as in most samples it was not above the detection limit, being confused with noise (not shown). The detection and quantification of the other ecdysteroids, 20E, MaA, and MuA was successful, and we followed with the analysis of those compounds.

Across all temperatures, both 20E and MaA exhibited broadly similar dynamics and appeared to scale uniformly with pupal development. Their concentrations peaked approximately at 35% of development and declined to near zero by 65% of development (Fig. 24) – consistent with previous reports. An exception was observed at 12°C, where both 20E and MaA showed a secondary increase around 80% of development- The cause of this secondary 'peak' remains unclear, but may reflect delayed clearance or altered feedback regulation of ecdysteroid metabolism at very low temperatures.

Temporal profiles of both molecules were generally bell-shaped, with a peak around 35% of development. Higher temporal resolution would be necessary to fully resolve the dynamics of ecdysteroid accumulation and clearance around the peak value. The current sampling interval

of 15% of developmental time likely underestimates subtle differences in peak timing across temperatures.

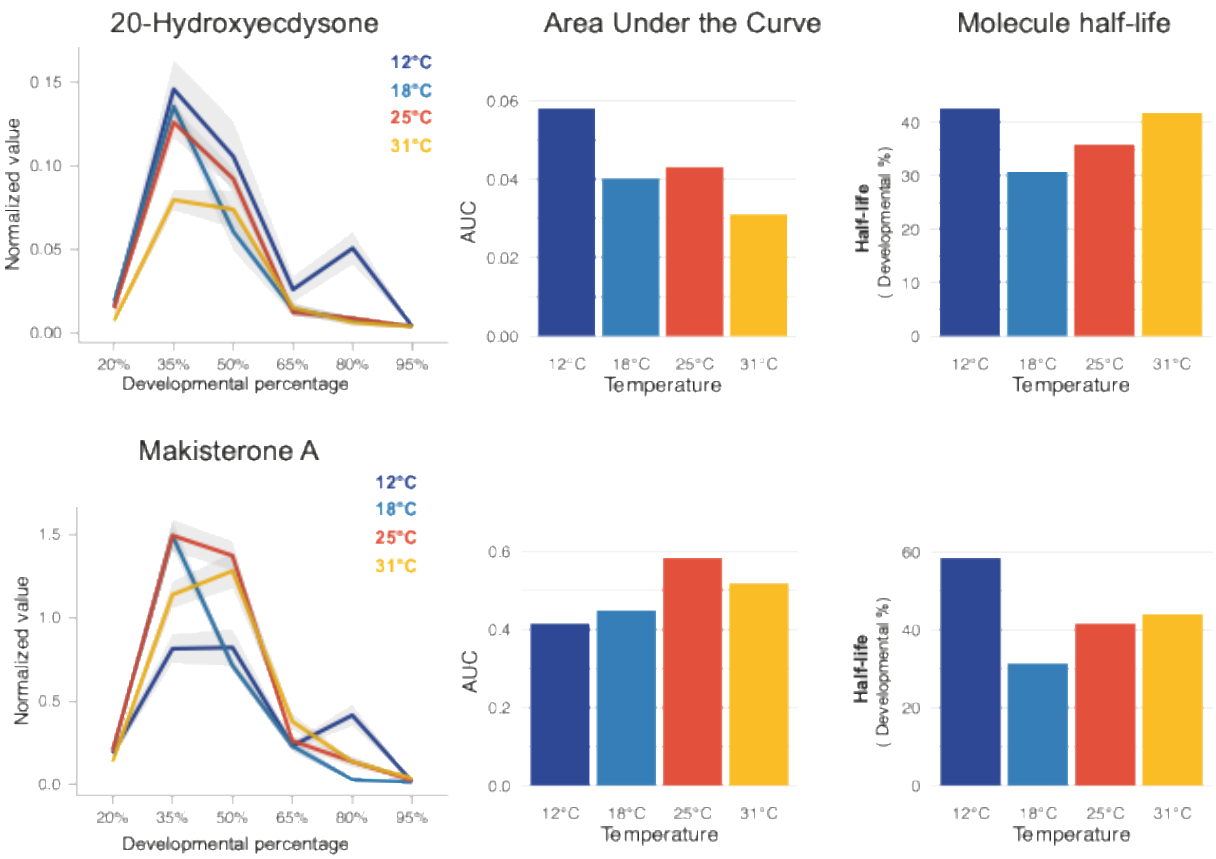

Figure 24. Temporal profiles of ecdysteroids across developmental temperatures. Quantified levels of 20-Hydroxyecdsone (top) and Makisterone A (bottom) in pupae reared at 12, 18, 25 and 31°C. Plots show (left to right) normalized values across across developmental time, area under the curve (AUC) and estimated half-life (percent of pupa development) values for each temperature. Each time point is composed of 6 independent replicates, each containing 6 pooled animals.

To estimate the amount of ecdysteroids produced throughout pupal development, I calculated the area under the curve (AUC) of normalized 20E and MaA levels for each temperature (Fig. 24). For 20E, pupae reared at 12 °C exhibited the highest overall levels – likely reflecting the secondary peak – whereas those at 31 °C had the lowest AUC. In contrast, MaA levels followed an opposite trend, increasing with temperature. These results indicate that developmental temperature differentially affects the abundance of 20E and MaA.

Although both molecules peaked at approximately 35% of development, their rates of decline may vary across temperatures. To assess this, I modeled normalized 20E and MaA levels as an

exponential decay over developmental time using nonlinear regression. I first fit a general decay model, then allowed temperature to modulate the decay rate, and finally fit separate models for each temperature. Each fit estimates a time decay constant (k), which I converted into half-life values ($\log_2/k$). Because samples represented independent populations at each developmental time point, the estimated decay parameters describe population-level dynamics rather than repeated measures from the same individuals.

For both 20E and MaA, pupae reared at 18°C showed the smallest half-life value, indicating a faster decline in its levels relative to other temperatures. Overall, 20E displayed an apparent similar temporal pattern across temperatures, suggesting that the overall coordination of body development remains conserved. This contrasts with the earlier increase of ecdysone-responsive genes observed in the RT-qPCR experiments, implying that the transcriptional shift is unlikely to arise directly from changes in ecdysteroids concentration. Instead, it could reflect temperature-dependent modulation of other regulatory downstream processes or tissue-specific transcriptional regulation.

5.4.3 Temporal scaling of gene expression across developmental temperatures

To investigate temperature-dependent transcriptional dynamics during pupal development, we performed bulk RNA sequencing (RNA-seq) of whole pupa across four rearing temperatures (12, 18, 25 and 31°C) and six developmental times, corresponding to those used for ecdysteroid quantification. In addition, samples from the late third instar (L3 wandering stage) and pupariation (P0) were included to capture the gene expression dynamics prior to temperature treatment. RNA extraction and RNA sequencing was performed by Novogene (See Methods, Section 4.8). Sequencing preprocessing, cleaning and preparation of the DESEq2 object was done by Dr. Federico Marini (see Methods, Section 4.8).

5.4.3.1 Validation of ecdysone-related gene expression by qPCR

I first compared the temporal gene expression profiles obtained by RT-qPCR with those derived from the RNA-seq dataset RNASeq. Although the two methods measure expression differently (fold change for RT-qPCR and normalized read counts for RNA-seq), most genes downstream of 20E presented similar temporal dynamics across 18 and 25°C in both datasets (Fig. 25).

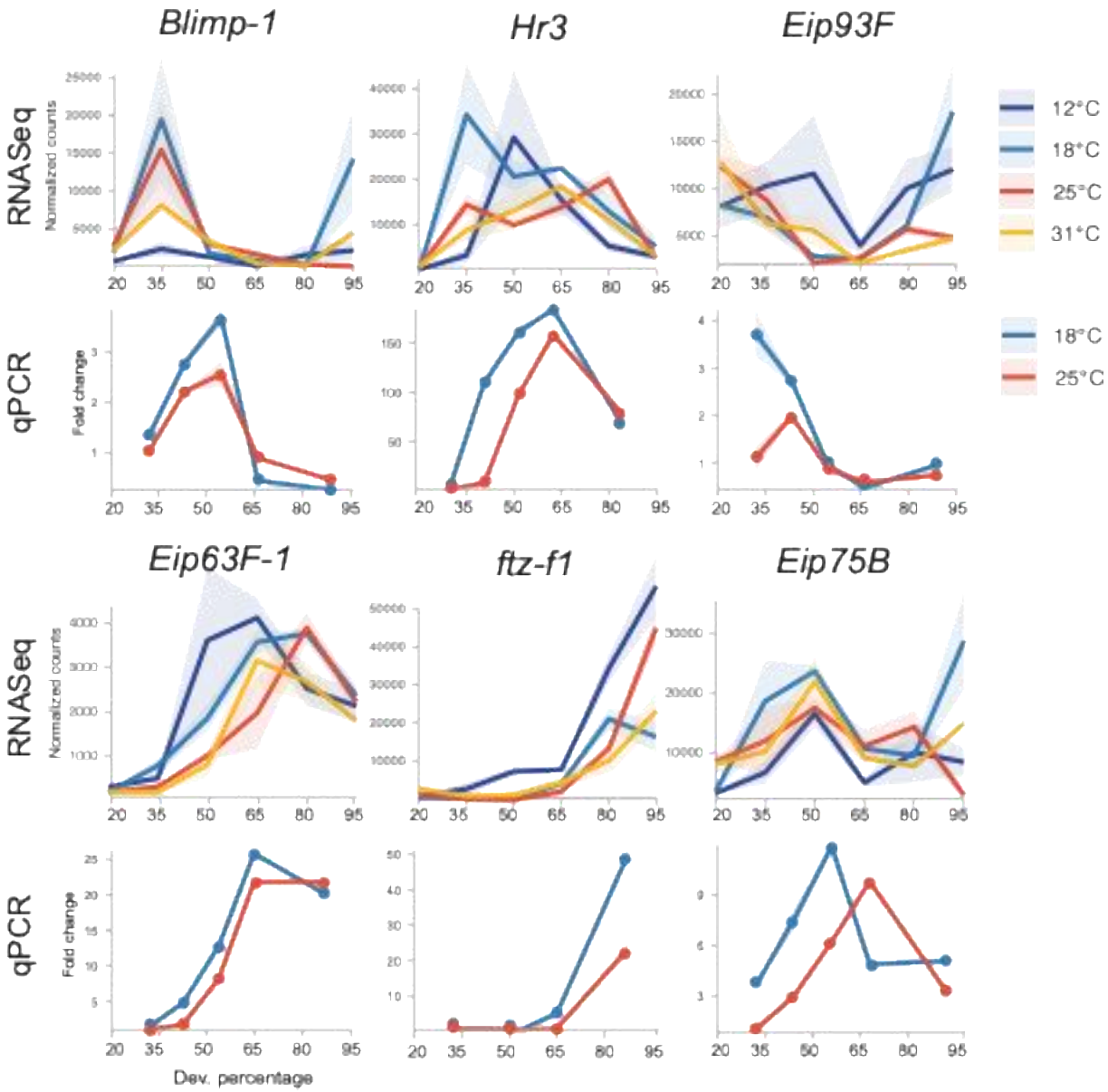

Figure 25. Comparison of RNA-seq and RT-qPCR temporal profiles for ecdysone downstream genes across developmental temperatures. Temporal expression patterns of ecdysone downstream genes obtained from RNA-seq (reads normalized by library size) and RT-qPCR (fold change in relation to first time point of 25°C). Developmental stages correspond to 20%, 35%, 50%, 65%, 80%, and 95% of pupal development for RNA-seq, and 25%, 30%, 40%, 55%, and 80% for RT-qPCR. Colors indicate rearing temperature: dark blue, 12 °C; blue, 18 °C; red, 25 °C; orange, 31 °C.

Specifically, *Eip63F-1, Hr3* and *ftz-f1* showed an earlier increase in expression at 18°C relative to 25°C in both assays, consistent with a possible temperature-dependent acceleration of their transcriptional activation.

I then examined the temporal dynamics of those genes across all four temperatures (12, 18, 25 and 31°C). Among the genes tested, *Eip63F-1* and *ftz-f1* displayed the clearest temporal profiles, with *Eip63F-1* peaking during mid-pupal development and *ftz-f1* showing a marked increase towards the end of metamorphosis. For both genes, lower temperatures were associated with an apparent earlier rise in expression, followed sequentially by higher temperatures. This pattern may indicate that transcriptional programs responding to ecdysone pulses are temporally shifted depending on developmental rate. For *Eip63F-1* and *ftz-f1* we can see that for 12 and 18°C, there is an earlier increase in expression, followed by the 25 and 31°C. *Eip63F-1* encodes an ecdysone-inducible transcription factor involved in developmental timing and neuronal differentiation (Berndt et al., 2015; Syed et al., 2017), whereas *ftz-f1* encodes a nuclear receptor that regulates late ecdysone-response genes during tissue maturation and metamorphic transitions (Broadus et al., 1999; Woodard et al., 1994). These genes therefore serve as broad indicators of developmental progression but are not tissue-specific, limiting our ability to distinguish differences between neural and non-neural developmental scaling across temperatures.

Together, these analyses confirm the temperature-dependent expression dynamics of ecdysone-responsive genes and demonstrate strong agreement between the RT-qPCR and RNA-seq datasets.

5.4.3.2 Expression dynamics of olfactory system genes

The development of projection neurons exhibited a non-uniform temporal shift between 18 °C and 25 °C (as shown in Section 5.3.1). To determine whether a similar temperature-dependent effect occurs in olfactory receptor neurons (ORNs), I examined the temporal expression profile of the odorant coreceptor *Orco*. *Orco* is expressed exclusively in olfactory sensory organs and serves as a reliable molecular marker for ORN development.

Orco expression increased progressively throughout pupal development at all temperatures (Fig. 26A). Across temperatures, its temporal dynamics followed the predicted non-uniform scaling pattern, with transcription rising first at 12 °C, followed by 18 °C, 25 °C, and 31 °C. These results provide clear evidence that developmental temperature modulates the timing of *Orco* expression, revealing a measurable shift in the onset of ORN differentiation even within bulk RNA-seq data.

To explore this further, I examined individual odorant receptor (*Or*) genes to assess whether they showed similar temperature-dependent trends. Most OR genes exhibited low read counts (fewer than 100 normalized reads), consistent with their expression in a limited number of antennal neurons and with their expected late onset during pupal development. To test for overall temperature effects, I pooled expression values across developmental stages for each temperature and performed a Kruskal–Wallis test followed by Dunn's post-hoc pairwise comparisons with Bonferroni correction. Out of the 34 *ORs* analyzed, six (*Or22b, Or1a, Or42a, Or71a, Or85c,* and *Or19b*) showed significant temperature-related differences in expression (Fig. 26B). However, given their low expression levels and lack of consistent directionality, these differences might reflect sampling variability rather than a robust temperature effect.

In addition to odorant receptors, several ionotropic receptors (*Irs*) contribute to olfactory detection. Most *Ir* genes exhibited similar temporal expression levels and dynamics across all four temperatures. Some ionotropic receptors (IRs) also act as co-receptors, analogous to *Orco*. I therefore examined the expression of IR co-receptors known to contribute to different sensory modalities: *Ir8a* (olfaction), *Ir93a* (thermosensation), and *Ir25a* and *Ir76b* (thermosensation and gustation). Among these, *Ir25a* showed the highest overall expression levels but displayed a distinct temporal pattern compared to *Orco*. Specifically, *Ir25a* transcripts tended to be higher at 12 °C and 18 °C than at 25 °C and 31 °C, although these differences were not statistically significant. The remaining IR co-receptors showed no notable temperature-dependent changes in transcript levels (Fig. 26C).

Overall we conclude that while global ORN development timing shifts with temperature, the expression of individual receptor subtypes remains largely stable – or not detectable through bulk RNA-seq.

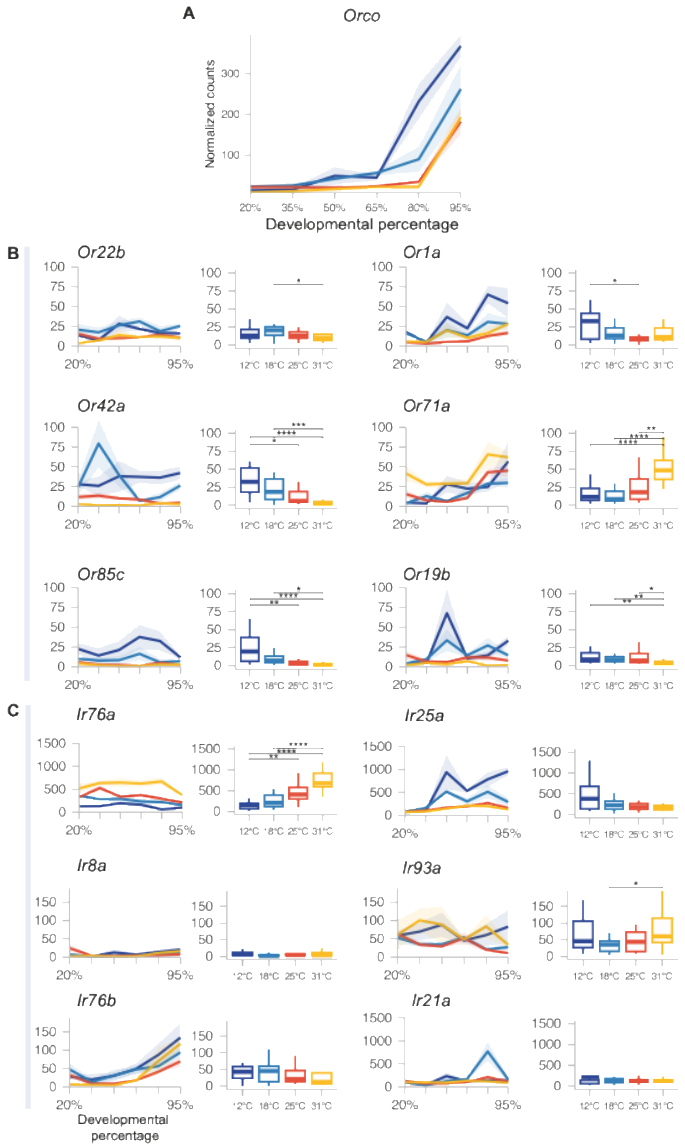

Figure 26. Temporal expression profiles of olfactory and ionotropic receptor genes across developmental temperatures. (A) Temporal expression profile of the odorant coreceptor *Orco* across four developmental temperatures. (B) Temporal dynamics (left) and total expression (right, represented as area under the curve, AUC) of individual odorant receptor (OR) genes. (C) Ionotropic receptors (IRs) analyzed in the same manner, including co-receptors involved in olfaction (Ir8a), thermosensation (Ir93a), and thermosensation/gustation (Ir25a and Ir76b). Colors indicate rearing temperature: dark blue, 12 °C; blue, 18 °C; red, 25 °C; orange, 31 °C. Statistical differences in AUC were assessed using a Kruskal–Wallis test followed by Dunn's post hoc pairwise comparisons with Bonferroni correction. Asterisks denote significance levels (* $p < 0.05$; **$p < 0.01$; **** $p < 0.0001$).

5.4.3.3 Expression of genes involved in energy metabolism (glycolysis, TCA cycle and electron transport chain)

From the model, we infer that the metabolically limiting rates of brain and body may differ across developmental temperatures. Motivated by this potential metabolic mismatch, I next examined the overall expression patterns of genes involved in central energy metabolism: glycolysis and the tricarboxylic acid (TCA) cycle. Glycolysis is a process that happens in the cell cytoplasm, and consists in transforming glucose into Pyruvate through 11 enzymes. Remarkably, all genes coding for those glycolytic enzymes were upregulated at lower developmental temperatures, starting to rise earlier in development at 12°C, followed by 18, 25 and 31°C (Fig. 27). The concurrent increase in glycolytic enzymes suggests enhanced availability of pyruvate for entry into the TCA cycle.

The pyruvate formed through glycolysis is then metabolized into Acetyl-CoA, which is transported from the cytoplasm to the mitochondrial matrix to fuel the tricarboxylic acid cycle (TCA). In the mitochondrial matrix, the TCA cycle produces NADH that will be used to transfer electrons to the electron transport chain (ETC), finally generating ATP. All enzymes in the TCA cycle were also upregulated at lower developmental temperatures, similarly to glycolysis enzymes.

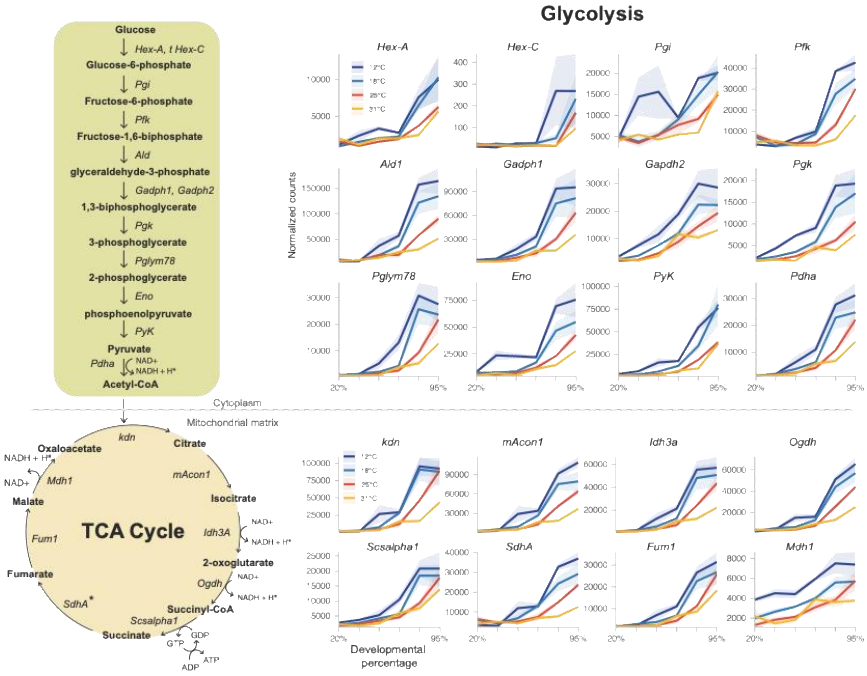

Figure 27. Coordinated upregulation of glycolytic and TCA cycle enzymes across developmental temperatures. Bulk RNA-seq data showing temporal expression patterns of

key enzymes in glycolysis (top) and the tricarboxylic acid (TCA) cycle (bottom) across pupal development. Expression levels increase earlier and reach higher values at cooler developmental temperatures (12 °C and 18 °C) compared with warmer conditions (25 °C and 31 °C), suggesting temperature-dependent enhancement of metabolic activity. Temperature color scheme: dark blue, 12 °C; blue, 18 °C; red, 25 °C; orange, 31 °C.

The mitochondrial electron transport chain (ETC) is a central component of oxidative phosphorylation process (OXPHOS). It consists of four main electron-transporting complexes (complexes I-IV) and ATP synthase (complex V). Electrons flow from NADH and FADH2 through complexes I and II to ubiquinone, then to complex III, cytochrome c and finally complex IV, where they reduce molecular oxygen – the terminal electron acceptor of the chain. As a result of this transport, complex I, III, and IV pump protons from the mitochondrial matrix to the intermembrane space, generating a proton motive force that is then used to generate ATP at the level of complex V (ATP synthase).

Following up on this, I next observed the transcription of genes of the core subunits of each complex. All core subunits of the ETC had a remarkable increase in gene expression similar to glycolysis and TCA cycle (Fig. 28), increasing first throughout development at 12°C, followed by 18°, 25° and 31°C.

The parallel upregulation of TCA and ETC components indicates that oxidative phosphorylation is also elevated, potentially leading to greater ATP production in pupae developing at lower temperatures. This pattern could reflect compensatory metabolic adjustments to maintain energy homeostasis under cooler conditions. For example, flies acclimated at 15°C show the highest activity of key metabolic cycle enzymes (hexokinase, glucose-6-phosphate dehydrogenase and cytochrome oxidase) when assayed at 25°C, compared with flies acclimatized at 25°C or 30°C (Burnell et al., 1991).

Cold acclimation reshapes both metabolome and transcriptome in adults (MacMillan et al., 2016). Flies lean harder on glycolysis during acute cold stress (Enriquez & Colinet, 2019; Williams et al., 2014). This is consistent with metabolomic quantifications of flies either developed or adapted to lower temperatures, in which sugars and classic energy-carrying molecules (NAD, NADP and AMP) are depleted (Hariharan et al., 2014; Schou et al., 2017). This could indirectly also indicate that at lower temperatures the pathways involved with those molecules (mostly glycolysis and TCA cycle) do not have only more transcripts, but are more active.

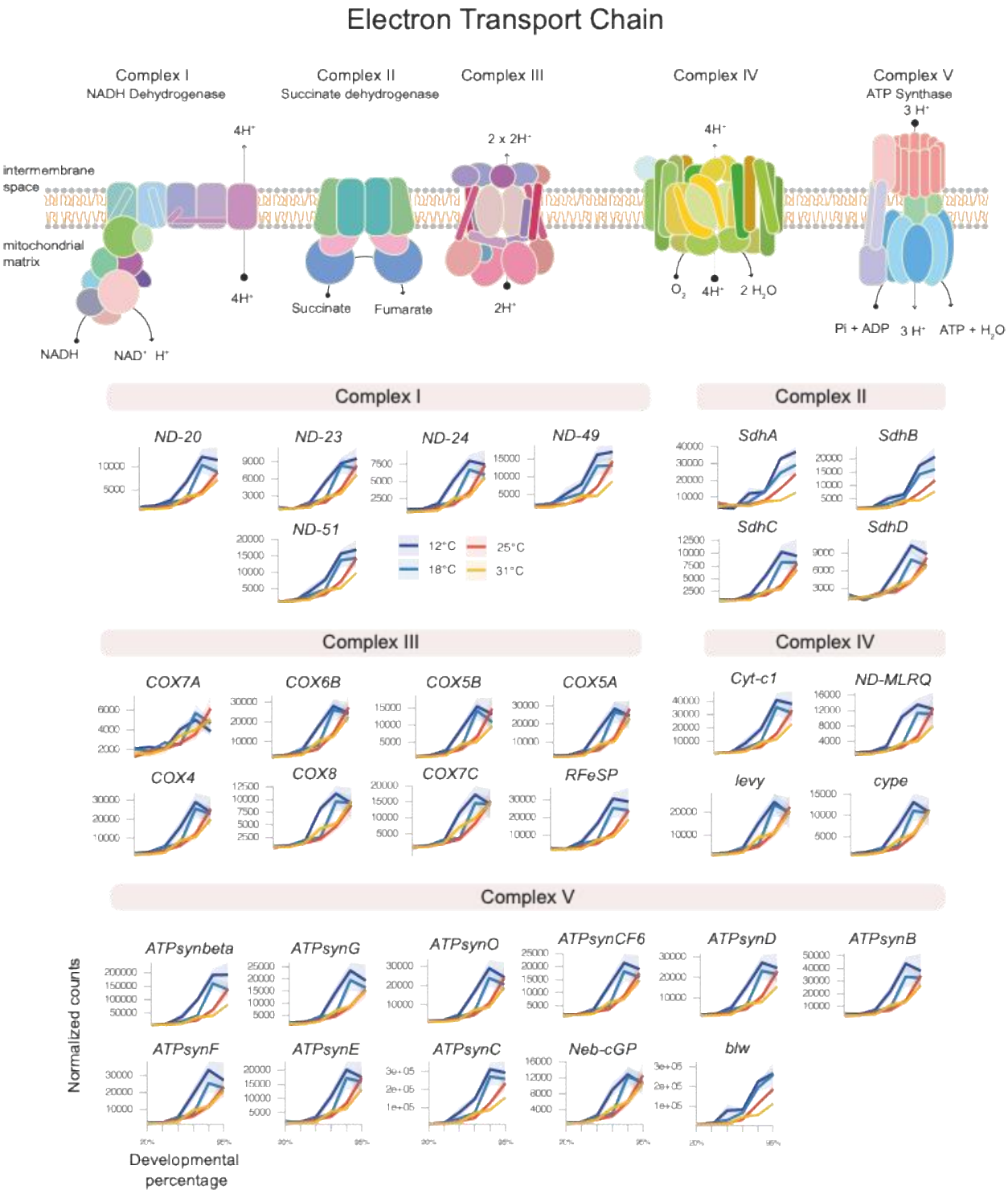

Figure 28. Coordinated upregulation of electron transport chain genes across developmental temperatures. Top: Schematic diagram of the electron transport chain showing its five major complexes (from left to right): Complex I (NADH dehydrogenase), Complex II (succinate dehydrogenase), Complex III, Complex IV, and Complex V (ATP

synthase). Each complex consists of core catalytic subunits and additional accessory components. Complex II is also of the tricarboxylic acid (TCA) cycle. The electron transport chain uses reducing equivalents (NADH) generated by the TCA cycle to drive proton translocation across the inner mitochondrial membrane, establishing an electrochemical gradient that powers ATP synthesis by Complex V. The ETC is located between the mitochondrial matrix and the intermembrane space. Bottom: Coordinated upregulation of electron transport chain core subunits across developmental temperatures, separated by ETC complex. Expression levels increase earlier and reach higher values at cooler developmental temperatures (12 °C and 18 °C) compared with warmer conditions (25 °C and 31 °C), suggesting temperature-dependent enhancement of metabolic activity. Temperature color scheme: dark blue, 12 °C; blue, 18 °C; red, 25 °C; orange, 31 °C.

On the other extreme, hot-evolved flies have lower baseline expression of TCA, glycolysis and oxidative phosphorylation (OXPHOS) genes than cold-evolved flies (Mallard et al., 2018). Similar decrease was also reported in transcriptomics of hot-evolved flies under fluctuating warm regimes (Aggarwal et al., 2025) and proteomics of flies developed at 31°C (Kristensen et al., 2019). Therefore, the increased transcripts at lower temperatures could indicate an 'adaptation' to the lower kinetics that the flies face during development.

5.4.3.3.1 Expression of mitochondrial-encoded electron transport chain genes

Only a few mitochondrial-encoded genes were detected in the dataset, all corresponding to ETC subunits. Interestingly, their expression profiles at 31°C followed a different dynamics than the expected from the previously shown nuclear encoded ETC genes (Fig. 29). Flies developing at 31°C presented an increase in the expression of those genes, which was not seen in the nuclear encoded ETC enzymes (Fig. 28). However, other temperatures followed a similar pattern as before. This divergence could reflect either temperature-specific disruption of mitochondrial transcription or an independent regulatory mechanism distinct from nuclear gene control.

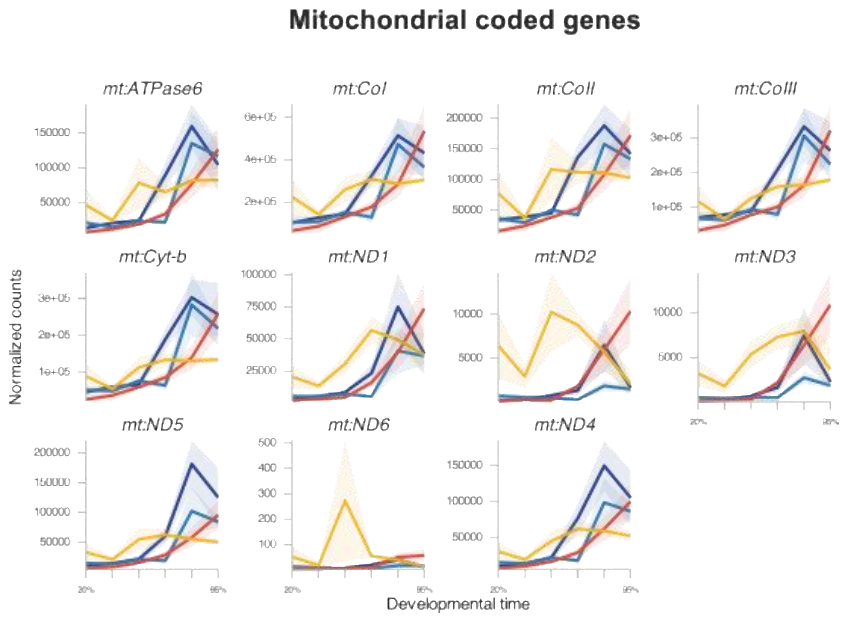

Figure 29. Expression of mitochondrial-encoded electron transport chain (ETC) genes across developmental temperatures. RNA-seq expression profiles of mitochondrial-encoded ETC genes are shown across developmental time. The x-axis represents developmental time, and the y-axis indicates normalized gene counts (adjusted by library size). Colors correspond to developmental temperatures as in previous figures (12 °C, dark blue; 18 °C, blue; 25 °C, red; 31 °C, yellow). At 31 °C, expression increases earlier in development compared to other temperatures, a pattern not observed for nuclear-encoded ETC genes in Figure 28.

5.4.4 Expression of genes involved in lipid metabolism (β-oxidation and lipogenesis)

To understand if other main metabolic pathways had the same pattern in expression across developmental temperature, I next investigated pathways associated with lipid metabolism. Both β-oxidation (in which fat acids are oxidized into Acetyl-CoA, used in the TCA cycle) and *de novo* lipogenesis (which produces new triacylglycerides) showed less pronounced temperature-dependent effects (Fig. 30). From the enzymes in these pathways, only *Acsl* and *Gdph1* exhibited similar profile as glycolysis and TCA cycle enzymes.

*Acsl (*Acyl-CoA synthetase long-chain*)* is important in the first step of β-oxidation, catalyzing the breakdown of fatty acids into Acyl CoA. The resulting Acyl CoA can be used for lipid synthesis, fatty acid degradation or membrane lipid remodeling (Mashek et al., 2007). Interestingly, *Acsl* regulates the composition of fatty acids and membrane lipids, which affects neuromuscular junction synapse development (Huang et al., 2016). *Acsl* also regulates axonal

transport of synaptic vesicles and is required for synaptic development and transmission (Liu et al., 2011).

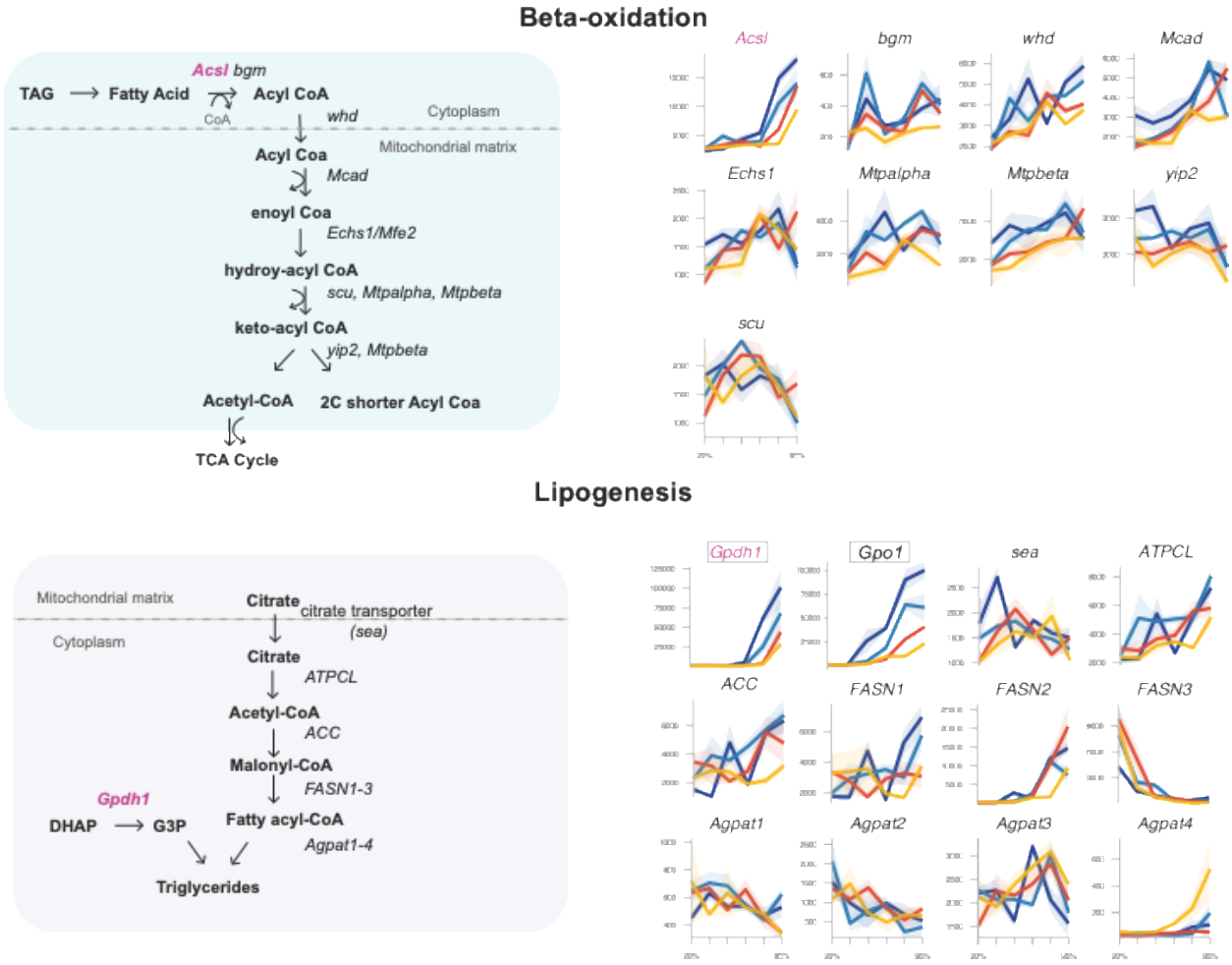

Figure 30. Temporal expression of genes involved in lipid metabolism across developmental temperatures. Top: β-oxidation pathway. Left: schematic overview of the β-oxidation process. Right: RNA-seq expression profiles of β-oxidation genes, with normalized gene counts (y-axis) plotted over developmental time (x-axis) for each temperature. Bottom: Lipogenesis pathway. Gene names with a grey box around (*Gpdh1* and *Gpo1*) are also involved in ETC ions shuttling.

Gpdh1 (glycerol-3-phosphate dehydrogenase 1) generates glycerol-3-phospate (G3P), which can be used in triacylglycerol synthesis in the fat body and as an oxidative substrate for electron transport in the adult flight muscle (Li et al., 2019; Merritt et al., 2006; Wojtas et al., 1997). In the latter, GP3 is used to shuttle electrons into the ETC for ATP synthesis. This is done in conjunction with the mitochondrial enzyme glycerophosphate oxidase 1 (GPO1), and supports the intense energy demands of insect flight (Carmon et al., 2010; Merritt et al., 2006; O'Brien

& Shimada, 1974). *Gpo1* expression pattern follows a similar temporal profile as *Gpdh1*, which could suggest that both enzymes are being co-regulated, increasing the outcome of the same pathway. This way, the upregulation of Gpdh1 and Gpo1 would also contribute to the generation of ATP.

Distinguishing whether this overall increase in energetics metabolism represents a true global metabolic increase or an earlier activation of developmental programs would require also sequencing flies after eclosion, for later time points. Given that the current time points finish at 95% of development, it remains unclear whether the elevated expression at low temperatures reflects a sustained upregulation or a temporal shift preceding comparable expression levels at higher temperatures. Moreover, tissue-specific transcriptomics and proteomics could be used to determine the effect of temperature across tissues. Such dataset would also allow to disentangle temporal aspects of gene regulation from proper gene upregulation, giving more insight into the metabolic constraints different tissues are subject to.

5.4.5 Expression of genes involved in heat and cold stress responses

A classic example of temperature in gene expression is the activation of heatshock proteins (Hsp) genes upon exposure to high temperatures, with the *Hsp70* and *Hsp90* families the most prominent (Feder et al., 1997; Mirault et al., 1978). Those proteins are chaperones, buffering environmental stresses by being involved in protein homeostasis. In *D. melanogaster*, expression of Hsp genes is not only rapidly up-regulated under environmental stresses, but is also regulated during normal development (Mason et al., 1984; Pauli et al., 1989). For example, *Hsp68* and *Hsp70* are expressed at very low levels in most developmental stages, but they are at higher concentration in pupae (Mason et al., 1984). Hsps are mostly present in the nucleus, endoplasmatic reticulum and cytosol (Li & Srivastava, 2004; Mayer & Bukau, 2005). In Drosophila, specific Hsp isoforms are mitochondrial chaperones (*mtHsp70*, *Hsp60*, *Hsp10*, and *Hsp22*) (Böttinger et al., 2015; Morrow et al., 2016; Voos & Röttgers, 2002) .

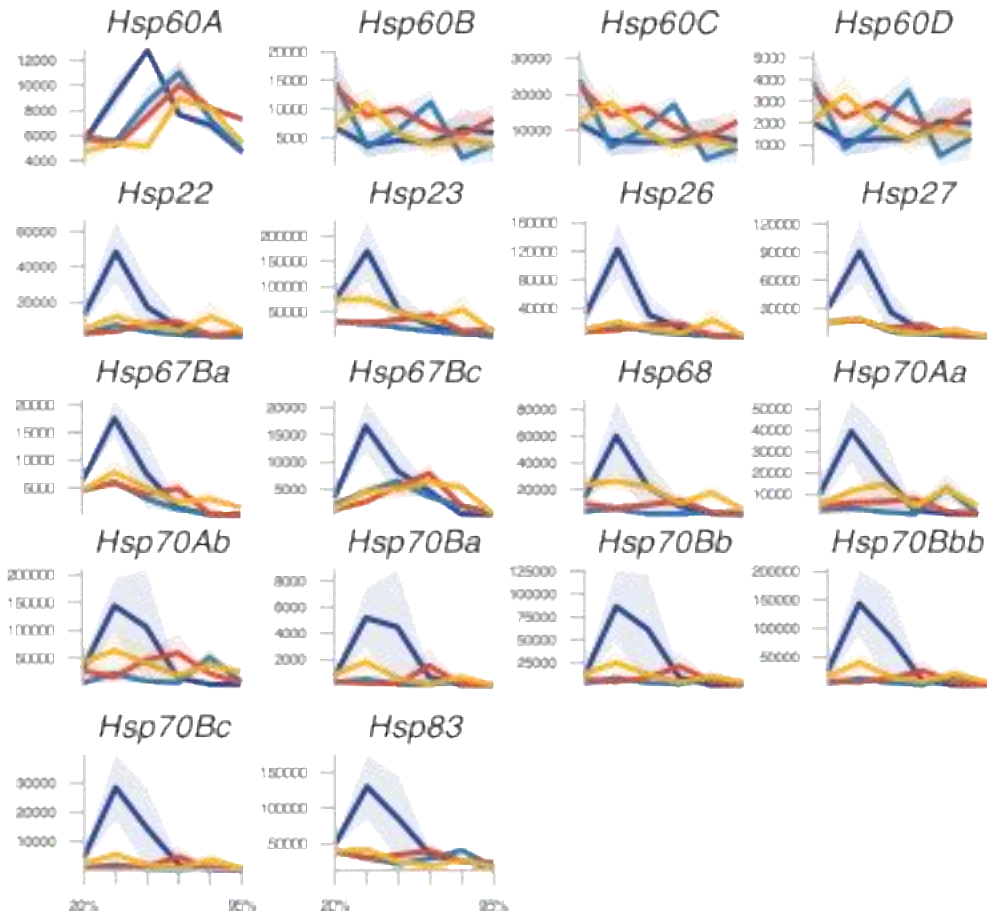

Figure 31. Temporal expression of heat shock protein genes is mostly upregulated at lower temperatures. Expression of heat shock protein genes across development and temperatures, with normalized gene counts (y-axis) plotted over developmental time (x-axis) for each temperature.

Therefore, we next analyzed all Hsp genes present in our dataset (Fig. 31). Most Hsp genes were impacted by temperature, with *Hsp60A* having a temporal dynamics with a peak of expression that shift in time from 12°C, to 31°C – similar to what was observed with metabolic genes. Only a few Hsp genes did not present a temperature related phenotype (*Hsp60B*, *Hsp60C* and *Hsp60D),* which has also been reported in a previous study (Chen et al., 2015b).

Intuitively, one would expect that most Hsp genes would be mostly expressed at higher temperatures (31°C). However, most of those genes were expressed the highest at 12°C during development, and not at 31°C (Fig. 31). This effect is in agreement with previous studies, which have shown that from the 15 temperature related Hsp genes we have in the dataset, 12 of those have been described to be Hsp genes that can be cold induced (Colinet et al., 2010; MacMillan et al., 2016; Qin et al., 2005).

Hsp60A shows the most interesting dynamics possibly of relevance for developmental coordination across the full range of viable temperatures. Hsp60A is a mitochondrial chaperone, with a role in normal Drosophila development, most notably in the embryo (Baena-López et al., 2008). Mitochondrial chaperones ensure oxidative phosphorylation is functional during cold exposure in insects, and their activity is linked to ROS management (Lubawy et al., 2022) and mitochondrial DNA replication and transmission (Jebara et al., 2017). Therefore, Hsp60A (rather than other broad cytosolic Hsps) could be more sensitive to changes in temperature during pupa development – relaying the appropriate modulation of oxidative phosphorylation in accordance to the temperature.

6 Discussion

In insects, temperature strongly modulates brain development during metamorphosis, a stage characterized by extensive neural growth and circuit reorganization. Perturbations in pupal temperature can alter the development and connectivity of neural circuits, resulting in persistent behavioral effects. Holometabolous insects thus serve as a powerful model for understanding how environmental variables are integrated into developmental programs to produce stable yet adaptable neural circuits.

Here, we propose that if developmental speed is constrained by varying metabolic reactions across cell types, then temperature manipulation could potentially disrupt the temporal coordination of their developmental programs. We demonstrate that this temporal mismatch can explain the change in neural growth and connectivity induced by developmental temperature. Although temperature shapes odor-driven behavior, it does not alter odor responses or sensitivity across glomeruli. Odor encoding is therefore preserved, even as network connectivity is scaled. In contrast, the organization of inputs onto LH neurons is modified, with possible consequences for behavior.

At the molecular level, we find that this rewiring does not arise from major changes in systemic developmental timing cues. Ecdysteroid hormone dynamics remain broadly conserved across temperatures. In contrast, downstream ecdysone-responsive transcription factors and metabolic gene programs are advanced at lower temperatures, revealing temperature-dependent modulation of transcription during development. While the endocrine dynamics appear largely conserved across temperatures, temperature-dependent shifts in transcriptional and metabolic timing may contribute to differences in developmental progression across tissues.

6.1 Temperature-dependent modulation of neural connectivity during pupal development

My investigation shows that developmental temperature exerts a strong and systematic influence on the formation and organization of synaptic connections in the olfactory system. Flies reared at lower temperatures develop more ORN synaptic partners (see Section 5.1.1), accompanied by an increase in presynaptic active zones (5.1.2) and mitochondrial content (5.1.3), suggesting enhanced synaptic capacity and metabolic support. These effects are not restricted to a single glomerulus but follow a consistent scaling across multiple olfactory

channels (5.1.4) and temperature ranges (5.1.5), pointing to a general developmental principle governing temperature-dependent wiring.

Collectively, prior studies have framed the effects of developmental temperature on neural wiring primarily through the lens of activity-dependent growth, with elevated temperatures often associated with synaptic or axonal overgrowth in both peripheral and central circuits. Developmental temperature has been shown to influence synaptic growth and organization across multiple neural systems, although the direction and underlying mechanisms of these effects vary by circuit and context. At the larval neuromuscular junction (NMJ) in Drosophila, the number of synaptic boutons increases when animals are reared at elevated temperatures (25–29°C or 32°C) (Sigrist et al., 2003). Importantly, this increase was interpreted not as a direct thermal effect on synaptogenesis, but rather as a consequence of increased neuronal activity at higher temperatures, leading to activity-dependent synaptic growth. Instead, our data indicate that developmental temperature acts as a developmental parameter that constrains wiring outcomes (see Section 5.3), revealing latent variability in circuit organization that is not captured by models based solely on neuronal activity or excitability.

Temperature-dependent modulation of neuronal growth has also been observed in central brain circuits. In larva, elevated temperature induces overgrowth of MB nerve terminals in the CNS, resembling the synaptic expansion seen at the peripheral NMJ (Sigrist et al., 2003; Zhong & Wu, 2004). In temperature manipulations in adults, axonal arborization of MB Kenyon cells is enhanced when flies are exposed to higher temperatures (30°C compared to 22°C), from 1 to 6 days post-eclosion (Peng et al., 2007). In the antennal lobe ORNs, developmental temperature modulates growth in a different way, with overgrowth of DM1-ORNs at lower developmental temperatures, instead of higher ones. One possible explanation for these differences is the timing of the temperature manipulation. In our data, temperature was manipulated exclusively during the pupal stage, a developmental period during which the animal is an energetically closed system. As a result, temperature acts directly on developmental processes, without secondary effects arising from changes in behavior or feeding.

Mechanistically, in the MB, exposure to higher temperatures was shown to act in a largely cell-autonomous manner by increasing neuronal excitability and spontaneous activity. This elevated activity is proposed to drive Ca^{2+} accumulation and activation of the cAMP signaling cascade, ultimately promoting activity-dependent changes in neuronal excitability and growth (Peng et al., 2007). In our data, the adult ORNs have the same spike counts across developmental

temperatures (18 and 25°C), without an increase in neuron excitability (see Züfle et al., 2025). The increase in neuronal excitability by Peng et a., therefore likely reflect acute effects of temperature exposure which we have not considered in our study.

In our view, temperature does not merely modulate the extent of growth, but actively participates in specifying how circuits are assembled. This perspective is consistent with findings by Kiral et al. (2021), which reported that lower developmental temperatures increased the number of postsynaptic partners of photoreceptors and dorsal cluster neurons. Kiral attributes this effect to a difference between the scaling of neural and animal growth rates, analyzed by filopodia dynamics (Kiral et al., 2021). We formalize this interpretation in a mathematical growth model, demonstrating that Drosophila developmental time scales exponentially with temperature, as predicted by models assuming metabolic constraints on growth (see Section 5.3).

Although this model offers a coherent explanation for temperature-dependent differences in circuit architecture, it is important to consider the limitations of the experimental methods used to infer synaptic connectivity. First, trans-Tango depends on the specificity and expression strength of the driver system, which may introduce bias in the labeling of synaptic partners. However, Talay et al. demonstrated that trans-Tango expression itself is not temperature-dependent, as assessed by receptor quantification (Talay et al., 2017). Second, it remains unclear whether the synaptic partners detected in the adult represent only stable connections formed throughout development or also transient contacts established during earlier stages. Approaches such as activity-dependent GRASP may provide complementary validation by more selectively reporting functional synaptic contacts (Shearin et al., 2018). However, in the case of ORN–PN connections examined here, we demonstrate that the postsynaptic neurons identified by trans-Tango are functionally connected, supporting the validity of this approach in this context (see Section 5.1.2).

In summary, we analyzed the effects of developmental temperature during pupal development and identified temperature-dependent differences in synaptic partner choice within the olfactory system. Importantly, these effects may not be uniform across circuits, and the scaling properties of connectivity could vary between different neural systems. A comprehensive assessment of this phenomenon would benefit from future analyses of connectomes from flies reared at different temperatures, using approaches such as light-microscopy-based connectomics (LICONN) (Tavakoli et al., 2025).

6.2 Functional robustness of the antennal lobe to changes in developmental temperature

Flies developed at lower temperatures presented an increase in ORN postsynaptic partners within the AL, which are functional and vary across glomeruli (Section 5.1). Next, to evaluate the effect of this increased connectivity on odor coding, we then imaged four glomeruli at the level of ORNs and PNs (Section 5.2.2). We observed that in flies developed at lower temperatures, ORNs responded to an odor stimulus with a higher calcium transient than flies developed at 25°C. Because ORNs are cholinergic, this increased presynaptic activity could lead to higher excitatory responses in postsynaptic PNs that send odor information to higher brain areas.

However in PNs (both uni- and multiglomerular) odor coding was robust to developmental temperatures, being constant across conditions (Section 5.2.2). This suggests that there is a compensation between the transmission of odor information between the ORNs to the PNs. This compensation might rely on inhibitory LNs that are recruited in larger numbers at lower temperatures.

The balance between excitation and inhibition is key for the function of healthy brains, and there is evidence that this balance is achieved developmentally during synapse formation (Cline, 2005). In the fly olfactory system, γ-aminobutyric acid (GABA) mediated inhibition is distributed at both pre- and post-synapses in ORN-uPN connections (Olsen & Wilson, 2008; Root et al., 2008). Additional ORN postsynaptic partners recruited at 18 °C include a substantial fraction of local interneurons, which are predominantly inhibitory, and multiglomerular projection neurons, many of which are GABAergic (Bates et al., 2020). This expansion of both excitatory outputs and inhibitory circuitry is consistent with a coordinated scaling of synaptic resources that maintains network balance rather than simply amplifying excitation. Presynaptic inhibition could therefore explain why in some glomeruli (DL1 and DL5) calcium transients are already compensated at the ORN axon terminals, although this remains to be confirmed experimentally, for example, by manipulating GABA receptors or local interneuron activity while measuring ORN calcium signals across developmental temperatures. Last, inhibition could be one component of a broader homeostatic mechanism that counter balancers developmental changes – in synapse strength, release probability, or intrinsic excitability (Böhme et al., 2019; Frank et al., 2020). Overall, we conclude that within a range of

temperatures, the peripheral olfactory system compensates for the developmental effects on circuit wiring and keeps odor information invariant to this environmental factor.

So far, our functional analyses were restricted to two developmental temperatures (18 and 25°C), whereas the anatomical analysis reveal drastic effects on circuit connectivity also for extreme temperatures (12 and 31°C). Extending this approach to additional temperatures and glomeruli – given that odor responses are combinatorial and involve the activity of multiple of those units – will be necessary to determine the full extent of temperature-dependent effects. Answering this question will be important to understand the evolutionary relevance of the developmental plasticity, specifically in the context of generating diversity in odor-driven behavior.

6.3 Developmental temperature shapes pn–lhn connectivity and behavioral responses

Although odor representations in the antennal lobe (AL) remain remarkably robust, developmental temperature strongly modulates behavioral responses to appetitive odor cues across two independent assays (Section 5.2.1). Flies reared at 18 °C display stronger attraction to the appetitive odor 2-butanone (and vinegar, see Züfle et al, 2025) than those developed at 25 °C in both tethered and free-walking assays. This suggests that temperature-dependent scaling of brain connectivity is not fully compensated at the functional level, and that odor-evoked activity in circuits downstream of the AL retains a dependence on developmental temperature.

Innate odor preference is computed in the lateral horn (LH), where projection neurons (PNs) synapse onto LH neurons (LHNs). LHNs then integrate inputs from subsets of glomeruli tuned to ecologically related odors (Dolan et al., 2019; Jeanne et al., 2018). Retro-Tango mapping indicates that PD2a1/b1 LHNs receive roughly twice as many PN inputs at 18 °C, accounting for both uPNs and mPNs (Section 5.2.3). The innervation density and AL symmetry observed in this dataset also suggests that more mPNs are connected to PD2a1/b1 at lower temperatures. However, this is was not comparable to the BacTrace analysis, as the driver line used labels only 2-3 mPNs (Cachero et al., 2020).

By focusing on the identity of glomeruli connected to the LHNs, the BacTrace analysis indicates temperature-dependent shifts in the likelihood of specific PN-LHN connections (5.2.3). However, as our dataset includes only about half of the uniglomerular PN types (due to

the specificity of the BacTrace driver) other additional, functionally important connections may not have been captured – such as those involving mPNs. Moreover, other LHN types that were not investigated in this study could also undergo parallel changes in wiring or odor responses, potentially contributing to the temperature-dependent functional effects.

Retro-Tango and BacTrace present similar limitations as trans-Tango (see Section 6.1). Both methods are dependent on driver specificity, and it remains uncertain whether they exclusively report functional, mature, synaptic connections. As trans-Tango, retro-Tango functions through a signaling cascade initiated by a ligand-receptor interaction. Those receptors are expressed exclusively in the synaptic zone, achieved by using the mouse intracellular adhesion molecule ICAM1 (in trans-Tango) and ICAM5 (in retro-Tango) (Sorkaç et al., 2023; Talay et al., 2017). In BacTrace, presynaptic neuron labeling is achieved through both ligand-receptor interaction and targeted neurotransmitter vesicles – which provides additional specificity but however does not fully guarantee that all labeled connections are functional (Cachero et al., 2020). For this reason, using multiple complementary synaptic tracing methods provides a more robust and reliable view of circuit connectivity.

In a functional analysis of PD2a1/b1 neurons in flies developed at different temperatures, the PD2b1 subtype shows reduced odor-evoked responses in its mushroom-body–projecting branch at lower temperatures (Section 5.2.3.3). Meanwhile, PD2a1/b1 neurons maintains a stable calcium response in the lateral horn. PD2a1/b1 neurons are required for memory retrieval (Dolan et al., 2018), yet their contribution to innate behavior is context dependent, varying with internal state and stimulus conditions (Lerner et al., 2020). Behaviorally, PD2a1/b1 neurons are associated with approach toward appetitive odors, but their activation alone does not elicit behavior (Dolan et al., 2019). Such findings suggest that PD2a1/b1 neurons operate synergistically or redundantly with other LHNs – whose connectivity may also be temperature dependent – within a circuit which organizing logic remains to be resolved. Behaviorally relevant differences therefore emerge not from wholesale reorganization but from subtle, circuit-specific rewiring and branch-specific tuning in higher-order neurons.

Finally, odor information reaches higher brain centers through both uniglomerular PNs (uPNs) and multiglomerular PNs (mPNs), the latter projecting to the LH and protocerebrum. We find that, likely, mPN connectivity to both ORNs and LHNs is likewise shaped by developmental temperature. Despite representing more than half of all PNs, the functional roles of mPNs remain poorly understood. Approximately half of mPNs are predicted to be GABAergic (Bates

et al., 2020), and these inhibitory neurons influence odor preference and discrimination, and their silencing reduces approach to appetitive odors (Liang et al., 2013; Parnas et al., 2013; Strutz et al., 2014). The remaining mPNs are predicted to be cholinergic (Bates et al., 2020), but their contributions to downstream processing and behavior are still unclear. A more complete understanding of mPN function and LH circuit organization will therefore be essential for linking temperature-dependent circuit plasticity to the behavioral changes we observe.

While certain computations in the olfactory system are robust, the circuit appears to have evolved to exploit developmental plasticity to generate adaptive phenotypes. Our experiments to date have examined only two developmental temperatures and a limited set of neurons. In this context, our measurements from a limited set of neurons represent only an initial step; whole-brain functional imaging across developmental temperatures will be an invaluable tool for understanding the effect of temperature across in overall stimulus coding.

6.4 Developmental tempo and circuit assembly: linking body growth to brain wiring

The development of a functional organism relies on the tightly coordinated growth of body tissues and the parallel assembly of synaptic connectivity in the brain. Because these developmental programs unfold within a precisely regulated temporal program, temperature-dependent changes in developmental speed raise fundamental questions about how such coordination is maintained.

Based on the observation that flies reared at lower temperatures exhibit an increased number of synaptic partners, Kiral et al. proposed that this effect arises from a mismatch between the growth rate of the nervous system and that of the organism as a whole. Here, we formalize this idea using a mathematical model of growth.

We show that total developmental time scales exponentially with temperature, in agreement with theories that assume that the growth rate has a temperature-dependent metabolic constraint (Section 5.3). Subsequently, we applied our model to neural growth and synapse formation, which successfully predicts brain wiring (i.e., postsynaptic partners number) under development at constant temperatures and at temperature cycles (see Züfle et al., 2025).

These findings raise important questions about the scaling of developmental tempo across tissues. Specifically, the brain may either follow a uniform scaling with the rest of the organism

or exhibit non-uniform scaling. Our model predicts that the increase in synaptic partners observed at lower temperatures arises because the nervous system progresses at its own intrinsic rate, faster than the overall pupa developmental duration. This interpretation suggests that neural development may not simply scale uniformly with body growth, but instead follows a distinct trajectory, which could have important implications for understanding how environmental factors such as temperature shape circuit assembly and connectivity.

While PN development at 18 and 25 °C supports the model's prediction of developmental tempo shifts, further experimental validation across other neural tissues and temperatures is still required. This could be addressed by quantifying the growth progress of defined neural populations across pupal development and a range of temperatures, for example in ORNs. Alternatively, to more directly assess potential mismatches between brain and body developmental tempo, one could compare the developmental trajectories of different tissues across time and temperature. Tissue-specific drivers targeting thoracic and peripheral organs – such as the wing, gut, or Malpighian tubules – could serve as proxies for overall body development, and compared with the brain tempo.

We propose that this disparity between brain and body developmental timing arises from differences in metabolic constraints, although direct experimental evidence for this hypothesis is currently lacking. However, Recent studies have highlighted a connection between developmental pace and metabolic rate. For instance, species-specific differences in developmental timing have been linked to variations in mitochondrial metabolism (Diaz-Cuadros et al., 2023; Iwata & Vanderhaeghen, 2024) and experimental manipulations of metabolic activity can directly alter the rate of development (Diaz-Cuadros et al., 2023).

Beyond this, several experimental approaches can be used to test this hypothesis. One possibility is to manipulate the metabolism of the brain specifically, for instance by targeting key neuronal energetic pathways. Candidate targets include the glucose transporter Glut1, alanine aminotransferase (Alat), and lactate dehydrogenase (Ldh), which mediate either the transfer or conversion of energetic substrates into pyruvate, supporting neuronal metabolism.

Finally, it is important to note that this metabolic hypothesis is grounded in biophysical principles and, as such, has limitations – such as not accounting for adaptation. Nevertheless, it provides a useful conceptual basis, generating testable predictions and new hypotheses, and serves as a valuable starting point for exploring the relationship between metabolism, developmental tempo, and neural circuit assembly.

6.5 Temporal dynamics of ecdysteroid are temperature-independent

Ecdysteroids are central regulators of developmental timing, coordinating both body growth and neural circuit assembly during pupal development. Their influence on metabolism and tissue-specific remodeling makes them a natural target to investigate how temperature shapes the coordination of development. Targeted quantification of 20-hydroxyecdysone (20E) and Makisterone A (MaA) across pupal development revealed broadly conserved temporal profiles across temperatures (Section 5.4.2). This suggests that major systemic signaling via ecdysone continues to follow the developmental pace independently to temperature.

Previous work in *Bicyclus anyana* reported temperature-dependent shifts in the peak of 20-hydroxyecdysone, with butterflies developed at higher temperatures presenting an earlier peak of the ecdysteroid (Oostra et al., 2011). In contrast, we did not observe a temperature-dependent shift in Drosophila. This discrepancy may reflect differences in developmental timing: pupal development in Drosophila is considerably faster (~4 days at 25 °C, ~20 days at 12 °C) than in *B. anyana* (~30 days at 25°C), which could limit the temporal window over which hormonal fluctuations can occur. Differences in sampling resolution might also contribute, as their study quantified ecdysteroids every 5% of development, whereas we quantified every 15% of development.

In contrast to the largely temperature-invariant dynamics of ecdysteroids levels, several ecdysone-responsive transcription factors that regulate neural wiring programs (Eip63F-1, ftz-f1, Hr3, Eip75B) exhibit earlier and often higher expression at lower temperatures (Section 5.4.1 and 5.4.3.1). These effects are unlikely driven solely by ecdysteroids levels, but rather by temperature-dependent regulation of downstream signaling, tissue-specific transcription, altered cellular sensitivity to ecdysteroids or cell intrinsic growth rates. Ecdysone thus provides a conserved temporal blueprint for development, while additional mechanisms fine-tune tissue-specific growth and coordination and circuit assembly.

6.6 Regulation of metabolic pathways by developmental temperature

The pace of neuronal development is tightly coupled to metabolic activity, particularly the rates of the TCA cycle and mitochondrial oxidative phosphorylation (Iwata & Vanderhaeghen, 2024). Metabolic rate represents a major source of temporal variability and is well suited to regulate developmental speed: it impacts nearly all biochemical reactions while also being adjustable locally to modulate tempo in specific regions, tissues, or cell types. Environmental temperature

profoundly influences the coordination of growth and neural circuit assembly, likely by altering these underlying metabolic processes.

Importantly, temperature affects not only the transcriptional control of metabolic enzymes but also the overall metabolic rate: consistent with Arrhenius kinetics, adult Drosophila metabolic rate increases with temperature (Jensen et al., 2014; Klepsatel et al., 2019). Yet how temperature shapes the transcriptional dynamics of metabolic pathways throughout development has remained largely unexplored.

To address this, we examined the transcriptional dynamics of key metabolic pathways across pupal development (Section 5.4). Development at lower temperatures lead to an earlier increase in the expression of genes involved in central energy metabolism, including glycolysis, the TCA cycle, and nuclear-encoded electron transport chain components (5.4.3.3).

This coordinated upregulation could suggests a compensatory response to maintain ATP production under slower developmental conditions, potentially offsetting the kinetic constraints imposed by cold. In cold-acclimated flies, Hexokinase, GPDH1 and Cytochrome Oxidase activities are increased to compensate for reduced kinetic energy at low temperatures and keep flux through glycolysis and the mitochondrial electron transport chain in comparison to warm-acclimated flies (Burnell et al., 1991). These findings suggest that temperature shapes developmental tempo not only by slowing or accelerating growth, but also by modulating the timing of metabolic programs, providing a potential mechanistic basis for differential scaling between tissues such as brain and body.

Temperature-dependent differences in the transcription of metabolic genes have been reported previously, though these studies do not capture the dynamic shifts across development in response to different rearing temperatures, as we do here. Nonetheless, examining the overall effects of temperature on metabolic gene expression provides valuable context.

Similarly to our findings, cold- and hot-adapted flies displayed a change in transcription of TCA cycle genes. In flies evolved at high temperatures, genes involved in the TCA cycle, oxidative phosphorylation, and key glycolytic enzymes are consistently downregulated in both *D. melanogaster* and *D. simulans* (Hariharan et al., 2014; Mallard et al., 2018). Metabolomic analyses confirm this transcriptional pattern, showing reduced levels of TCA intermediates, indicating a coordinated decline in both enzyme expression and metabolic flux under warm conditions (Hariharan et al., 2014). In contrast to heat-acclimated flies, cold-acclimated ones

exhibit extensive reorganization of both the transcriptome and metabolome, with pronounced upregulation of genes in carbohydrate and TCA pathways. Metabolite profiling mirrors these changes, suggesting that transcriptional adjustments are closely linked to altered flux through central metabolic pathways (MacMillan et al., 2016).

While these studies illustrate temperature-driven shifts in transcription and metabolic flux at the organismal level, our model predicts that brain and body may respond differently to temperature due to their distinct metabolic rates. Consequently, bulk transcriptional changes likely represent an average across tissues, potentially obscuring tissue-specific adaptations in metabolism and energy allocation. Beyond global temperature effects, different cell types and tissues exhibit distinct metabolic challenges, and therefore likely face different metabolic constraints. As a result, temperature may impact tissues in specific and heterogeneous ways. Even within the brain, metabolism is uniquely organized: neuronal energy demands are tightly coupled to glial support, making the brain metabolically distinct from the rest of the body. For example, glucose metabolism is spatially organized within the brain, with astrocytes exhibiting higher glycolytic activity than neurons. This arrangement creates a lactate gradient from astrocytes to neurons, enabling neurons to prioritize glucose use for maintaining redox balance rather than directly for energy production (Dienel, 2018; Miyamoto & Amrein, 2019). Importantly, the brain may be buffered against developmental temperature effects due to its unique metabolic requirements and the phenomenon of brain sparing. Under limited resources, energy allocation may prioritize the brain, allowing neuronal development to proceed at a relatively stable pace while other tissues adjust more flexibly (Maurange & Lanet, 2014).

Therefore, while our dataset captures transcriptional dynamics across the entire pupa, resolving tissue-specific differences remains an important next step. Our model predicts that the effect of temperature on metabolic rates and therefore developmental speed may vary between tissues, particularly between the brain and the rest of the body. Therefore, conclusions about tissue-specific metabolic effects of temperature would benefit from tissue-specific data. Future studies could, for example, separately profile the brain and body of flies reared at different temperatures to quantify gene expression in each compartment. Alternatively, bulk RNA-seq combined with FACS-based isolation of the brain could distinguish transcripts originating from neural versus non-neural tissues. An intriguing possibility is that metabolic regulation varies even further at the level of individual cell types, particularly neurons, though this remains to be determined. Supporting this idea, recent single-cell transcriptomic analyses in zebrafish revealed cell type–

specific effects of developmental temperature on proteostasis, with potential implications for the pace of development (Bourn & Dorrity, 2024; Dorrity et al., 2023).

Finally, an important open question is how temperature affects the balance between bioenergetic and biosynthetic demands: although we observed earlier upregulation of genes encoding key energetic enzymes, it remains unclear whether this leads to more ATP production or supports other cellular processes. Temperature modulates mitochondrial efficiency via influencing the non-ATP producing respiration (Chamberlin, 2004; Hardewig et al., 1999; Martinez et al., 2017). For example, *Manduca sexta* developed at elevated temperatures display a higher proportion of substrate that is used without generating ATP, which reduces cellular energy budget and indirectly increases costs of maintenance (Martinez et al., 2017). However, transcriptomic data alone provide only a partial view of metabolic activity in the intact animal. A more complete understanding of energy allocation and expenditure could be gained through calorimetry, oxygen consumption measurements, extracellular flux assays, or live imaging approaches using pyruvate or NAD+/NADH FRET sensors (Bulusu et al., 2017; Hemalatha et al., 2025). These complementary approaches will be crucial to determine the functional consequences of temperature-dependent transcriptional changes in metabolism.

Beyond the analyses presented here, this dataset can serve as a foundation for further studies investigating the regulatory logic and temporal coordination of temperature-sensitive genes during development. For example, genes could be grouped according to their temporal expression dynamics and how these patterns shift across temperatures, potentially revealing biologically meaningful clusters of temperature-sensitive genes. More sophisticated statistical modeling could identify overarching regulatory trends or infer gene networks. Investigating the transcription factors controlling these genes could further illuminate how developmental temperature modulates gene regulatory programs. To our knowledge, this is the first dataset tracking transcription throughout pupal development across multiple temperatures, making it a valuable resource for understanding how temperature influences developmental processes and, ultimately, adult phenotypes.

6.7 Concluding remarks

In conclusion, our study provides a unique, dynamic view of how temperature shapes development and brain outcome. Two main insights emerge from this work. First, we demonstrate a link between developmental temperature and metabolic regulation; as well as a link between developmental tempo and brain wiring. Second, despite those pronounced

temperature-dependent changes in developmental tempo and circuit wiring, core sensory computations remain functionally robust, while behavioral outputs retain flexibility. This combination of robustness and plasticity suggests that evolution has shaped developmental programs that buffer essential neural functions yet preserve the capacity for adaptive behavioral variation in response to environmental conditions.

Importantly, our analyses focus on acute temperature effects, assessed after re-adaptation to 25 °C. Many questions remain about how sustained or fluctuating thermal conditions influence development, particularly when considering potential adaptive roles of metabolism that extend beyond purely biophysical constraints. Future work combining transcriptional, metabolic, and functional assays will be key to fully understanding how temperature interacts with intrinsic developmental programs.

7 Bibliography

Ables, E. T., Bois, K. E., Garcia, C. A., & Drummond-Barbosa, D. (2015). Ecdysone response gene E78 controls ovarian germline stem cell niche formation and follicle survival in Drosophila. *Developmental Biology*, *400*(1), 33–42. https://doi.org/10.1016/j.ydbio.2015.01.013

Aggarwal, D., Mishra, P., Patel, Y., Singh, M., Sharma, V., Korol, A. B., & Michalak, P. (2025). Experimental evolution-induced transcriptome and phenotype responses of Drosophila melanogaster to novel thermal environments. *Journal of Experimental Biology*, *228*(19), jeb251365. https://doi.org/10.1242/jeb.251365

Amiel, J. J., Lindström, T., & Shine, R. (2014). Egg incubation effects generate positive correlations between size, speed and learning ability in young lizards. *Animal Cognition*, *17*(2), 337–347. https://doi.org/10.1007/s10071-013-0665-4

Amiel, J. J., & Shine, R. (2012). Hotter nests produce smarter young lizards. *Biology Letters*, *8*(3), 372–374. https://doi.org/10.1098/rsbl.2011.1161

Angilletta Jr., M. J. (2009). *Thermal Adaptation: A Theoretical and Empirical Synthesis*. Oxford University Press. https://doi.org/10.1093/acprof:oso/9780198570875.001.1

Angilletta, M. J., Steury, T. D., & Sears, M. W. (2004). Temperature, growth rate, and body size in ectotherms: Fitting pieces of a life-history puzzle. *Integrative and Comparative Biology*, *44*(6), 498–509. https://doi.org/10.1093/icb/44.6.498

Arrhenius, S. (1889). Über die Dissociationswärme und den Einfluss der Temperatur auf den Dissociationsgrad der Elektrolyte. *Zeitschrift für Physikalische Chemie*, *4U*(1), 96–116. https://doi.org/10.1515/zpch-1889-0408

Ashburner, M. (1974). Sequential gene activation by ecdysone in polytene chromosomes of Drosophila melanogaster. II. The effects of inhibitors of protein synthesis. *Developmental Biology*, *39*(1), 141–157. https://doi.org/10.1016/s0012-1606(74)80016-3

Aso, Y., Sitaraman, D., Ichinose, T., Kaun, K. R., Vogt, K., Belliart-Guérin, G., Plaçais, P.-Y., Robie, A. A., Yamagata, N., Schnaitmann, C., Rowell, W. J., Johnston, R. M., Ngo, T.-T. B., Chen, N., Korff, W., Nitabach, M. N., Heberlein, U., Preat, T., Branson, K. M., … Rubin, G.

M. (2014). Mushroom body output neurons encode valence and guide memory-based action selection in Drosophila. *eLife*, *3*, e04580. https://doi.org/10.7554/eLife.04580

Awasaki, T., Huang, Y., O'Connor, M. B., & Lee, T. (2011). Glia instruct developmental neuronal remodeling through TGF-[beta] signaling. *Nature Neuroscience*. https://doi.org/10.1038/NN.2833

Baena-López, L. A., Alonso, J., Rodriguez, J., & Santarén, J. F. (2008). The Expression of Heat Shock Protein HSP60A Reveals a Dynamic Mitochondrial Pattern in Drosophila melanogaster Embryos. *Journal of Proteome Research*, *7*(7), 2780–2788. https://doi.org/10.1021/pr800006x

Bates, A. S., Phelps, J. S., Kim, M., Yang, H. H., Matsliah, A., Ajabi, Z., Perlman, E., Delgado, K. M., Osman, M. A. M., Salmon, C. K., Gager, J., Silverman, B., Renauld, S., Collie, M. F., Fan, J., Pacheco, D. A., Zhao, Y., Patel, J., Zhang, W., … Lee, W.-C. A. (2025). Distributed control circuits across a brain-and-cord connectome. *bioRxiv: The Preprint Server for Biology*, 2025.07.31.667571. https://doi.org/10.1101/2025.07.31.667571

Bates, A. S., Schlegel, P., Roberts, R. J. V., Drummond, N., Tamimi, I. F. M., Turnbull, R., Zhao, X., Marin, E. C., Popovici, P. D., Dhawan, S., Jamasb, A., Javier, A., Serratosa Capdevila, L., Li, F., Rubin, G. M., Waddell, S., Bock, D. D., Costa, M., & Jefferis, G. S. X. E. (2020). Complete Connectomic Reconstruction of Olfactory Projection Neurons in the Fly Brain. *Curr. Biol.*, *30*(16), 3183-3199.e6.

Bear, A., & Monteiro, A. (2013). Male courtship rate plasticity in the butterfly Bicyclus anynana is controlled by temperature experienced during the pupal and adult stages. *PloS One*, *8*(5), e64061. https://doi.org/10.1371/journal.pone.0064061

Beatty, J., Fauth, T., Callender, J. L., Spindler-Barth, M., & Henrich, V. C. (2006). Analysis of transcriptional activity mediated by Drosophila melanogaster ecdysone receptor isoforms in a heterologous cell culture system. *Insect Molecular Biology*, *15*(6), 785–795. https://doi.org/10.1111/j.1365-2583.2006.00683.x

Beckstead, R. B., Lam, G., & Thummel, C. S. (2005). The genomic response to 20-hydroxyecdysone at the onset of Drosophila metamorphosis. *Genome Biology*, *6*(12), R99. https://doi.org/10.1186/gb-2005-6-12-r99

Benton, R., Sachse, S., Michnick, S. W., & Vosshall, L. B. (2006). Atypical membrane topology and heteromeric function of Drosophila odorant receptors in vivo. *PLoS Biology*, *4*(2), e20. https://doi.org/10.1371/journal.pbio.0040020

Berenbaum, M. (2017). Insect Biodiversity – Millions and Millions. In *Insect Biodiversity* (pp. 783–792). John Wiley & Sons, Ltd. https://doi.org/10.1002/9781118945568.ch25

Berke, B., Wittnam, J., McNeill, E., Vactor, D. L. V., & Keshishian, H. (2013). Retrograde BMP Signaling at the Synapse: A Permissive Signal for Synapse Maturation and Activity-Dependent Plasticity. *Journal of Neuroscience*, *33*(45), 17937–17950. https://doi.org/10.1523/JNEUROSCI.6075-11.2013

Berndt, A. J. E., Tang, J. C. Y., Ridyard, M. S., Lian, T., Keatings, K., & Allan, D. W. (2015). Gene Regulatory Mechanisms Underlying the Spatial and Temporal Regulation of Target-Dependent Gene Expression in Drosophila Neurons. *PLoS Genetics*, *11*(12), e1005754. https://doi.org/10.1371/journal.pgen.1005754

Bleckert, A., & Wong, R. O. L. (2011). Identifying roles for neurotransmission in circuit assembly: Insights gained from multiple model systems and experimental approaches. *BioEssays*, *33*(1), 61–72. https://doi.org/10.1002/bies.201000095

Bleckert, A., Zhang, C., Turner, M. H., Koren, D., Berson, D. M., Park, S. J. H., Demb, J. B., Rieke, F., Wei, W., & Wong, R. O. (2018). GABA release selectively regulates synapse development at distinct inputs on direction-selective retinal ganglion cells. *Proceedings of the National Academy of Sciences*, *115*(51), E12083–E12090. https://doi.org/10.1073/pnas.1803490115

Bogovic, J. A., Otsuna, H., Heinrich, L., Ito, M., Jeter, J., Meissner, G., Nern, A., Colonell, J., Malkesman, O., Ito, K., & Saalfeld, S. (2020). An unbiased template of the Drosophila brain and ventral nerve cord. *PLOS ONE*, *15*(12), e0236495. https://doi.org/10.1371/journal.pone.0236495

Böhme, M. A., McCarthy, A. W., Grasskamp, A. T., Beuschel, C. B., Goel, P., Jusyte, M., Laber, D., Huang, S., Rey, U., Petzoldt, A. G., Lehmann, M., Göttfert, F., Haghighi, P., Hell, S. W., Owald, D., Dickman, D., Sigrist, S. J., & Walter, A. M. (2019). Rapid active zone remodeling consolidates presynaptic potentiation. *Nature Communications*, *10*(1), 1085. https://doi.org/10.1038/s41467-019-08977-6

Bond, N. D., Hoshizaki, D. K., & Gibbs, A. G. (2010). The role of 20-hydroxyecdysone signaling in Drosophila pupal metabolism. *Comparative Biochemistry and Physiology. Part A, Molecular & Integrative Physiology*, *157*(4), 398–404. https://doi.org/10.1016/j.cbpa.2010.08.025

Bornstein, B., Zahavi, E. E., Gelley, S., Zoosman, M., Yaniv, S. P., Fuchs, O., Porat, Z., Perlson, E., & Schuldiner, O. (2015). Developmental Axon Pruning Requires Destabilization of Cell Adhesion by JNK Signaling. *Neuron*. https://doi.org/10.1016/J.NEURON.2015.10.023

Böttinger, L., Oeljeklaus, S., Guiard, B., Rospert, S., Warscheid, B., & Becker, T. (2015). Mitochondrial Heat Shock Protein (Hsp) 70 and Hsp10 Cooperate in the Formation of Hsp60 Complexes *. *Journal of Biological Chemistry*, *290*(18), 11611–11622. https://doi.org/10.1074/jbc.M115.642017

Boulanger, A., Clouet-Redt, C., Farge, M., Flandre, A., Guignard, T., Fernando, C., Juge, F., & Dura, J. (2011). Ftz-f1 and Hr39 opposing roles on EcR expression during Drosophila mushroom body neuron remodeling. *Nature Neuroscience*. https://doi.org/10.1038/NN.2700

Bourn, J. J., & Dorrity, M. W. (2024). Degrees of freedom: Temperature's influence on developmental rate. *Current Opinion in Genetics and Development*. https://doi.org/10.1016/j.gde.2024.102155

Boyce, W. T., Sokolowski, M. B., & Robinson, G. E. (2020). Genes and environments, development and time. *Proceedings of the National Academy of Sciences*, *117*(38), 23235–23241. https://doi.org/10.1073/pnas.2016710117

Broadus, J., McCabe, J. R., Endrizzi, B., Thummel, C. S., & Woodard, C. T. (1999). The Drosophila beta FTZ-F1 orphan nuclear receptor provides competence for stage-specific responses to the steroid hormone ecdysone. *Molecular Cell*, *3*(2), 143–149. https://doi.org/10.1016/s1097-2765(00)80305-6

Bruyne, M. de, Clyne, P. J., & Carlson, J. R. (1999). Odor Coding in a Model Olfactory Organ: TheDrosophila Maxillary Palp. *Journal of Neuroscience*, *19*(11), 4520–4532. https://doi.org/10.1523/JNEUROSCI.19-11-04520.1999

Bulusu, V., Prior, N., Snaebjornsson, M. T., Kuehne, A., Sonnen, K. F., Kress, J., Stein, F., Schultz, C., Sauer, U., & Aulehla, A. (2017). Spatiotemporal Analysis of a Glycolytic Activity

Gradient Linked to Mouse Embryo Mesoderm Development. *Developmental Cell*, *40*(4), 331-341.e4. https://doi.org/10.1016/j.devcel.2017.01.015

Burnell, A. M., Reaper, C., & Doherty, J. (1991). The effect of acclimation temperature on enzyme activity in Drosophila melanogaster. *Comparative Biochemistry and Physiology B, Comparative Biochemistry*, *98*(4), 609–614. https://doi.org/10.1016/0305-0491(91)90263-d

Cáceres, L., Necakov, A., Schwartz, C., Kimber, S., Roberts, I. J. H., & Krause, H. M. (2011). Nitric oxide coordinates metabolism, growth, and development via the nuclear receptor E75. *Genes & Development*. https://doi.org/10.1101/GAD.2064111

Cachero, S., Gkantia, M., Bates, A. S., Frechter, S., Blackie, L., McCarthy, A., Sutcliffe, B., Strano, A., Aso, Y., & Jefferis, G. S. X. (2020). *BAcTrace a new tool for retrograde tracing of neuronal circuits*.

Carmon, A., Chien, J., Sullivan, D., & MacIntyre, R. (2010). The α glycerophosphate cycle in Drosophila melanogaster V. Molecular analysis of α glycerophosphate dehydrogenase and α glycerophosphate oxidase mutants. *Journal of Heredity*, *101*(2), 218–224.

Caron, S. J. C., Ruta, V., Abbott, L. F., & Axel, R. (2013). Random convergence of olfactory inputs in the Drosophila mushroom body. *Nature*, *497*(7447), 113–117.

Caygill, E. E., & Brand, A. H. (2016). The GAL4 System: A Versatile System for the Manipulation and Analysis of Gene Expression. In C. Dahmann (Ed.), *Drosophila: Methods and Protocols* (pp. 33–52). Springer. https://doi.org/10.1007/978-1-4939-6371-3_2

Chamberlin, M. E. (2004). Top-down control analysis of the effect of temperature on ectotherm oxidative phosphorylation. *American Journal of Physiology. Regulatory, Integrative and Comparative Physiology*, *287*(4), R794-800. https://doi.org/10.1152/ajpregu.00240.2004

Chávez, V. M., Marqués, G., Delbecque, J. P., Kobayashi, K., Hollingsworth, M., Burr, J., Natzle, J. E., & O'Connor, M. B. (2000). The Drosophila disembodied gene controls late embryonic morphogenesis and codes for a cytochrome P450 enzyme that regulates embryonic ecdysone levels. *Development*, *127*(19), 4115–4126. https://doi.org/10.1242/dev.127.19.4115

Chen, Akin, O., Nern, A., Tsui, C. Y. K., Pecot, M. Y., & Zipursky, S. L. (2014). Cell-type-Specific Labeling of Synapses In Vivo through Synaptic Tagging with Recombination. *Neuron*, *81*(2), 280–293. https://doi.org/10.1016/j.neuron.2013.12.021

Chen, J., Nolte, V., & Schlötterer, C. (2015a). Temperature Stress Mediates Decanalization and Dominance of Gene Expression in Drosophila melanogaster. *PLOS Genetics*, *11*(2), e1004883. https://doi.org/10.1371/journal.pgen.1004883

Chen, J., Nolte, V., & Schlötterer, C. (2015b). Temperature-Related Reaction Norms of Gene Expression: Regulatory Architecture and Functional Implications. *Molecular Biology and Evolution*, *32*(9), 2393–2402. https://doi.org/10.1093/molbev/msv120

Cheung, D., & Ma, J. (2015). Probing the impact of temperature on molecular events in a developmental system. *Scientific Reports*, *5*, 13124. https://doi.org/10.1038/srep13124

Chou, Y.-H., Spletter, M. L., Yaksi, E., Leong, J. C. S., Wilson, R. I., & Luo, L. (2010). Diversity and Wiring Variability of Olfactory Local Interneurons in the Drosophila Antennal Lobe. *Nature Neuroscience*, *13*(4), 439–449. https://doi.org/10.1038/nn.2489

Clarke, A. (2017). *Principles of Thermal Ecology: Temperature, Energy, and Life*. Oxford University Press. https://doi.org/10.1093/oso/9780199551668.001.0001

Cline, H. (2005). Synaptogenesis: A balancing act between excitation and inhibition. *Current Biology: CB*, *15*(6), R203-205. https://doi.org/10.1016/j.cub.2005.03.010

Colinet, H., Lee, S. F., & Hoffmann, A. (2010). Temporal expression of heat shock genes during cold stress and recovery from chill coma in adult Drosophila melanogaster. *The FEBS Journal*, *277*(1), 174–185. https://doi.org/10.1111/j.1742-4658.2009.07470.x

Couto, A., Alenius, M., & Dickson, B. J. (2005). Molecular, anatomical, and functional organization of the Drosophila olfactory system. *Current Biology: CB*, *15*(17), 1535–1547. https://doi.org/10.1016/j.cub.2005.07.034

Cruz, J., Ureña, E., Iñiguez, L. P., Irimia, M., Franch-Marro, X., & Martín, D. (2024). E93 controls adult differentiation by repressing broad in Drosophila. *Proceedings of the National Academy of Sciences of the United States of America*, *121*(51), e2403162121. https://doi.org/10.1073/pnas.2403162121

Das, A., Sen, S., Lichtneckert, R., Okada, R., Ito, K., Rodrigues, V., & Reichert, H. (2008). Drosophila olfactory local interneurons and projection neurons derive from a common neuroblast lineage specified by the empty spiracles gene. *Neural Dev.*, *3*, 33.

Davidson, J. (1944). On the Relationship between Temperature and Rate of Development of Insects at Constant Temperatures. *Journal of Animal Ecology*, *13*(1), 26–38. https://doi.org/10.2307/1326

de Belle & Heisenberg. (1994). Associative odor learning in Drosophila abolished by chemical ablation of mushroom bodies. *Science*, *263*(5147), 692–695. https://doi.org/10.1126/science.8303280

De Jong, M. J., Alton, L. A., White, C. R., O'Bryan, M. K., Chapple, D. G., & Wong, B. B. M. (2023). Long-term effects of incubation temperature on growth and thermal physiology in a small ectotherm. *Philosophical Transactions of the Royal Society of London. Series B, Biological Sciences*, *378*(1884), 20220137. https://doi.org/10.1098/rstb.2022.0137

de Rosny, E., de Groot, A., Jullian-Binard, C., Borel, F., Suarez, C., Le Pape, L., Fontecilla-Camps, J. C., & Jouve, H. M. (2008). DHR51, the Drosophila melanogaster homologue of the human photoreceptor cell-specific nuclear receptor, is a thiolate heme-binding protein. *Biochemistry*. https://doi.org/10.1021/BI801691B

Devarakonda, S., Harp, J. M., Kim, Y., Ozyhar, A., & Rastinejad, F. (2003). Structure of the heterodimeric ecdysone receptor DNA-binding complex. *The EMBO Journal*, *22*(21), 5827–5840. https://doi.org/10.1093/emboj/cdg569

Devineni, A. V., & Scaplen, K. M. (2021). Neural Circuits Underlying Behavioral Flexibility: Insights From Drosophila. *Frontiers in Behavioral Neuroscience*, *15*, 821680. https://doi.org/10.3389/fnbeh.2021.821680

Diaz-Cuadros, M., Miettinen, T. P., Skinner, O. S., Sheedy, D., Díaz-García, C. M., Gapon, S., Hubaud, A., Yellen, G., Manalis, S. R., Oldham, W. M., & Pourquié, O. (2023). Metabolic regulation of species-specific developmental rates. *Nature*, *613*(7944), 550–557. https://doi.org/10.1038/s41586-022-05574-4

Dienel, G. A. (2018). Brain Glucose Metabolism: Integration of Energetics with Function. *Physiological Reviews*. (Bethesda, MD). https://doi.org/10.1152/physrev.00062.2017

Dolan, M.-J., Belliart-Guérin, G., Bates, A. S., Frechter, S., Lampin-Saint-Amaux, A., Aso, Y., Roberts, R. J. V., Schlegel, P., Wong, A., Hammad, A., Bock, D., Rubin, G. M., Preat, T., Plaçais, P.-Y., & Jefferis, G. S. X. E. (2018). Communication from Learned to Innate Olfactory

Processing Centers Is Required for Memory Retrieval in Drosophila. *Neuron*, *100*(3), 651-668.e8. https://doi.org/10.1016/j.neuron.2018.08.037

Dolan, M.-J., Frechter, S., Bates, A. S., Dan, C., Huoviala, P., Roberts, R. J., Schlegel, P., Dhawan, S., Tabano, R., Dionne, H., Christoforou, C., Close, K., Sutcliffe, B., Giuliani, B., Li, F., Costa, M., Ihrke, G., Meissner, G. W., Bock, D. D., … Jefferis, G. S. (2019). Neurogenetic dissection of the Drosophila lateral horn reveals major outputs, diverse behavioural functions, and interactions with the mushroom body. *Elife*, *8*. https://doi.org/10.7554/eLife.43079

Dorkenwald, S., Matsliah, A., Sterling, A. R., Schlegel, P., Yu, S.-C., McKellar, C. E., Lin, A., Costa, M., Eichler, K., Yin, Y., Silversmith, W., Schneider-Mizell, C., Jordan, C. S., Brittain, D., Halageri, A., Kuehner, K., Ogedengbe, O., Morey, R., Gager, J., … FlyWire Consortium. (2024). Neuronal wiring diagram of an adult brain. *Nature*, *634*(8032), 124–138. https://doi.org/10.1038/s41586-024-07558-y

Dorrity, M. W., Saunders, L. M., Duran, M., Srivatsan, S. R., Barkan, E., Jackson, D. L., Sattler, S. M., Ewing, B., Queitsch, C., Shendure, J., Raible, D. W., Kimelman, D., & Trapnell, C. (2023). Proteostasis governs differential temperature sensitivity across embryonic cell types. *Cell*, *186*(23), 5015-5027.e12. https://doi.org/10.1016/j.cell.2023.10.013

Duch, C., Vonhoff, F., & Ryglewski, S. (2008). Dendrite elongation and dendritic branching are affected separately by different forms of intrinsic motoneuron excitability. *Journal of Neurophysiology*, *100*(5), 2525–2536.

Enriquez, T., & Colinet, H. (2019). Cold acclimation triggers major transcriptional changes in Drosophila suzukii. *BMC Genomics*, *20*(1), 413. https://doi.org/10.1186/s12864-019-5745-7

Etheridge, K. (2011). Maria Sibylla Merian and the metamorphosis of natural history. *Endeavour*, *35*(1), 16–22. https://doi.org/10.1016/j.endeavour.2010.10.002

Falibene, A., Roces, F., Rössler, W., & Groh, C. (2016). Daily Thermal Fluctuations Experienced by Pupae via Rhythmic Nursing Behavior Increase Numbers of Mushroom Body Microglomeruli in the Adult Ant Brain. *Frontiers in Behavioral Neuroscience*, *10*. https://doi.org/10.3389/fnbeh.2016.00073

Fan, X. L., Lin, Z. H., & Scheffers, B. R. (2021). Physiological, developmental, and behavioral plasticity in response to thermal acclimation. *Journal of Thermal Biology*, *97*, 102866. https://doi.org/10.1016/j.jtherbio.2021.102866

Feder, M., Blair, N., & Figueras, H. (1997). Natural thermal stress and heat-shock protein expression in Drosophila larvae and pupae. *Functional Ecology*, *11*(1), 90–100.

Fişek, M., & Wilson, R. I. (2014). Stereotyped connectivity and computations in higher-order olfactory neurons. *Nat. Neurosci.*, *17*(2), 280–288. https://doi.org/10.1038/nn.3613

Formicola, N., Heim, M., Dufourt, J., Lancelot, A.-S., Nakamura, A., Lagha, M., & Besse, F. (2021). Tyramine induces dynamic RNP granule remodeling and translation activation in the Drosophila brain. *eLife*, *10*, e65742. https://doi.org/10.7554/eLife.65742

Frank, C. A., James, T. D., & Müller, M. (2020). Homeostatic control of Drosophila neuromuscular junction function. *Synapse (New York, N.y.)*, *74*(1), e22133. https://doi.org/10.1002/syn.22133

Frechter, S., Bates, A. S., Tootoonian, S., Dolan, M.-J., Manton, J., Jamasb, A. R., Kohl, J., Bock, D., & Jefferis, G. (2019). Functional and anatomical specificity in a higher olfactory centre. *Elife*, *8*. https://doi.org/10.7554/eLife.44590

Gilbert, L. I. (2004). Halloween genes encode P450 enzymes that mediate steroid hormone biosynthesis in *Drosophila melanogaster*. *Molecular and Cellular Endocrinology, Proceedings of the Serono Foundation for the Advancement of Medical Science Workshop on Molecular Steroidogenesis*, *215*(1), 1–10. https://doi.org/10.1016/j.mce.2003.11.003

Gillooly, J. F., Brown, J. H., West, G. B., Savage, V. M., & Charnov, E. L. (2001). Effects of Size and Temperature on Metabolic Rate. *Science*, *293*(5538), 2248–2251. https://doi.org/10.1126/science.1061967

Gillooly, J. F., Charnov, E. L., West, G. B., Savage, V. M., & Brown, J. H. (2002). Effects of size and temperature on developmental time. *Nature*, *417*(6884), 70–73. https://doi.org/10.1038/417070a

Grimaldi, D., & Engel, M. S. (2005). *Evolution of the Insects*. Cambridge University Press.

Groh, C., Tautz, J., & Rössler, W. (2004). Synaptic organization in the adult honey bee brain is influenced by brood-temperature control during pupal development. *Proceedings of the National Academy of Sciences*, *101*(12), 4268–4273. https://doi.org/10.1073/pnas.0400773101

Groothuis, J., & Smid, H. M. (2017). Nasonia parasitic wasps escape from Haller's rule by diphasic, partially isometric brain-body size scaling and selective neuropil adaptations. *Brain Behavior and Evolution*, *90*(3), 243–254.

Hakim, Y., Yaniv, S. P., & Schuldiner, O. (2014). Astrocytes Play a Key Role in Drosophila Mushroom Body Axon Pruning. *PLoS ONE*, *9*(1), e86178. https://doi.org/10.1371/journal.pone.0086178

Hales, K. G., Korey, C. A., Larracuente, A. M., & Roberts, D. M. (2015). Genetics on the Fly: A Primer on the Drosophila Model System. *Genetics*, *201*(3), 815–842. https://doi.org/10.1534/genetics.115.183392

Hardewig, I., Pörtner, H. O., & Peck, L. S. (1999). Thermal sensitivity of mitochondrial function in the Antarctic Notothenioid Lepidonotothen nudifrons. *Journal of Comparative Physiology B*, *169*(8), 597–604. https://doi.org/10.1007/s003600050260

Hariharan, R., Hoffman, J. M., Thomas, A. S., Soltow, Q. A., Jones, D. P., & Promislow, D. E. (2014). Invariance and plasticity in the Drosophila melanogastermetabolomic network in response to temperature. *BMC Systems Biology*, *8*(1), 139. https://doi.org/10.1186/s12918-014-0139-6

Hartwig, C. L., Worrell, J., Levine, R. B., Ramaswami, M., & Sanyal, S. (2008). Normal dendrite growth in Drosophila motor neurons requires the AP-1 transcription factor. *Developmental Neurobiology*, *68*(10), 1225–1242. https://doi.org/10.1002/dneu.20655

Havird, J. C., Neuwald, J. L., Shah, A. A., Mauro, A., Marshall, C. A., & Ghalambor, C. K. (2020). Distinguishing between active plasticity due to thermal acclimation and passive plasticity due to Q10 effects: Why methodology matters. *Functional Ecology*, *34*(5), 1015–1028. https://doi.org/10.1111/1365-2435.13534

Heimbeck, G., Bugnon, V., Nanaë Gendre, Keller, A., Reinhard F. Stocker, & Stocker, R. F. (2001). A central neural circuit for experience-independent olfactory and courtship behavior in Drosophila melanogaster. *Proceedings of the National Academy of Sciences of the United States of America*, *98*(26), 15336–15341. https://doi.org/10.1073/pnas.011314898

Heisenberg, M. (2003). Mushroom body memoir: From maps to models. *Nat. Rev. Neurosci.*, *4*(4), 266–275. https://doi.org/10.1038/nrn1074

Heisenberg, M., Borst, A., Wagner, S., & Byers, D. (1985). Drosophila mushroom body mutants are deficient in olfactory learning. *Journal of Neurogenetics*, *2*(1), 1–30. https://doi.org/10.3109/01677068509100140

Heisenberg, M., Heusipp, M., & Wanke, C. (1995). Structural plasticity in the Drosophila brain. *Journal of Neuroscience*, *15*(3), 1951–1960.

Hemalatha, A., Li, Z., Gonzalez, D. G., Matte-Martone, C., Tai, K., Lathrop, E., Gil, D., Ganesan, S., Gonzalez, L. E., Skala, M., Perry, R. J., & Greco, V. (2025). Metabolic rewiring in skin epidermis drives tolerance to oncogenic mutations. *Nature Cell Biology*, *27*(2), 218–231. https://doi.org/10.1038/s41556-024-01574-w

Hochachka, P. W., & Somero, G. N. (2002). *Biochemical Adaptation: Mechanism and Process in Physiological Evolution*. Oxford University Press. https://doi.org/10.1093/oso/9780195117028.001.0001

Homem, C. C. F., Steinmann, V., Burkard, T. R., Jais, A., Esterbauer, H., & Knoblich, J. A. (2014). Ecdysone and mediator change energy metabolism to terminate proliferation in Drosophila neural stem cells. *Cell*, *158*(4), 874–888. https://doi.org/10.1016/j.cell.2014.06.024

Honda, T. (2022). Optogenetic and thermogenetic manipulation of defined neural circuits and behaviors in Drosophila. *Learning & Memory (Cold Spring Harbor, N.Y.)*, *29*(4), 100–109. https://doi.org/10.1101/lm.053556.121

Hong, W., Mosca, T. J., & Luo, L. (2012). Teneurins Instruct Synaptic Partner Matching in an Olfactory Map. *Nature*, *484*(7393), 201–207. https://doi.org/10.1038/nature10926

Hong, W., Zhu, H., Potter, C. J., Barsh, G., Kurusu, M., Zinn, K., & Luo, L. (2009). Leucine-rich repeat transmembrane proteins instruct discrete dendrite targeting in an olfactory map. *Nat. Neurosci.*, *12*(12), 1542–1550. https://doi.org/10.1038/nn.2442

Huang, Y., Huang, S., Lam, S. M., Liu, Z., Shui, G., & Zhang, Y. Q. (2016). Acsl, the Drosophila ortholog of intellectual-disability-related ACSL4, inhibits synaptic growth by altered lipids. *Journal of Cell Science*, *129*(21), 4034–4045. https://doi.org/10.1242/jcs.195032

Issman-Zecharya, N., & Schuldiner, O. (2014). The PI3K class III complex promotes axon pruning by downregulating a Ptc-derived signal via endosome-lysosomal degradation. *Developmental Cell*. https://doi.org/10.1016/J.DEVCEL.2014.10.013

Ito, K., Sass, H., Urban, J., Hofbauer, A., & Schneuwly, S. (1997). GAL4-responsive UAS-tau as a tool for studying the anatomy and development of the Drosophila central nervous system. *Cell and Tissue Research*, *290*(1), 1–10. https://doi.org/10.1007/s004410050901

Iwata, R., & Vanderhaeghen, P. (2024). Metabolic mechanisms of species-specific developmental tempo. *Developmental Cell*, *59*(13), 1628–1639. https://doi.org/10.1016/j.devcel.2024.05.027

Jain, S., Lin, Y., Kurmangaliyev, Y. Z., Valdes-Aleman, J., LoCascio, S. A., Mirshahidi, P., Parrington, B., & Zipursky, S. L. (2022). A global timing mechanism regulates cell-type-specific wiring programmes. *Nature*, *603*(7899), 112–118. https://doi.org/10.1038/s41586-022-04418-5

Jeanne, J. M., Fişek, M., & Wilson, R. I. (2018). The Organization of Projections from Olfactory Glomeruli onto Higher-Order Neurons. *Neuron*, *98*(6), 1198-1213.e6.

Jebara, F., Weiss, C., & Azem, A. (2017). Hsp60 and Hsp70 Chaperones: Guardians of Mitochondrial Proteostasis. In *Encyclopedia of Life Sciences* (pp. 1–9). John Wiley & Sons, Ltd. https://doi.org/10.1002/9780470015902.a0027152

Jefferis, G. S. X. E., Marin, E. C., Stocker, R. F., & Luo, L. (2001). Target neuron prespecification in the olfactory map of Drosophila. *Nature*, *414*(6860), 204–208. https://doi.org/10.1038/35102574

Jefferis, G. S. X. E., Potter, C. J., Chan, A. M., Marin, E. C., Rohlfing, T., Maurer, C. R., Jr, & Luo, L. (2007). Comprehensive maps of Drosophila higher olfactory centers: Spatially segregated fruit and pheromone representation. *Cell*, *128*(6), 1187–1203. https://doi.org/10.1016/j.cell.2007.01.040

Jefferis, G. S. X. E., Vyas, R. M., Berdnik, D., Ramaekers, A., Stocker, R. F., Tanaka, N. K., Ito, K., & Luo, L. (2004). Developmental origin of wiring specificity in the olfactory system of Drosophila. *Development*, *131*(1).

Jensen, P., Overgaard, J., Loeschcke, V., Schou, M. F., Malte, H., & Kristensen, T. N. (2014). Inbreeding effects on standard metabolic rate investigated at cold, benign and hot temperatures in *Drosophila melanogaster*. *Journal of Insect Physiology*, *62*, 11–20. https://doi.org/10.1016/j.jinsphys.2014.01.003

Jindra, M., Palli, S. R., & Riddiford, L. M. (2013). The juvenile hormone signaling pathway in insect development. *Annual Review of Entomology*, *58*, 181–204. https://doi.org/10.1146/annurev-ento-120811-153700

Johnston, D. M., Sedkov, Y., Petruk, S., Riley, K. M., Fujioka, M., Jaynes, J. B., & Mazo, A. (2011). Ecdysone- and NO-Mediated Gene Regulation by Competing EcR/Usp and E75A Nuclear Receptors during Drosophila Development. *Molecular Cell*. https://doi.org/10.1016/J.MOLCEL.2011.07.033

Jones, J. C., Myerscough, M. R., Graham, S., & Oldroyd, B. P. (2004). Honey Bee Nest Thermoregulation: Diversity Promotes Stability. *Science*, *305*(5682), 402–404. https://doi.org/10.1126/science.1096340

Kagey, M. H., Newman, J. J., Bilodeau, S., Zhan, Y., Orlando, D. A., van Berkum, N. L., Ebmeier, C. C., Goossens, J., Rahl, P. B., Levine, S. S., Taatjes, D. J., Dekker, J., & Young, R. A. (2010). Mediator and cohesin connect gene expression and chromatin architecture. *Nature*, *467*(7314), 430–435. https://doi.org/10.1038/nature09380

Kanamori, T., Kanai, M. I., Dairyo, Y., Yasunaga, K., Morikawa, R., & Emoto, K. (2013). Compartmentalized Calcium Transients Trigger Dendrite Pruning in Drosophila Sensory Neurons. *Science*. https://doi.org/10.1126/SCIENCE.1234879

Kanamori, T., Yoshino, J., Yasunaga, K., Dairyo, Y., & Emoto, K. (2015). Local endocytosis triggers dendritic thinning and pruning in Drosophila sensory neurons. *Nature Communications*. https://doi.org/10.1038/NCOMMS7515

Kiral, F. R., Dutta, S. B., Linneweber, G. A., Hilgert, S., Poppa, C., Duch, C., von Kleist, M., Hassan, B. A., & Hiesinger, P. R. (2021). Brain connectivity inversely scales with developmental temperature in Drosophila. *Cell Rep.*, *37*(12), 110145. https://doi.org/10.1016/j.celrep.2021.110145

Kiral, F. R., Linneweber, G. A., Mathejczyk, T., Georgiev, S. V., Wernet, M. F., Hassan, B. A., von Kleist, M., & Hiesinger, P. R. (2020). Autophagy-dependent filopodial kinetics restrict synaptic partner choice during Drosophila brain wiring. *Nature Communications*, *11*(1), 1325. https://doi.org/10.1038/s41467-020-14781-4

Klepsatel, P., Wildridge, D., & Gáliková, M. (2019). Temperature induces changes in Drosophila energy stores. *Scientific Reports*, *9*(1), 5239. https://doi.org/10.1038/s41598-019-41754-5

Koyama, T., Saeed, U., Rewitz, K., & Halberg, K. V. (2025). The Integrative Physiology of Hormone Signaling: Insights from Insect Models. *Physiology (Bethesda, Md.)*, *40*(4), 0. https://doi.org/10.1152/physiol.00030.2024

Kristensen, T. N., Loeschcke, V., Tan, Q., Pertoldi, C., & Mengel-From, J. (2019). Sex and age specific reduction in stress resistance and mitochondrial DNA copy number in Drosophila melanogaster. *Scientific Reports*, *9*(1), 12305. https://doi.org/10.1038/s41598-019-48752-7

Kucharski, R., Maleszka, J., Foret, S., & Maleszka, R. (2008). Nutritional control of reproductive status in honeybees via DNA methylation. *Science*, *319*(5871), 1827–1830.

Kuo, C. T., Jan, L. Y., & Jan, Y. N. (2005). Dendrite-specific remodeling of Drosophila sensory neurons requires matrix metalloproteases, ubiquitin-proteasome, and ecdysone signaling. *Proceedings of the National Academy of Sciences of the United States of America*. https://doi.org/10.1073/PNAS.0507393102

Lai, S.-L., Awasaki, T., Ito, K., & Lee, T. (2008). Clonal analysis of Drosophila antennal lobe neurons: Diverse neuronal architectures in the lateral neuroblast lineage. *Development*, *135*(17), 2883–2893. https://doi.org/10.1242/dev.024380

Lavrynenko, O., Rodenfels, J., Carvalho, M., Dye, N. A., Lafont, R., Eaton, S., & Shevchenko, A. (2015). The ecdysteroidome of Drosophila: Influence of diet and development. *Development (Cambridge, England)*, *142*(21), 3758–3768. https://doi.org/10.1242/dev.124982

Lee, T., Lee, Arthur, & Luo, L. (1999). Development of the Drosophila mushroom bodies: Sequential generation of three distinct types of neurons from a neuroblast. *Development*.

Lee, T., Liqun Luo, & Luo, L. (1999). Mosaic analysis with a repressible cell marker for studies of gene function in neuronal morphogenesis. *Neuron*, *22*(3), 451–461. https://doi.org/10.1016/s0896-6273(00)80701-1

Lee, T., Marticke, S., Sung, C., Robinow, S., & Luo, L. (2000). Cell-autonomous requirement of the USP/EcR-B ecdysone receptor for mushroom body neuronal remodeling in Drosophila. *Neuron*, *28*(3), 807–818. https://doi.org/10.1016/s0896-6273(00)00155-0

Lerner, H., Rozenfeld, E., Rozenman, B., Huetteroth, W., & Parnas, M. (2020). Differential Role for a Defined Lateral Horn Neuron Subset in Naïve Odor Valence in Drosophila. *Sci. Rep.*, *10*(1), 6147. https://doi.org/10.1038/s41598-020-63169-3

Li, H., Rai, M., Buddika, K., Sterrett, M. C., Luhur, A., Mahmoudzadeh, N. H., Julick, C. R., Pletcher, R. C., Chawla, G., & Gosney, C. J. (2019). Lactate dehydrogenase and glycerol-3-phosphate dehydrogenase cooperatively regulate growth and carbohydrate metabolism during Drosophila melanogaster larval development. *Development*, *146*(17), dev175315.

Li, & Srivastava. (2004). Heat-shock proteins. *Current Protocols in Immunology*, *Appendix 1*, Appendix 1T. https://doi.org/10.1002/0471142735.ima01ts58

Liang, L., Li, Y., Potter, C. J., Yizhar, O., Deisseroth, K., Tsien, R. W., & Luo, L. (2013). GABAergic projection neurons route selective olfactory inputs to specific higher-order neurons. *Neuron*, *79*(5), 917–931. https://doi.org/10.1016/j.neuron.2013.06.014

Lin, S., Kao, C.-F., Yu, H.-H., Huang, Y., & Lee, T. (2012). Lineage analysis of Drosophila lateral antennal lobe neurons reveals notch-dependent binary temporal fate decisions. *PLoS Biol.*, *10*(11), e1001425. https://doi.org/10.1371/journal.pbio.1001425

Liou, N.-F., Lin, S.-H., Chen, Y.-J., Tsai, K.-T., Yang, C.-J., Lin, T.-Y., Wu, T.-H., Lin, H.-J., Chen, Y.-T., Gohl, D. M., Silies, M., & Chou, Y.-H. (2018). Diverse populations of local interneurons integrate into the Drosophila adult olfactory circuit. *Nature Communications*, *9*(1), Article 1. https://doi.org/10.1038/s41467-018-04675-x

Liu, Z., Huang, Y., Zhang, Y., Chen, D., & Zhang, Y. Q. (2011). Drosophila Acyl-CoA Synthetase Long-Chain Family Member 4 Regulates Axonal Transport of Synaptic Vesicles and Is Required for Synaptic Development and Transmission. *Journal of Neuroscience*, *31*(6), 2052–2063. https://doi.org/10.1523/JNEUROSCI.3278-10.2011

Livak, K. J., & Schmittgen, T. D. (2001). Analysis of relative gene expression data using real-time quantitative PCR and the 2(-Delta Delta C(T)) Method. *Methods (San Diego, Calif.)*, *25*(4), 402–408. https://doi.org/10.1006/meth.2001.1262

Lnenicka, G. A., Spencer, G. M., & Keshishian, H. (2003). Effect of reduced impulse activity on the development of identified motor terminals in Drosophila larvae. *Journal of Neurobiology*, *54*(2), 337–345. https://doi.org/10.1002/neu.10133

Low, L. K., & Cheng, H.-J. (2006). Axon pruning: An essential step underlying the developmental plasticity of neuronal connections. *Philosophical Transactions of the Royal Society B: Biological Sciences*. https://doi.org/10.1098/RSTB.2006.1883

Lubawy, J., Chowański, S., Adamski, Z., & Słocińska, M. (2022). Mitochondria as a target and central hub of energy division during cold stress in insects. *Frontiers in Zoology*, *19*(1), 1. https://doi.org/10.1186/s12983-021-00448-3

Luo, & O'Leary. (2005). Axon retraction and degeneration in development and disease. *Annual Review of Neuroscience*. https://doi.org/10.1146/ANNUREV.NEURO.28.061604.135632

Luo, S. X., Axel, R., & Abbott, L. F. (2010). Generating sparse and selective third-order responses in the olfactory system of the fly. *Proc. Natl. Acad. Sci. U. S. A.*, *107*(23), 10713–10718. https://doi.org/10.1073/pnas.1005635107

MacMillan, H. A., Knee, J. M., Dennis, A. B., Udaka, H., Marshall, K. E., Merritt, T. J. S., & Sinclair, B. J. (2016). Cold acclimation wholly reorganizes the Drosophila melanogaster transcriptome and metabolome. *Scientific Reports*, *6*(1), 28999. https://doi.org/10.1038/srep28999

Mallard, F., Nolte, V., Tobler, R., Kapun, M., & Schlötterer, C. (2018). A simple genetic basis of adaptation to a novel thermal environment results in complex metabolic rewiring in Drosophila. *Genome Biology*, *19*(1), 119. https://doi.org/10.1186/s13059-018-1503-4

Manenti, T., Kjærsgaard, A., Schou, T. M., Pertoldi, C., Moghadam, N. N., & Loeschcke, V. (2021). Responses to Developmental Temperature Fluctuation in Life History Traits of Five Drosophila Species (Diptera: Drosophilidae) from Different Thermal Niches. *Insects*, *12*(10), 925. https://doi.org/10.3390/insects12100925

Marder, E. (2011). Variability, compensation, and modulation in neurons and circuits. *Proceedings of the National Academy of Sciences*, *108*(supplement_3), 15542–15548. https://doi.org/10.1073/pnas.1010674108

Marin, E. C., Jefferis, G. S. X. E., Komiyama, T., Zhu, H., & Luo, L. (2002). Representation of the glomerular olfactory map in the Drosophila brain. *Cell*, *109*(2), 243–255. https://doi.org/10.1016/s0092-8674(02)00700-6

Marmor-Kollet, N., & Schuldiner, O. (2016). Contrasting developmental axon regrowth and neurite sprouting of Drosophila mushroom body neurons reveals shared and unique molecular mechanisms. *Developmental Neurobiology*. https://doi.org/10.1002/DNEU.22312

Martinez, E., Menze, M. A., & Agosta, S. J. (2017). Reduced Mitochondrial Efficiency Explains Mismatched Growth and Metabolic Rate at Supraoptimal Temperatures. *Physiological and Biochemical Zoology: PBZ*, *90*(2), 294–298. https://doi.org/10.1086/689871

Mashek, D. G., Li, L. O., & Coleman, R. A. (2007). Long-Chain Acyl-Coa Synthetases And Fatty Acid Channeling. *Future Lipidology*, *2*(4), 465–476. https://doi.org/10.2217/17460875.2.4.465

Mason, P. J., Hall, L. M. C., & Gausz, J. (1984). The expression of heat shock genes during normal development in Drosophila melanogaster (heat shock/abundant transcripts/developmental regulation). *Molecular and General Genetics MGG*, *194*(1), 73–78. https://doi.org/10.1007/BF00383500

Maurange, C., & Lanet, E. (2014). Building a brain under nutritional restriction: Insights on sparing and plasticity from Drosophila studies. *Frontiers in Physiology*, *5*. https://doi.org/10.3389/fphys.2014.00117

Mayer, M. P., & Bukau, B. (2005). Hsp70 chaperones: Cellular functions and molecular mechanism. *Cellular and Molecular Life Sciences: CMLS*, *62*(6), 670–684. https://doi.org/10.1007/s00018-004-4464-6

Merian, M. S. (1705). *Metamorphosis insectorum surinamensium.* Voor den auteur, als ook by G. Valck. https://www.biodiversitylibrary.org/item/129308

Merritt, T. J., Sezgin, E., Zhu, C.-T., & Eanes, W. F. (2006). Triglyceride pools, flight and activity variation at the Gpdh locus in Drosophila melanogaster. *Genetics*, *172*(1), 293–304.

Mirault, M.-E., Goldschmidt-Clermont, M., Moran, L., Arrigo, A., & Tissieres, A. (1978). *The effect of heat shock on gene expression in Drosophila melanogaster*. *42*, 819–827.

Miyamoto, T., & Amrein, H. (2019). Neuronal Gluconeogenesis Regulates Systemic Glucose Homeostasis in Drosophila melanogaster. *Current Biology*, *29*(8), 1263-1272.e5. https://doi.org/10.1016/j.cub.2019.02.053

Moore, R. J. D., Taylor, G. J., Paulk, A. C., Pearson, T., van Swinderen, B., & Srinivasan, M. V. (2014). FicTrac: A visual method for tracking spherical motion and generating fictive animal paths. *Journal of Neuroscience Methods*, *225*, 106–119. https://doi.org/10.1016/j.jneumeth.2014.01.010

Morrow, G., Le Pécheur, M., & Tanguay, R. M. (2016). Drosophila melanogaster mitochondrial Hsp22: A role in resistance to oxidative stress, aging and the mitochondrial unfolding protein response. *Biogerontology*, *17*(1), 61–70. https://doi.org/10.1007/s10522-015-9591-y

Mosca, T. J., Carrillo, R. A., White, B. H., & Keshishian, H. (2005). Dissection of synaptic excitability phenotypes by using a dominant-negative Shaker K+ channel subunit. *Proceedings of the National Academy of Sciences*, *102*(9), 3477–3482.

Nakagawa, Y., & Henrich, V. C. (2009). Arthropod nuclear receptors and their role in molting. *The FEBS Journal*, *276*(21), 6128–6157. https://doi.org/10.1111/j.1742-4658.2009.07347.x

Neuhaus, E. M., Gisselmann, G., Zhang, W., Dooley, R., Störtkuhl, K., & Hatt, H. (2005). Odorant receptor heterodimerization in the olfactory system of Drosophila melanogaster. *Nature Neuroscience*, *8*(1), 15–17. https://doi.org/10.1038/nn1371

Niwa, R., Matsuda, T., Yoshiyama, T., Namiki, T., Mita, K., Fujimoto, Y., & Kataoka, H. (2004). CYP306A1, a cytochrome P450 enzyme, is essential for ecdysteroid biosynthesis in the prothoracic glands of Bombyx and Drosophila. *The Journal of Biological Chemistry*, *279*(34), 35942–35949. https://doi.org/10.1074/jbc.M404514200

O'Brien, S. J., & Shimada, Y. (1974). THE α-GLYCEROPHOSPHATE CYCLE IN DROSOPHILA MELANOGASTER: IV. Metabolic, Ultrastructural, and Adaptive Consequences of α Gpdh-1" Null" Mutations. *The Journal of Cell Biology*, *63*(3), 864–882.

Ohmer, M. E. B., Hammond, T. T., Switzer, S., Wantman, T., Bednark, J. G., Paciotta, E., Coscia, J., & Richards-Zawacki, C. L. (2023). Developmental environment has lasting effects on amphibian post-metamorphic behavior and thermal physiology. *Journal of Experimental Biology*, *226*(9), jeb244883. https://doi.org/10.1242/jeb.244883

Okamoto, N., Raghuvir Viswanatha, Viswanatha, R., Riyan Bittar, Bittar, R., Zhongchi Li, Li, Z., Sachiko Haga-Yamanaka, Haga-Yamanaka, S., Norbert Perrimon, Perrimon, N., Naoaki Yamanaka, & Yamanaka, N. (2018). A Membrane Transporter Is Required for Steroid

Hormone Uptake in Drosophila. *Developmental Cell*, *47*(3), 294. https://doi.org/10.1016/j.devcel.2018.09.012

Olsen, S. R., & Wilson, R. (2008). Lateral presynaptic inhibition mediates gain control in an olfactory circuit. *Nature*, *452*(7190), 956–960. https://doi.org/10.1038/nature06864

Oostra, V., de Jong, M. A., Invergo, B. M., Kesbeke, F., Wende, F., Brakefield, P. M., & Zwaan, B. J. (2011). Translating environmental gradients into discontinuous reaction norms via hormone signalling in a polyphenic butterfly. *Proceedings. Biological Sciences*, *278*(1706), 789–797. https://doi.org/10.1098/rspb.2010.1560

Özel, M. N., Kulkarni, A., Hasan, A., Brummer, J., Moldenhauer, M., Daumann, I.-M., Wolfenberg, H., Dercksen, V. J., Kiral, F. R., Weiser, M., Prohaska, S., von Kleist, M., & Hiesinger, P. R. (2019). Serial Synapse Formation through Filopodial Competition for Synaptic Seeding Factors. *Developmental Cell*, *50*(4), 447-461.e8. https://doi.org/10.1016/j.devcel.2019.06.014

Pallotta, M. M., Turano, M., Ronca, R., Mezzasalma, M., Petraccioli, A., Odierna, G., & Capriglione, T. (2017). Brain Gene Expression is Influenced by Incubation Temperature During Leopard Gecko (Eublepharis macularius) Development. *Journal of Experimental Zoology Part B: Molecular and Developmental Evolution*, *328*(4), 360–370. https://doi.org/10.1002/jez.b.22736

Parnas, M., Lin, A. C., Huetteroth, W., & Miesenböck, G. (2013). Odor Discrimination in Drosophila: From Neural Population Codes to Behavior. *Neuron*, *79*(5), 932–944. https://doi.org/10.1016/j.neuron.2013.08.006

Patro, R., Duggal, G., Love, M. I., Irizarry, R. A., & Kingsford, C. (2017). Salmon provides fast and bias-aware quantification of transcript expression. *Nature Methods*, *14*(4), 417–419. https://doi.org/10.1038/nmeth.4197

Pauli, D., Arrigo, A.-P., Vazquez, J., Tonka, C.-H., & Tissières, A. (1989). Expression of the small heat shock genes during Drosophila development: Comparison of the accumulation of hsp23 and hsp27 mRNAs and polypeptides. *Genome*, *31*(2), 671–676. https://doi.org/10.1139/g89-123

Peng, I.-F., Berke, B. A., Zhu, Y., Lee, W.-H., Chen, W., & Wu, C.-F. (2007). Temperature-dependent developmental plasticity of Drosophila neurons: Cell-autonomous roles of

membrane excitability, Ca2+ influx, and cAMP signaling. *The Journal of Neuroscience: The Official Journal of the Society for Neuroscience*, *27*(46), 12611–12622. https://doi.org/10.1523/JNEUROSCI.2179-07.2007

Pétavy, G., Morin, J. P., Moreteau, B., & David, J. R. (1997). Growth temperature and phenotypic plasticity in two Drosophila sibling species: Probable adaptive changes in flight capacities. *Journal of Evolutionary Biology*, *10*(6), 875–887.

Petryk, A., Warren, J. T., Marqués, G., Jarcho, M. P., Gilbert, L. I., Kahler, J., Parvy, J.-P., Li, Y., Dauphin-Villemant, C., & O'Connor, M. B. (2003). Shade is the Drosophila P450 enzyme that mediates the hydroxylation of ecdysone to the steroid insect molting hormone 20-hydroxyecdysone. *Proceedings of the National Academy of Sciences of the United States of America*, *100*(24), 13773–13778. https://doi.org/10.1073/pnas.2336088100

Popov, V. I., & Bocharova, L. S. (1992). Hibernation-induced structural changes in synaptic contacts between mossy fibres and hippocampal pyramidal neurons. *Neuroscience*, *48*(1), 53–62. https://doi.org/10.1016/0306-4522(92)90337-2

Prieto-Godino, L. L., Diegelmann, S., & Bate, M. (2012). Embryonic Origin of Olfactory Circuitry in Drosophila: Contact and Activity-Mediated Interactions Pattern Connectivity in the Antennal Lobe. *PLOS Biology*, *10*(10), e1001400. https://doi.org/10.1371/journal.pbio.1001400

Prokop, A., Beaven, R., Qu, Y., & Sánchez-Soriano, N. (2013). Using fly genetics to dissect the cytoskeletal machinery of neurons during axonal growth and maintenance. *Journal of Cell Science*. https://doi.org/10.1242/JCS.126912

Qin, W., Neal, S. J., Robertson, R. M., Westwood, J. T., & Walker, V. K. (2005). Cold hardening and transcriptional change in Drosophila melanogaster. *Insect Molecular Biology*, *14*(6), 607–613. https://doi.org/10.1111/j.1365-2583.2005.00589.x

Rabinovich, D., Mayseless, O., & Schuldiner, O. (2015). Long term ex vivo culturing of Drosophila brain as a method to live image pupal brains: Insights into the cellular mechanisms of neuronal remodeling. *Front. Cell. Neurosci.* https://doi.org/10.3389/FNCEL.2015.00327

Rabinovich, D., Yaniv, S. P., Alyagor, I., & Schuldiner, O. (2016). Nitric Oxide as a Switching Mechanism between Axon Degeneration and Regrowth during Developmental Remodeling. *Cell*. https://doi.org/10.1016/J.CELL.2015.11.047

Raghuram, S., Stayrook, K. R., Huang, P., Rogers, P. M., Nosie, A. K., McClure, D. B., Burris, L. L., Khorasanizadeh, S., Burris, T. P., & Rastinejad, F. (2007). Identification of heme as the ligand for the orphan nuclear receptors REV-ERBα and REV-ERBβ. *Nature Structural &Molecular Biology*. https://doi.org/10.1038/NSMB1344

Reinking, J., Lam, M. M., Pardee, K., Sampson, H. M., Liu, S., Yang, P., Williams, S. P., White, W. L., Lajoie, G., Edwards, A. M., & Krause, H. M. (2005). The Drosophila Nuclear Receptor E75 Contains Heme and Is Gas Responsive. *Cell*. https://doi.org/10.1016/J.CELL.2005.07.005

Riabinina, O., & Potter, C. J. (2016). The Q-System: A Versatile Expression System for Drosophila. *Methods in Molecular Biology (Clifton, N.J.)*, *1478*, 53–78. https://doi.org/10.1007/978-1-4939-6371-3_3

Riddiford, L. M., Hiruma, K., Zhou, X., & Nelson, C. A. (2003). Insights into the molecular basis of the hormonal control of molting and metamorphosis from *Manduca sexta* and *Drosophila melanogaster*. *Insect Biochemistry and Molecular Biology, Tribute to Lawrence Gilbert*, *33*(12), 1327–1338. https://doi.org/10.1016/j.ibmb.2003.06.001

Robinow, S., Talbot, W. S., Hogness, D. S., & Truman, J. W. (1993). Programmed cell death in the Drosophila CNS is ecdysone-regulated and coupled with a specific ecdysone receptor isoform. *Development (Cambridge, England)*, *119*(4), 1251–1259. https://doi.org/10.1242/dev.119.4.1251

Root, C. M., Masuyama, K., Green, D. S., Enell, L. E., Nässel, D. R., Lee, C.-H., & Wang, J. W. (2008). A Presynaptic Gain Control Mechanism Fine-Tunes Olfactory Behavior. *Neuron*, *59*(2), 311–321. https://doi.org/10.1016/j.neuron.2008.07.003

Sakuma, C., Anzo, M., Miura, M., & Chihara, T. (2014). Development of olfactory projection neuron dendrites that contribute to wiring specificity of the Drosophila olfactory circuit. *Genes & Genetic Systems*, *89*(1), 17–26. https://doi.org/10.1266/ggs.89.17

Scheffer, L. K., Xu, C. S., Januszewski, M., Lu, Z., Takemura, Shin-ya, Hayworth, K. J., Huang, G. B., Shinomiya, K., Maitlin-Shepard, J., Berg, S., Clements, J., Hubbard, P. M., Katz, W. T., Umayam, L., Zhao, T., Ackerman, D., Blakely, T., Bogovic, J., Dolafi, T., … Plaza, S. M. (2020). A connectome and analysis of the adult Drosophila central brain. *eLife*, *9*, e57443. https://doi.org/10.7554/eLife.57443

Schlegel, P., Bates, A. S., Stürner, T., Jagannathan, S. R., Drummond, N., Hsu, J., Serratosa Capdevila, L., Javier, A., Marin, E. C., Barth-Maron, A., Tamimi, I. F., Li, F., Rubin, G. M., Plaza, S. M., Costa, M., & Jefferis, G. S. X. E. (2021). Information flow, cell types and stereotypy in a full olfactory connectome. *Elife*, *10*. https://doi.org/10.7554/eLife.66018

Schou, M. F., Kristensen, T. N., Pedersen, A., Karlsson, B. G., Loeschcke, V., & Malmendal, A. (2017). Metabolic and functional characterization of effects of developmental temperature in *Drosophila melanogaster*. *American Journal of Physiology-Regulatory, Integrative and Comparative Physiology*, *312*(2), R211–R222. https://doi.org/10.1152/ajpregu.00268.2016

Schubiger, M., Wade, A. A., Carney, G. E., Truman, J. W., & Bender, M. (1998). Drosophila EcR-B ecdysone receptor isoforms are required for larval molting and for neuron remodeling during metamorphosis. *Development (Cambridge, England)*, *125*(11), 2053–2062. https://doi.org/10.1242/dev.125.11.2053

Schuldiner, O., Berdnik, D., Levy, J. M., Wu, J., Luginbuhl, D. J., Gontang, A. C., & Luo, L. (2008). piggyBac-Based Mosaic Screen Identifies a Postmitotic Function for Cohesin in Regulating Developmental Axon Pruning. *Developmental Cell*. https://doi.org/10.1016/J.DEVCEL.2007.11.001

Schuldiner, O., & Yaron, A. (2015). Mechanisms of developmental neurite pruning. *Cellular and Molecular Life Sciences*. https://doi.org/10.1007/S00018-014-1729-6

Schuman, E. M., Dynes, J. L., & Steward, O. (2006). Synaptic regulation of translation of dendritic mRNAs. *The Journal of Neuroscience: The Official Journal of the Society for Neuroscience*, *26*(27), 7143–7146. https://doi.org/10.1523/JNEUROSCI.1796-06.2006

Schwedes, C. C., & Carney, G. E. (2012). Ecdysone signaling in adult Drosophila melanogaster. *Journal of Insect Physiology*, *58*(3), 293–302. https://doi.org/10.1016/j.jinsphys.2012.01.013

Seebacher, F., White, C. R., & Franklin, C. E. (2015). Physiological plasticity increases resilience of ectothermic animals to climate change. *Nature Climate Change*, *5*(1), 61–66. https://doi.org/10.1038/nclimate2457

Shearin, H. K., Quinn, C. D., Mackin, R. D., Macdonald, I. S., & Stowers, R. S. (2018). T-GRASP, a targeted GRASP for assessing neuronal connectivity. *J. Neurosci. Methods*, *306*, 94–102. https://doi.org/10.1016/j.jneumeth.2018.05.014

Shi, Y. Y., Yan, W. Y., Huang, Z. Y., Wang, Z. L., Wu, X. B., & Zeng, Z. J. (2013). Genomewide analysis indicates that queen larvae have lower methylation levels in the honey bee (Apis mellifera). *Naturwissenschaften*, *100*(2), 193–197.

Shimizu, K., & Stopfer, M. (2017). A Population of Projection Neurons that Inhibits the Lateral Horn but Excites the Antennal Lobe through Chemical Synapses in Drosophila. *Front. Neural Circuits*, *11*, 30. https://doi.org/10.3389/fncir.2017.00030

Shimono, K., Fujimoto, A., Tsuyama, T., Yamamoto-Kochi, M., Sato, M., Hattori, Y., Sugimura, K., Usui, T., Kimura, K., & Uemura, T. (2009). Multidendritic sensory neurons in the adult Drosophila abdomen: Origins, dendritic morphology, and segment- and age-dependent programmed cell death. *Neural Development*, *4*(1), 37. https://doi.org/10.1186/1749-8104-4-37

Sigrist, S. J., Reiff, D. F., Thiel, P. R., Steinert, J. R., & Schuster, C. M. (2003). Experience-Dependent Strengthening of Drosophila Neuromuscular Junctions. *Journal of Neuroscience*, *23*(16), 6546–6556. https://doi.org/10.1523/JNEUROSCI.23-16-06546.2003

Song, Q., Sun, X., & Jin, X.-Y. (2003). 20E-regulated USP expression and phosphorylation in *Drosophila melanogaster*. *Insect Biochemistry and Molecular Biology, Tribute to Lawrence Gilbert*, *33*(12), 1211–1218. https://doi.org/10.1016/j.ibmb.2003.06.005

Sorkaç, A., Moşneanu, R. A., Crown, A. M., Savaş, D., Okoro, A. M., Memiş, E., Talay, M., & Barnea, G. (2023). Retro-Tango enables versatile retrograde circuit tracing in Drosophila. *eLife*, *12*, e85041. https://doi.org/10.7554/eLife.85041

Spencer, K. A., Belgacem, Y. H., Visina, O., Shim, S., Genus, H., & Borodinsky, L. N. (2019). Growth at Cold Temperature Increases the Number of Motor Neurons to Optimize Locomotor Function. *Current Biology*, *29*(11), 1787-1799.e5. https://doi.org/10.1016/j.cub.2019.04.072

Stocker, R. F. (1994). The organization of the chemosensory system in Drosophila melanogaster: A rewiew. *Cell and Tissue Research*, *275*(1), 3–26. https://doi.org/10.1007/BF00305372

Stocker, R. F., Lienhard, M. C., Borst, A., & Fischbach, K. F. (1990). Neuronal architecture of the antennal lobe in Drosophila melanogaster. *Cell Tissue Res.*, *262*(1), 9–34. https://doi.org/10.1007/BF00327741

Strutz, A., Soelter, J., Baschwitz, A., Farhan, A., Grabe, V., Rybak, J., Knaden, M., Schmuker, M., Hansson, B. S., & Sachse, S. (2014). Decoding odor quality and intensity in the Drosophila brain. *Elife*, *3*, e04147. https://doi.org/10.7554/eLife.04147

Sweeney, L. B., Chou, Y.-H., Wu, Z., Joo, W., Komiyama, T., Potter, C. J., Kolodkin, A. L., Garcia, K. C., & Luo, L. (2011). Secreted Semaphorins from Degenerating Larval ORN Axons Direct Adult Projection Neuron Dendrite Targeting. *Neuron*, *72*(5), 734–747. https://doi.org/10.1016/j.neuron.2011.09.026

Syed, M. H., Mark, B., & Doe, C. Q. (2017). Steroid hormone induction of temporal gene expression in Drosophila brain neuroblasts generates neuronal and glial diversity. *eLife*, *6*, e26287. https://doi.org/10.7554/eLife.26287

Takesian, A. E., & Hensch, T. K. (2013). Balancing plasticity/stability across brain development. *Progress in Brain Research*, *207*, 3–34. https://doi.org/10.1016/B978-0-444-63327-9.00001-1

Talay, M., Ethan Richman, Richman, E. B., Snell, N., Hartmann, G., Fisher, J. D., Sorkaç, A., Santoyo, J. F., Chou-Freed, C., Nair, N., Johnson, M. A., Johnson, M., Szymanski, J., & Barnea, G. (2017). Transsynaptic Mapping of Second-Order Taste Neurons in Flies by trans-Tango. *Neuron*, *96*(4), 783. https://doi.org/10.1016/j.neuron.2017.10.011

Talbot, W. S., Swyryd, E. A., & Hogness, D. S. (1993). Drosophila tissues with different metamorphic responses to ecdysone express different ecdysone receptor isoforms. *Cell*, *73*(7), 1323–1337. https://doi.org/10.1016/0092-8674(93)90359-x

Tanaka, N. K., Awasaki, T., Shimada, T., & Ito, K. (2004). Integration of Chemosensory Pathways in the Drosophila Second-Order Olfactory Centers. *Current Biology*, *14*(6), 449–457. https://doi.org/10.1016/j.cub.2004.03.006

Tanaka, N. K., Endo, K., & Ito, K. (2012). Organization of antennal lobe-associated neurons in adult Drosophila melanogaster brain. *J. Comp. Neurol.*, *520*(18), 4067–4130.

Tang, L. S., Goeritz, M. L., Caplan, J. S., Taylor, A. L., Fisek, M., & Marder, E. (2010). Precise Temperature Compensation of Phase in a Rhythmic Motor Pattern. *PLOS Biology*, *8*(8), e1000469. https://doi.org/10.1371/journal.pbio.1000469

Tasdemir-Yilmaz, O. E., & Freeman, M. (2014). Astrocytes engage unique molecular programs to engulf pruned neuronal debris from distinct subsets of neurons. *Genes & Development*. https://doi.org/10.1101/GAD.229518.113

Tautz, J., Maier, S., Groh, C., Rossler, W., & Brockmann, A. (2003). Behavioral performance in adult honey bees is influenced by the temperature experienced during their pupal development. *Proceedings of the National Academy of Sciences of the United States of America*, *100*(12), 7343–7347. https://doi.org/10.1073/pnas.1232346100

Tavakoli, M. R., Lyudchik, J., Januszewski, M., Vistunou, V., Agudelo Dueñas, N., Vorlaufer, J., Sommer, C., Kreuzinger, C., Oliveira, B., Cenameri, A., Novarino, G., Jain, V., & Danzl, J. G. (2025). Light-microscopy-based connectomic reconstruction of mammalian brain tissue. *Nature*, *642*(8067), 398–410. https://doi.org/10.1038/s41586-025-08985-1

Thomas, M. G., Pascual, M. L., Maschi, D., Luchelli, L., & Boccaccio, G. L. (2014). Synaptic control of local translation: The plot thickens with new characters. *Cellular and Molecular Life Sciences: CMLS*, *71*(12), 2219–2239. https://doi.org/10.1007/s00018-013-1506-y

Thum, A. S., & Gerber, B. (2023). The making of a maggot brain. *eLife*, *12*, e86696. https://doi.org/10.7554/eLife.86696

Thummel, C. S. (2002). Ecdysone-regulated puff genes 2000. *Insect Biochemistry and Molecular Biology*, *32*(2), 113–120. https://doi.org/10.1016/S0965-1748(01)00112-6

Tristan Walter & Iain D Couzin. (2021). *TRex, a fast multi-animal tracking system with markerless identification, and 2D estimation of posture and visual fields | eLife*. https://elifesciences.org/articles/64000

Trotta, V., Calboli, F. C., Ziosi, M., Guerra, D., Pezzoli, M. C., David, J. R., & Cavicchi, S. (2006). Thermal plasticity in Drosophila melanogaster: A comparison of geographic populations. *BMC Evolutionary Biology*, *6*(1), 67.

Truman, J. W. (2019). The Evolution of Insect Metamorphosis. *Current Biology*, *29*(23), R1252–R1268. https://doi.org/10.1016/j.cub.2019.10.009

Truman, J. W., Price, J., Miyares, R. L., & Lee, T. (2023). Metamorphosis of memory circuits in Drosophila reveals a strategy for evolving a larval brain. *eLife*, *12*, e80594. https://doi.org/10.7554/eLife.80594

Truman, J. W., & Riddiford, L. M. (2023). Drosophila postembryonic nervous system development: A model for the endocrine control of development. *Genetics*, *223*(3), iyac184. https://doi.org/10.1093/genetics/iyac184

Truman, J. W., Talbot, W. S., Fahrbach, S. E., & Hogness, D. S. (1994). Ecdysone receptor expression in the CNS correlates with stage-specific responses to ecdysteroids during Drosophila and Manduca development. *Development (Cambridge, England)*, *120*(1), 219–234. https://doi.org/10.1242/dev.120.1.219

Voos, W., & Röttgers, K. (2002). Molecular chaperones as essential mediators of mitochondrial biogenesis. *Biochimica et Biophysica Acta (BBA) - Molecular Cell Research, Protein Transport into Mitochondria and Chloroplasts Part II*, *1592*(1), 51–62. https://doi.org/10.1016/S0167-4889(02)00264-1

Vosshall, L. B., Wong, A. M., & Axel, R. (2000). An olfactory sensory map in the fly brain. *Cell*, *102*(2), 147–159. https://doi.org/10.1016/s0092-8674(00)00021-0

Wang, H., Liu, Z., Wang, Y., Ma, L., Zhang, W., & Xu, B. (2020). Genome-wide differential DNA methylation in reproductive, morphological, and visual system differences between queen bee and worker bee (Apis mellifera). *Frontiers in Genetics*, *11*, 770.

Wang, K., Gong, J., Wang, Q., Li, H., Cheng, Q., Liu, Y., Zeng, S., & Wang, Z. (2014). Parallel pathways convey olfactory information with opposite polarities in Drosophila. *Proceedings of the National Academy of Sciences*, *111*(8), 3164–3169. https://doi.org/10.1073/pnas.1317911111

Warm, D., Schroer, J., & Sinning, A. (2022). Gabaergic Interneurons in Early Brain Development: Conducting and Orchestrated by Cortical Network Activity. *Frontiers in Molecular Neuroscience*, *14*. https://doi.org/10.3389/fnmol.2021.807969

Warren, J. T., Petryk, A., Marques, G., Jarcho, M., Parvy, J.-P., Dauphin-Villemant, C., O'Connor, M. B., & Gilbert, L. I. (2002). Molecular and biochemical characterization of two P450 enzymes in the ecdysteroidogenic pathway of Drosophila melanogaster. *Proceedings of the National Academy of Sciences of the United States of America*, *99*(17), 11043–11048. https://doi.org/10.1073/pnas.162375799

Warren, J. T., Petryk, A., Marqués, G., Parvy, J.-P., Shinoda, T., Itoyama, K., Kobayashi, J., Jarcho, M., Li, Y., O'Connor, M. B., Dauphin-Villemant, C., & Gilbert, L. I. (2004). Phantom

encodes the 25-hydroxylase of *Drosophila melanogaster* and *Bombyx mori*: A P450 enzyme critical in ecdysone biosynthesis. *Insect Biochemistry and Molecular Biology*, *34*(9), 991–1010. https://doi.org/10.1016/j.ibmb.2004.06.009

Watts, R. J., Hoopfer, E. D., & Luo, L. (2003). Axon pruning during Drosophila metamorphosis: Evidence for local degeneration and requirement of the ubiquitin-proteasome system. *Neuron*. https://doi.org/10.1016/S0896-6273(03)00295-2

Werner, E. E. (1988). Size, Scaling, and the Evolution of Complex Life Cycles. In B. Ebenman & L. Persson (Eds.), *Size-Structured Populations* (pp. 60–81). Springer. https://doi.org/10.1007/978-3-642-74001-5_6

West, G. B., Brown, J. H., & Enquist, B. J. (1997). A general model for the origin of allometric scaling laws in biology. *Science*, *276*(5309), 122–126. https://doi.org/10.1126/science.276.5309.122

Whyte, W. A., Orlando, D. A., Hnisz, D., Abraham, B. J., Lin, C. Y., Kagey, M. H., Rahl, P. B., Lee, T. I., & Young, R. A. (2013). Master transcription factors and mediator establish super-enhancers at key cell identity genes. *Cell*, *153*(2), 307–319. https://doi.org/10.1016/j.cell.2013.03.035

Williams, C. M., Watanabe, M., Guarracino, M. R., Ferraro, M. B., Edison, A. S., Morgan, T. J., Boroujerdi, A. F. B., & Hahn, D. A. (2014). Cold adaptation shapes the robustness of metabolic networks in Drosophila melanogaster. *Evolution; International Journal of Organic Evolution*, *68*(12), 3505–3523. https://doi.org/10.1111/evo.12541

Winding, M., Pedigo, B. D., Barnes, C. L., Patsolic, H. G., Park, Y., Kazimiers, T., Fushiki, A., Andrade, I. V., Khandelwal, A., Valdes-Aleman, J., Li, F., Randel, N., Barsotti, E., Correia, A., Fetter, R. D., Hartenstein, V., Priebe, C. E., Vogelstein, J. T., Cardona, A., & Zlatic, M. (2023). The connectome of an insect brain. *Science*, *379*(6636), eadd9330. https://doi.org/10.1126/science.add9330

Wojtas, K., Slepecky, N., von Kalm, L., & Sullivan, D. (1997). Flight muscle function in Drosophila requires colocalization of glycolytic enzymes. *Molecular Biology of the Cell*, *8*(9), 1665–1675. https://doi.org/10.1091/mbc.8.9.1665

Wong, A. M., Wang, J. W., & Axel, R. (2002). Spatial representation of the glomerular map in the Drosophila protocerebrum. *Cell*, *109*(2), 229–241. https://doi.org/10.1016/s0092-8674(02)00707-9

Woodard, C. T., Baehrecke, E. H., & Thummel, C. S. (1994). A molecular mechanism for the stage specificity of the Drosophila prepupal genetic response to ecdysone. *Cell*, *79*(4), 607–615. https://doi.org/10.1016/0092-8674(94)90546-0

Yadav, P., Shinde, P., & Singh, A. (2025). Brain rewiring during development: A comparative analysis of larval and adult Drosophila melanogaster connectomes. *Network Neuroscience*, *9*(4), 1299–1322. https://doi.org/10.1162/NETN.a.26

Yamanaka, N., Rewitz, K. F., & O'Connor, M. B. (2013). Ecdysone Control of Developmental Transitions: Lessons from Drosophila Research. *Annual Review of Entomology*, *58*(Volume 58, 2013), 497–516. https://doi.org/10.1146/annurev-ento-120811-153608

Yaniv, S. P., Issman-Zecharya, N., Oren-Suissa, M., Podbilewicz, B., & Schuldiner, O. (2012). Axon Regrowth during Development and Regeneration Following Injury Share Molecular Mechanisms. *Current Biology*. https://doi.org/10.1016/J.CUB.2012.07.044

Yaniv, S. P., & Schuldiner, O. (2016). A fly's view of neuronal remodeling. *Wiley Interdisciplinary Reviews-Developmental Biology*. https://doi.org/10.1002/wdev.241

Yao, T.-P., Forman, B. M., Jiang, Z., Cherbas, L., Chen, J.-D., McKeown, M., Cherbas, P., & Evans, R. M. (1993). Functional ecdysone receptor is the product of EcR and Ultraspiracle genes. *Nature*, *366*(6454), 476–479. https://doi.org/10.1038/366476a0

Zhang, B., Sato, K., & Yamamoto, D. (2018). Ecdysone signaling regulates specification of neurons with a male-specific neurite in Drosophila. *Biology Open*, *7*(2), bio029744. https://doi.org/10.1242/bio.029744

Zheng, Z., Lauritzen, J. S., Perlman, E., Robinson, C. G., Nichols, M., Milkie, D., Torrens, O., Price, J., Fisher, C. B., Sharifi, N., Calle-Schuler, S. A., Kmecova, L., Ali, I. J., Karsh, B., Trautman, E. T., Bogovic, J. A., Hanslovsky, P., Jefferis, G. S. X. E., Kazhdan, M., … Bock, D. D. (2018). A Complete Electron Microscopy Volume of the Brain of Adult Drosophila melanogaster. *Cell*, *174*(3), 730-743.e22. https://doi.org/10.1016/j.cell.2018.06.019

Zhong, Y., & Wu, C.-F. (2004). Neuronal activity and adenylyl cyclase in environment-dependent plasticity of axonal outgrowth in Drosophila. *Journal of Neuroscience*, *24*(6), 1439–1445.

Zhu, H., Hummel, T., Clemens, J. C., Berdnik, D., Zipursky, S. L., & Luo, L. (2006). Dendritic patterning by Dscam and synaptic partner matching in the Drosophila antennal lobe. *Nature Neuroscience*, *9*(3), 349–355. https://doi.org/10.1038/nn1652

Züfle, P., Batista, L. L., Brandão, S. C., D'Uva, G., Daniel, C., & Martelli, C. (2025). Impact of developmental temperature on neural growth, connectivity, and function. *Science Advances*, *11*(3), eadp9587. https://doi.org/10.1126/sciadv.adp9587

8 Acknowledgments

9 Curriculum vitae

10 Eigenständigkeitserklärung

Hiermit erkläre ich,

dass ich die vorliegende Arbeit selbstständig verfasst und keine anderen als die angegebenen Quellen und Hilfsmittel (dazu zählen auch KI-basierte Anwendungen oder Werkzeuge[1]) benutzt habe. Sämtliche wörtlichen oder sinngemäßen Übernahmen und Zitate sind kenntlich gemacht und nachgewiesen. Ich versichere, dass ich keine Hilfsmittel verwendet habe, deren Nutzung die Prüferin oder der Prüfer explizit ausgeschlossen hat.

Mit Abgabe der vorliegenden Leistung übernehme ich die Verantwortung für das eingereichte Gesamtprodukt. Ich verantworte damit auch jegliche KI-generierten Inhalte, die ich in meine Arbeit übernommen habe. Die Richtigkeit übernommener (KI-generierter) Aussagen und Inhalte habe ich nach bestem Wissen und Gewissen geprüft.

Ich habe die Arbeit nicht zum Erwerb eines anderen Leistungsnachweises in gleicher oder ähnlicher Form eingereicht.

Mir ist bekannt, dass ein Verstoß gegen die genannten Punkte prüfungsrechtliche Konsequenzen hat und insbesondere dazu führen kann, dass die Studien- und Prüfungsleistung als mit „nicht bestanden“ bewertet wird. Die Einschreibung kann für bis zu zwei Jahre widerrufen werden, wenn Studierende zweimal oder häufiger bei Prüfungsleistungen täuschen (§ 69 Abs. 4 und 5 HochSchG).

_____

Ort, Datum und Unterschrift

AI-TOOL	PURPOSE
ChatGPT	Help improve minor parts of the text
Anara	Help with finding relevant papers

Note: I carefully reviewed and validated all concepts and literature. This dissertation is the result of my writing, critical thinking and interpretations.

[1] Weiterführende Informationen zu KI-basierte Anwendungen oder Werkzeuge unter: https://digitale-lehre.uni-mainz.de/lehren-pruefen/ki-in-der-hochschulbildung/